Effect of novel ryanodine receptor modulators in mouse and human models of Duchenne muscular dystrophy

Garazi Aldanondo Aristizabal

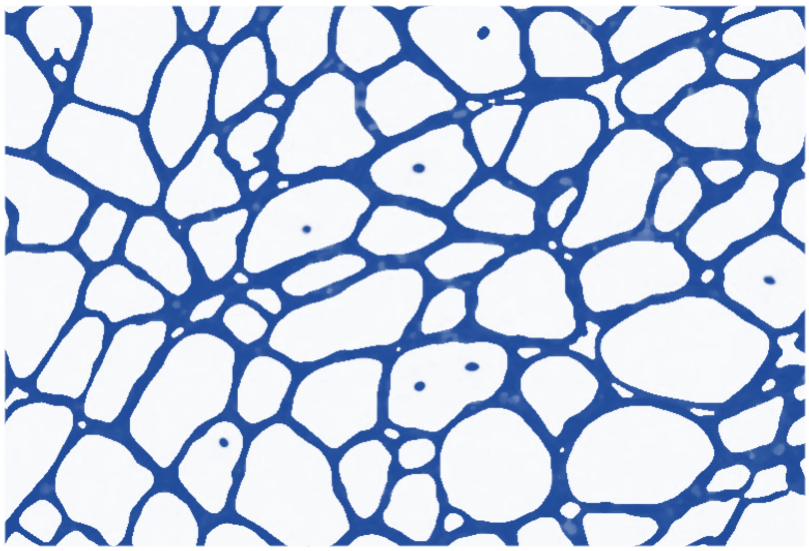

PhD THESIS

DEPARTMENT OF PHARMACOLOGY

2017

eman ta zabal zazu

Universidad del País Vasco
Euskal Herriko Unibertsitatea
The University of the Basque Country

(c)2017 GARAZI ALDANONDO ARISTIZABAL

CONTENTS

LABURPENA

SUMMARY

LABURPENA

Doktoretza-tesi honen helburu nagusia da Ahulken (AHK) deituriko konposatu-familia berri baten efektua ikertzea Duchenne distrofia muskularraren (DMD) tratamendurako. DMD gaixotasun genetiko bat da, eta X kromosomari lotutako herentzia errezesiboa du. Distrofina kodetzen duen genean gertatzen diren mutazioek sortzen dute gaixotasuna. Mutazio horiek muskuluetan distrofina proteinaren gabezia eragiten dute; gabezia horrek muskulu zuntzen degenerazio progresibo larria eragiten du, eta, ondorioz, pazienteen mugikortasuna mugatzen du. Gaixotasuna aurrera doan heinean, degenerazioa arnasketa-muskuluetara eta bihotzera hedatzen da, eta horrek pazienteen heriotza goiztiarra eragiten du. Gaixotasun honek 3500-4000 haurretatik bati eragiten dio, mutikoei nagusiki. Tamalez, gaur egun ez dago gaixotasun honen aurkako tratamendu eraginkorrik, eta pazienteen bizi-itxaropena 20-30 urte ingurukoa da.

AHK konposatuak Euskal Herriko Unibertsitateko Jesús María Aizpurua doktorearen taldearekin kolaborazioan diseinatu dira, rianodina-hartzaileen (RyR) eta kalstabina (Calst) proteinaren arteko elkarrekintza indartzea helburu. RyR muskulu-zuntzetan kaltzioaren (Ca^{2+}) askapenaz arduratzen den kanal nagusia da. Haren aktibitatea molekula zein proteina ugarik erregulatzen dute. Horien artean, ikusi da Calst proteina txikiak RyR kanala egonkortzen duela. Zehazki, Calst proteinak RyR-en konformazio itxia egonkortzen du. Zenbait egoera patologikotan, aldiz, DMD kasu, RyR-ak hainbat eraldaketa post-tanskripzional jasaten ditu; fosforilazioa eta nitrosilazioa, besteak beste. Ikusi da aldaketa horiek RyR eta Calst arteko elkarrekintza murrizten dutela. Ondorioz, RyR ez da behar bezala ixten, eta erretikulu sarkoplasmatikotik (ES) Ca^{2+} galtzen da zitoplasmarantz. Kaltzio-irteera horrek, zelula barneko Ca^{2+}-mailak handitzen ditu, eta, hala, muskulu-zuntzaren heriotza eragiten duten prozesu zelularrak aktibatzen ditu. Mekanismo hori DMD gaixotasunean gertatzen den muskulu-endekapenaren oinarrietako bat dela proposatu da.

Aurrekoan oinarrituta, **lehen kapituluan**, AHK konposatuen toxikotasuna eta ekintza mekanismoa aztertzen dira. Atal honetan, S107 (Armgo Pharma) erreferentziazko konposatu gisa erabili zen, RyR-Calst interakzioa handitzeko eta mdx saguetan (DMDren eredua) fenotipo distrofikoa hobetzeko erakutsitako eraginkortasunagatik. Konposatuen toxikotasuna sagu eta giza zeluletan ikertu zen. Horretarako, muskulu-zelula diferentziatuak konposatuen kontzentrazio ezberdinekin inkubatu ziren gau batez. Ondoren, laktato deshidrogenasaren mailak neurtu ziren zelulen medioan, toxikotasun-markatzaile gisa. Oro har, ikusi zen AHK konposatuek toxikotasun-maila oso txikiak eragin zituztela, baita kontzentrazio altuetan ere. Zehazki, A6 eta A7 konposatuek ez zuten toxikotasunik eragin, ez saguen zeluletan, ez giza zeluletan. Aitzitik, S107 konposatua ez zen toxikoa izan aurretik saguetan ikertu zen kontzentrazioetan, baina kultiboko zelula guztien heriotza eragin zuen 1-2 mM-eko kontzentrazioetan.

Jarraian, konposatuen ekintza-mekanismoa ikertzeko, giza zelula osasuntsu batzuetan RyR1 hartzailearen fosforilazioa eta nitrosilazioa eragin zen, SIN-1 peroxinitrito emailea erabiliz. *In situ* gertutasun bidezko ligazio (PLA) teknika erabili zen RyR1-en aldaketa post-transkripzionalak eta RyR1-Calst1 elkarrekintza kuantifikatzeko. Egiaztatu zen zelula osasuntsuak SIN-1-en eraginpean jartzeak RyR1-ren fosforilazioa eta nitrosilazioa handitzen zituela. Era berean, ikusi zen aldaketa post-transkripzional horien ondorioz RyR1 eta Calst1-en arteko interakzioa modu esanguratsuan gutxitzen zela. Hala, eredu zelular hori erabili zen AHK konposatuen ekintza-mekanismoa egiaztatzeko. Era horretan, ikusi zen A6 eta A7 konposatuek, eta baita S107-ek ere, RyR1 eta Calst1 arteko interakzioa handitzeko gaitasuna dutela.

Bigarren kapituluan konposatuek DMD gaixotasunean duten eragina mdx saguetan *in vivo* ikertu zen. Mdx sagua DMD animalia eredu nagusia da. Nahiz eta saguek duten fenotipo distrofikoa pazienteena baino askoz arinagoa izan, mdx saguek, pazienteek bezala, indar muskularra gutxitua dute, serumean kreatina kinasa (CK) maila altuak dituzte, eta euren muskuluetan degenerazio eta birsortze zikloak antzeman daitezke. Atal honetan, konposatuak aho-bidez eman ziren, edateko uretan disolbatuta.

Saguak 5 astez tratatu ziren, hilabete bateko adina zutenean hasita. Tratamenduak iraun zuen bitartean, korrika egiteko zinta batean trebatu ziren saguak, fenotipo distrofikoa larriagotzeko asmoz. Horrez gain, astero saguen indarra neurtu zen, *grip strength* neurgailua erabiliz. Tratamenduaren amaieran, aurreko tibia-muskulua isolatu, eta haren indar muskularra neurtu zen. Aldi berean, muskulu- eta odol-laginak jaso ziren, gaixotasunaren eboluzioa aztertzeko. Bestetik, behatzetako muskulu flexoreetatik (FDB) muskulu-zuntzak isolatu ziren, haien barneko Ca^{2+}-mailak neurtzeko. Esperimentu horren emaitzek frogatu zuten sagu distrofikoen muskulu-zuntzetan Ca^{2+}-mailak altuagoak zirela kontrol-saguetan baino. Horrez gain, A6 eta A7 konposatuek modu eraginkorrean jatsi zituzten mdx saguen muskulu-zuntzen Ca^{2+}-mailak, eta baita S107-k ere.

Jarraian, Ca^{2+}-mailen normalizazio horrek muskuluen funtzioan eragiten ote zuen ikertu zen. Kasu horretan ere, konposatuek sagu distrofikoen indarra handitzen zutela frogatu zen. Esan bezala, indarra bi modu ezberdinetara neurtu zen: batetik, *in vivo,* saguen aurreko hanketako indarra neurtu zen, *grip strength* neurgailua erabiliz, eta, bestetik, *ex vivo,* aurreko tibia-muskuluaren indarra. Bi teknika horien bitartez frogatu zen A6 tratamendua eraginkorra dela mdx saguen indarra handitzeko. Hala ere, bi teknikekin antzeman ziren efektuak desberdinak izan ziren. Izan ere, *in vivo* egindako saioetan A6 konposatuak % 30 handitu zuen sagu distrofikoen indarra; eta *ex vivo* saioetan % 16 besterik ez. Era berean, bi teknika horien bidez lorturiko emaitzen arteko korrelazioa sendoa izan zen tratatu gabeko animaliak aztertzean, baina ahuldu egiten zen tratatutako saguak gehitzean. Efektu horren zergatia ulertzeko ikerketa sakonagoak behar diren arren, emaitza hauek iradokitzen dute A6 konposatuak muskuluan duen eraginaz gain, beste efekturen bat izan dezakeela.

Tratamenduek degenerazio muskularrean duten efektua ikertzeko asmoz saguen serumean CK-mailak neurtu ziren. Espero bezala, agerian gelditu zen mdx saguek sagu osasuntsuek baino CK-maila altuagoak zituztela. Aldi berean, A6-rekin tratatuko saguek CK-maila baxuagoak zituztela frogatu zen. Ondoren, diafragma eta aurreko tibia-muskuluen azterketa histologikoa egin zen. Azterketa horietan nukleo zentrala zuten

muskulu-zuntzen kopurua kuantifikatu zen. Modu horretan min muskular baten eraginez birsortzen ari diren zuntzak identifikatzen dira, eta parametro hori degenerazio muskularraren kuantifikazio gisa erabil daiteke. Nukleo zentrala zuten zuntzen ehunekoa oso baxua izan zen sagu osasuntsuen muskuluetan. Mdx saguetan, aldiz, ikusi zen diafragman zuntzen % 43-ak eta aurreko tibia-muskuluan zuntzen % 57-ak nukleo zentrala zutela. AHK zein S107-rekin trataturiko saguen muskuluetan, aldiz, portzentaje hau % 25 txikiagoa izan zen. Ondorioz, atal honetan frogatu zen AHK konposatuak eraginkorrak direla mdx saguetan Ca^{2+}-kontzentrazioak jaisteko, funtzio muskularra hobetzeko eta degenerazio muskularra arintzeko.

DMD gaixotasuna ikertzeko eta terapia berrien garapenerako animalia ereduen erabilera oso hedatua dagoen arren, emaitzak pazienteetara estrapolatzea erronka handia da. Horrexegatik, giza ereduen garapena ezinbestekoa da terapia berriek pazienteetan izan dezaketen efektua iragartzeko. Azken atal honetan (**hirugarren kapiluan**), hilezkortutako giza mioblastoetan oinarritutako bi eredu aztertu ziren, AHK konposatuen efektua aztertzeko eredu zelular egokiena aukeratzeko asmoz.

Miotuboen diferentziazioak aurrera egin ahala Ca^{2+}-aren homeostasiarekin erlazionaturiko proteinen espresioa handitu egiten da, eta horrek aldaketak eragiten ditu zelula-barneko Ca^{2+} kontzentrazioetan. Hori dela eta, zelula osasuntsu eta distrofikoekin lan egitean ezinbestekoa da diferentziazio-maila berean dauden zelulak konparatzea. Horretarako, atal honetan, zelulak *in vitro* diferentziatu ostean, miotuboen morfologia eta diferentziazio-maila aztertu ziren. Morfologia miotuboen zabalera neurtuz aztertu zen. Diferentziazio maila neurtzeko, aldiz, miotuboak homogeneizatu ondoren, batetik, CK-ren aktibitatea neurtu zen, eta, bestetik, RNA mezulari (RNAm) eta proteina-mailan hainbat diferentziazio-markatzaileren espresioak konparatu ziren.

Lehenik, bi paziente osasuntsutatik eta DMD paziente batetik isolatutako zelula hilezkortuak konparatu ziren. Zortzi egunez diferentziatu ostean, miotuboen zabalera aztertu zen. Bi kontrol osasuntsuen artean desberdintasun esanguratsuak aurkitu ziren, bai eta bigarren kontrol osasuntsuaren eta DMD pazientearen zelulen artean ere.

Bestetik, diferentziazio-mailan ere hiru pazienteen zelulen artean desberdintasun nabarmenak hauteman ziren. RNAm-mailan bigarren kontrola izan zen DMD zelulekiko antzekoena. Proteina-mailan, aldiz, lehen kontrola izan zen antzekoagoa. Emaitza guzti horiek kontuan hartuta, aztertutako bi kontrol-zelulek eta DMD pazientetik eratorritakoek diferentziazio-maila ezberdinak zituztela ondorioztatu zen, eta, beraz, aztertutako bi kontrolak ez zirela DMD zelulekin konparagarriak.

Pazientetatik isolatutako zeluletan ikusitako aldakortasuna gutxitzeko asmoz, zelula osasuntsuetan distrofinaren genea isildu zen shRNA plasmidodun birusen bitartez. Eredu horrekin, zelula-lerro berean distrofinaren gabeziak eragiten dituen aldaketa patologikoak ikertu ziren. Lehenik eta behin, plasmido kontrol batez infektaturiko zelulak (NS-shRNA) eta distrofina isiltzeko plasmidoaz infektatutako zelulak (DYST-shRNA) diferentziatu, eta paziente zelulekin egin zen bezala, morfologia eta diferentziazio maila aztertu ziren. Kasu honetan ez zen desberdintasun adierazgarririk aurkitu zelula kontrol eta distrofikoen artean, CK aktibitate zein RNAm eta proteina mailako diferentziazio-markatzaileei dagokienez. Horregatik, zelula hauek aukeratu ziren distrofina-gabeziak RyR eta Calst interakzioan, zein zelula barneko Ca^{2+}kontzentrazioetan, eragiten dituen aldaketa patologikoak ikertzeko.

Mdx saguetan egindako beste ikerketa batzuek erakutsi dutenez, sagu distrofikoen muskuluetan RyR1 kanalak gehiegizko fosforilazio eta nitrosilazioa jasaten ditu; eta, gainera, aldaketa horiek Calst1-ekiko interakzioa jaisten dute. Lan honetan, antzeko emaitzak lortu ziren distrofina gabeko giza zeluletan ere. Distrofina gabeko zelulak zelula kontrolekin alderatzean, ikusi zen RyR1-en fosforilazioa % 62 handiagoa zela distrofikoetan. Aldi berean, antzeman zen RyR1-en nitrosilazioa ere ia bikoiztua zegoela. Espero bezala, RyR1-en aldaketa horiek RyR1-Calst1 interakzioan eragiten zuten. Hala, zelula distrofikoetan RyR1-Calst1 interakzioa ia % 50 jaitsi zen.

Bestalde, Calst1-ek RyR1-en konformazio itxia egonkortzen duenez, interakzioaren jatsiera horrek RyR1-en ixteko gaitasuna eragiten duela ikusi zuten mdx saguetan. Ondorioz, RyR1-ek ES-tik Ca^{2+} irteten uzten du, eta zelularen Ca^{2+}

kontzentrazioa handitzen du. Distrofina gabeko giza zeluletan egindako Ca^{2+} neurketak emaitza horiekin bat etorri ziren. Zelula kontrolekin konparatuz, distrofina gabeko zeluletan Ca^{2+}-maila modu esanguratsuan handitu zen. Emaitza guztiak kontuan hartuz, frogatu zen distrofina isilduz sortutako bigarren eredu honek DMD gaixotasunaren zenbait ezaugarri adierazten dituela. Beraz, AHK konposatuen efektua ikertzeko erabili zen eredu hori.

Hala, DMD giza eredu horretan aztertu zen A6 eta A7 konposatuek zer gaitasun duten RyR1-Calst1 interakzioa indartzeko eta zelula barneko Ca^{2+} mailak normalizatzeko. Frogatu zen bi konposatuak eraginkorrak zirela RyR1-Calst1 mailak handitzeko. Halaber, zelulak 50 nM A6 edo A7 konposaturekin tratatzean, antzeman zen Ca^{2+}-mailak balio kontroletara jaisten zirela. Konposatuen kontzentrazioa 150 nM-era handitu zenean, aldiz, A6-k Ca^{2+}-aren erregulazioan zuen efektua txikitu egin zen, eta A7-rena galdu. Halaber, zelula kontroletan 150 nM-eko tratamenduak Ca^{2+} mailak handitzen zituela ikusi zen. Emaitza hauen arabera, AHK konposatuek RyR1-Calst1 interakzioan efektu alosteriko bat izan lezaketela ondoriozta genezake. Hau da, baliteke AHK konposatuek kontzentrazioaren arabera aldaketa konformazional ezberdin bat eragitea RyR1-Calst1 interakzioan, eta, ondorioz, kanala konformazio itxi edo irekian egonkortzea. Ezinbestean, sakonago ikertu beharko litzateke efektu bifasiko hori ziurrago azaldu ahal izateko.

Laburbilduz, tesi honetan ondorioztatu da AHK konposatuak eraginkorrak izan daitezkeela DMD gaitzaren tratamendurako. Batetik, erakutsi da AHK konposatuek toxikotasun baxua dutela. Bestetik, mdx saguetan egindako esperimentuetan ikusi da konposatuek saguen indar muskularra hobetu eta degenerazio muskularra arintzen dutela. Eta, azkenik, *in vitro* sorturiko giza eredu batean erakutsi da AHK konposatuek gaitasuna dutela RyR1-Calst1 interakzioa berreskuratzeko, eta horrek zelula muskularren Ca^{2+}-mailak jaisten dituela. Bestalde, ikusi da muskulu-zuntzen Ca^{2+}-maila altuek DMD patologiaren garapenean eragin zuzena dutela; beraz, Ca^{2+}-maila horiek jaisteko gaitasuna duten AHK konposatuak erabilgarriak izan daitezke gaixoen bizi-kalitatea hobetzeko.

SUMMARY

The main objective of this thesis is to evaluate the effect of a novel family of compounds, named Ahulken (AHK), as a therapy for Duchenne muscular dystrophy (DMD). DMD is an inherited X-linked disorder caused by mutations in the *DMD* gene which lead to absence of dystrophin (DYST) protein. As a consequence of DYST deficiency, muscles show membrane fragility and increased intracellular calcium levels that cause muscle degeneration, weakness and premature death. In this context, AHK compounds have been designed to enhance ryanodine (RyR) and calstabin (Calst) binding in pathological conditions, such as DMD, where due to nitro-oxidative stress, RyR1 is found to suffer abnormal post-translational modifications that result in calcium leakage from the sarcoplasmic reticulum. This mechanism has been proposed to contribute to the abnormal calcium homeostasis observed in dystrophic patients.

In a first study, the toxicity of AHK compounds and their ability to enhance RyR1-Calst1 binding was evaluated (**Chapter 1**). The RyR stabiliser S107 (Armgo Pharma) was used as a reference compound due to its ability to enhance RyR1-Calst1 binding and to improve dystrophic phenotype *in vivo* in mdx mice. The toxicity of the compounds was determined in mouse and human myotube cultures after 24 hours of treatment. Overall, AHK compounds showed very low or undetectable toxicity up to 1-2 mM concentration. In contrast, the reference compound S107 displayed high toxicity at 1-2mM concentrations, resulting in 100% death of mouse and human cells in culture. On the other hand, in order to study the mechanism of action of AHK compounds, a human cellular model where RyR1 nitrosylation, phosphorylation and Calst1 depletion were achieved with the peroxinitrite donor SIN-1 was used. Using this model and *in situ* proximity ligation assay (PLA) technique, A6 and A7 AHK compounds, as well as the reference compound S107, proved to efficiently increase RyR1-Calst1 binding in SIN-1 stressed human myotubes.

In the second section (**Chapter 2**), AHK compounds were tested in mdx mouse model of DMD. A6, A7 AHK compounds and S107 reference compound were administered to 1-month-old male mice for 5 weeks in drinking water. During this period, mice were exercised weekly in a treadmill in order to aggravate dystrophic phenotype and forelimb strength was assessed using a grip strength meter. At the end of the experiment, *tibialis anterior* muscle strength was evaluated *ex vivo* in isolated muscle, creatine kinase was measured in serum and muscles were dissected for histological analysis. In addition, resting intracellular calcium levels were measured in isolated fibres from *flexor digitorum brevis* muscles. The results obtained in this section indicate that in mdx mice A6, A7 and S107 efficiently reduce resting intracellular calcium levels in dystrophic muscles, ameliorating the biochemical and histopathological features of muscular dystrophy and improving overall muscle function.

In a final work (**Chapter 3**), a human *in vitro* model based on immortalised myoblasts was validated as a model of DMD. Although animal models have been widely used to study DMD pathophysiology as well as for in vivo preclinical testing of potential therapies, there are many examples in the literature illustrating that effective therapies in DMD animal models may not necessarily yield the same outcomes in humans. Therefore, a relevant and reproducible human *in vitro* DMD model for drug screening is needed in order to advance in the generation of specific therapies for DMD as well as to predict patients' response to experimental therapies. Hence, shRNA mediated dystrophin (DYST) knocking down was used to generate a DYST-deficient human myoblast line. After differentiation, silenced myotubes showed several DMD features such as reduced α-sarcoglycan expression, Calst1 depletion from RyR1 macromolecular complex and elevated resting intracellular calcium levels. In contrast, myotubes from different donors displayed high variability with regard to features such as morphology, differentiation and maturation, making comparison between healthy and dystrophic myotubes very challenging. For these reasons, DYST-shRNA infected human myoblasts model was used to evaluate the effect of AHK compounds on RyR1-Calst1

binding and calcium homeostasis. After overnight treatment, A6 and A7 compounds were able to efficiently restore RyR1-Calst1 binding and normalise resting intracellular calcium levels in dystrophic myotubes. Since increased intracellular calcium levels have been proposed as a pathological mechanism that triggers dystrophic phenotype in DMD patients, compounds as AHK that are able to regulate intracellular calcium levels could constitute an effective therapeutic alternative for these patients.

GENERAL INTRODUCTION

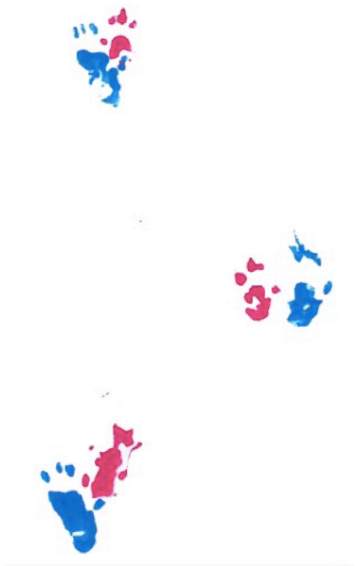

GENERAL INTRODUCTION

The muscular system is one of the largest organ in the body. Muscles are attached to the bones by tendons and they are responsible for body movement, help to maintain the posture and allow blood circulation all over the body. Three different muscle types are described: smooth, cardiac and skeletal muscle. Within them, skeletal muscle represents the majority of the system and is responsible for all our voluntary movements.

In the body, muscles are protected by different layers of connective tissue (Figure 1). The fascia is located beneath the skin and separates muscles and other organs. Each individual muscle is surrounded by a layer, called *epimysium*. Inside, the muscle is divided in several portions that are called fascicles and are surrounded by the *perimysium*. Each fasciculus is composed by a bundle of myofibres. The muscle fibre or myofibre is the functional unit of the muscle and it is surrounded by a layer called *endomysium*[1].

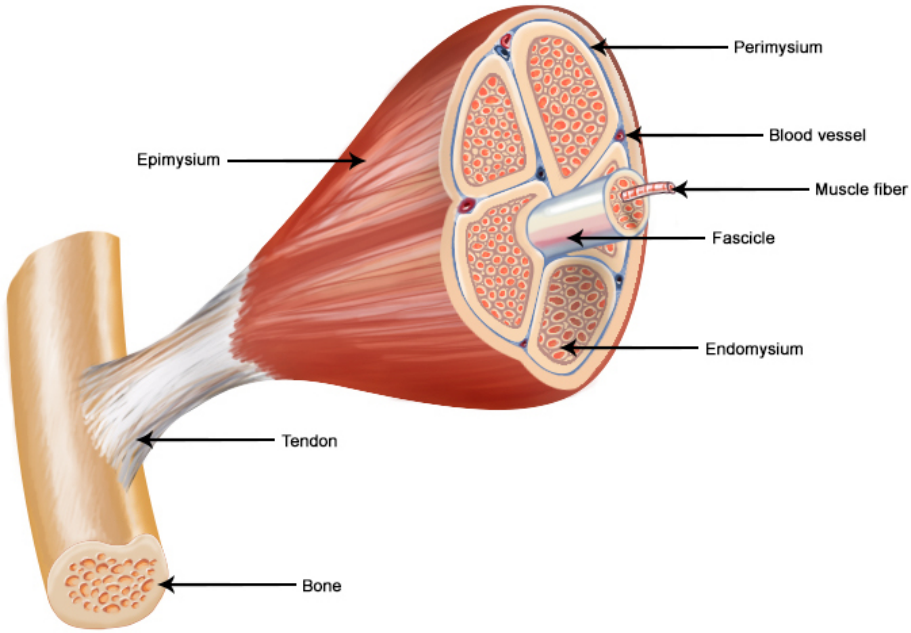

Figure 1. Structure of skeletal muscle. From whole muscle with bone insertion to single muscle fibre. From SEER Training Modules, *Muscular System*. U. S. National Institutes of Health, National Cancer Institute. 10 February 2017 <*https://training.seer.cancer.gov/*>.

Satellite cells are the stem cell population of the muscle. They are located between the basal lamina and the sarcolemma (plasma membrane) of the muscle fibre in a quiescent state and they are activated when muscle regeneration is needed providing myoblasts that fuse with each other to form new myofibres[2].

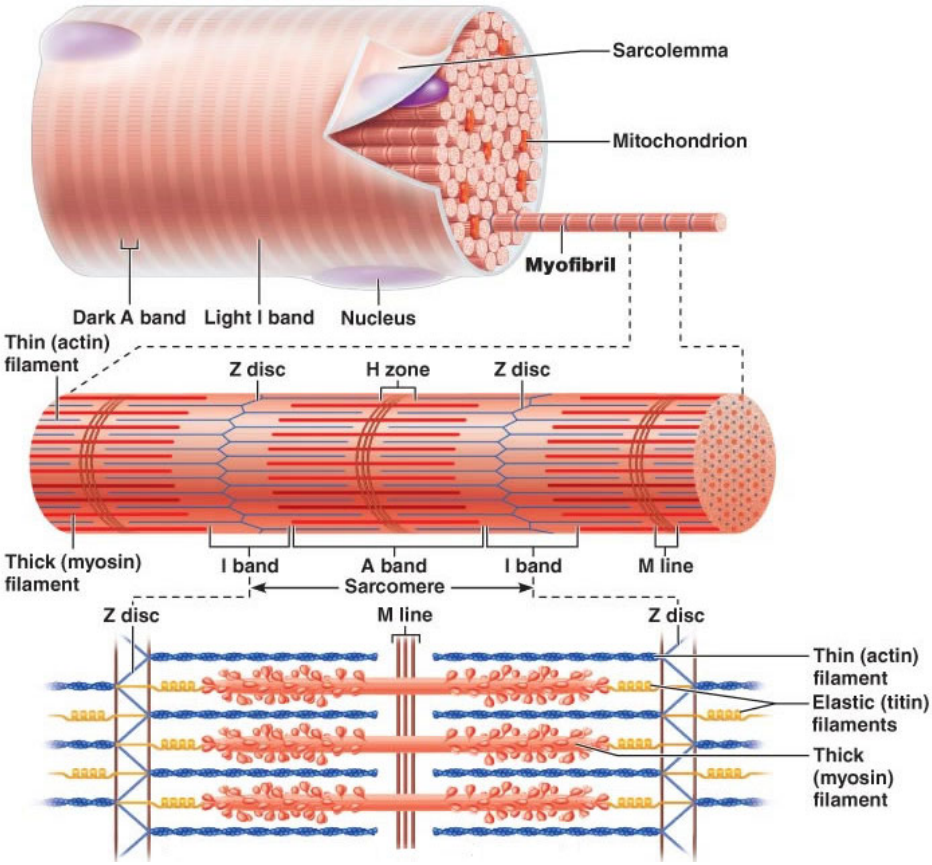

Figure 2. Structure of the skeletal muscle fibre and sarcomere organisation. From top to bottom: a single muscle fibre, a myofibril and the sarcomere. Copyright © 2013 Pearson Education, Inc.

Myofibres are long, cylindrical and multinucleated cells. Their nuclei are localised in the periphery of the fibre underneath the sarcolemma. The cytoplasm of the fibre (sarcoplasm) is filled by myofibrils, which constitute the contractile apparatus of the cell. Myofibrils are mainly composed by actin and myosin filaments arranged in a repeating unit called sarcomere[3] (Figure 2). Myosin, which is the molecular motor of the cell, produces movement via ATP-dependent cross-bridge formation with actin[4].

This interaction is regulated by two proteins, troponin and tropomyosin, that directly interact with actin, controlling its myosin binding site[5]. In the presence of calcium (Ca^{2+}), troponin changes its conformation, producing tropomyosin movement and the liberation of the myosin binding site of actin. Then, cross-bridge is formed between actin and myosin, leading to muscle contraction[6,7].

Filaments confer a characteristic striated pattern to the skeletal muscle. Thin filaments of actin, troponin and tropomyosin are alternated with thick myosin filaments[8]. The sarcomere is delimited by Z disks. Around Z disks, several proteins, such as vinculin and the dystrophin-glycoprotein complex (DCG), constitute the costamere, which links the sarcomere with the sarcolemma and has an important role in force transduction[9].

Other cellular elements present in the muscle sarcoplasm are the sarcoplasmic reticulum (SR), T-tubules and mitochondria. Mitochondria are located between the myofibrils and their amount is dependent on the fibre type (slow, fast, …)[10,11]. On the other hand, T-tubules are invaginations of the sarcolemma that enter into the cell and form a structure called triad together with the terminal cisterns of the SR (Figure 3). Triads are highly specialised structures where excitation-contraction coupling process occur[12].

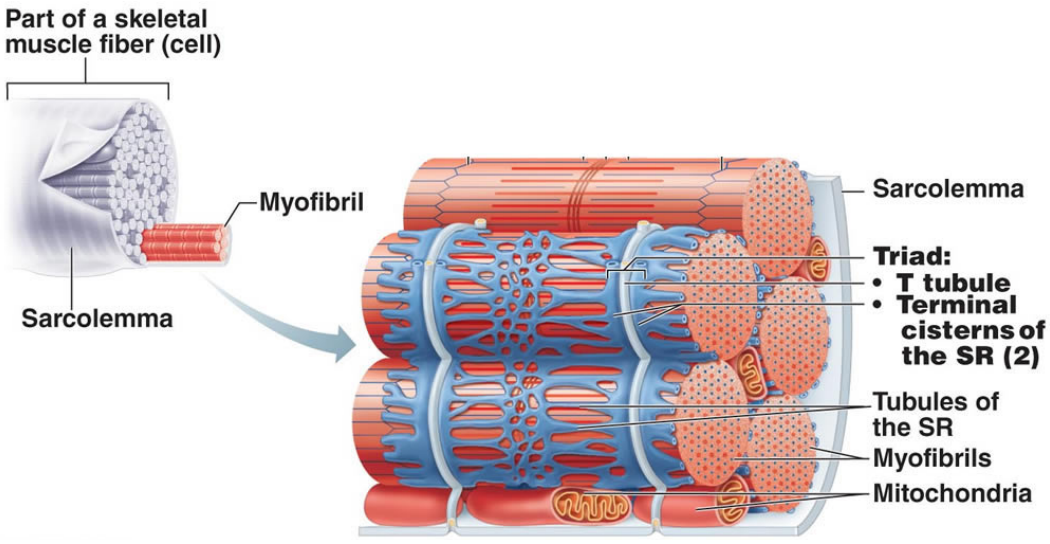

Figure 3. Sarcolemma forming T-tubules that dip into the cell and form a structure called triad in contact with terminal cisterns of SR. Copyright © 2013 Pearson Education, Inc.

Different muscle fibre types are defined based on their contraction velocity and fatigue resistance[13]. Slow-twitch or oxidative fibres (type I, IIA), present slow contraction and high resistance to fatigue. They contain high number of mitochondria and generate ATP through aerobic metabolism. In contrast, fast-twitch or glycolytic fibres (Type IIX, IIB) show rapid contraction but lower resistance to fatigue. In addition, they have low mitochondrial content and ATP production occur through anaerobic metabolism[8,10]. Differences in Ca^{2+} handling have also been described between fast and slow fibres. Hence, fast fibres release larger amounts of Ca^{2+} and present faster decline and relaxation[8,14].

Fibre type composition of a muscle can change in response to different physiological needs owing to the high plasticity that muscles present[15]. In fact, affectation of specific fibre types or fibre type transition has also been described in several muscular dystrophies, such as Duchenne muscular dystrophy, where fast to slow muscle transition occur[16,17] or Limb-girdle muscular dystrophy type 2A (LGMD2A), in which slow fibres are preferentially affected[18].

CALCIUM HOMEOSTASIS IN SKELETAL MUSCLE

Skeletal muscle is under the voluntary control of the somatic nervous system. Motor neurons connect to the muscle at the neuromuscular junctions, where acetylcholine release produces depolarisation of the sarcolemma starting excitation-contraction coupling (EC-coupling)[14,19]. This process translates the electric action potential of the neuron into mechanical muscle contraction (Figure 4).

Sarcolemma depolarisation is propagated down the T-tubular system activating dihydropyridine receptors (DHPR or Cav1.1). Activation of DHPRs produces a change in their conformation that activates ryanodine receptors (RyR)[20]. RyR are the main Ca^{2+} release channel of the SR. They are located into the SR membrane in close proximity to DHPRs and their activation lead to SR Ca^{2+} release to the cytosol[21]. Ca^{2+} diffuses through the sarcomere and binds troponins initiating contraction process through actin

and myosin interaction. After contraction, relaxation is initiated with the action of the sarco/endoplasmic reticulum Ca^{2+} pump SERCA, which transfers Ca^{2+} back to the SR[22,23]. Alternatively, other mechanisms have also been involved in relaxation process by removing Ca^{2+} to the extracellular space, such as the sarcolemmal Na^{+}/Ca^{2+} exchanger (NCX) and the plasmalemmal Ca^{2+}-ATPase (PMCA) (Figure 5)[24].

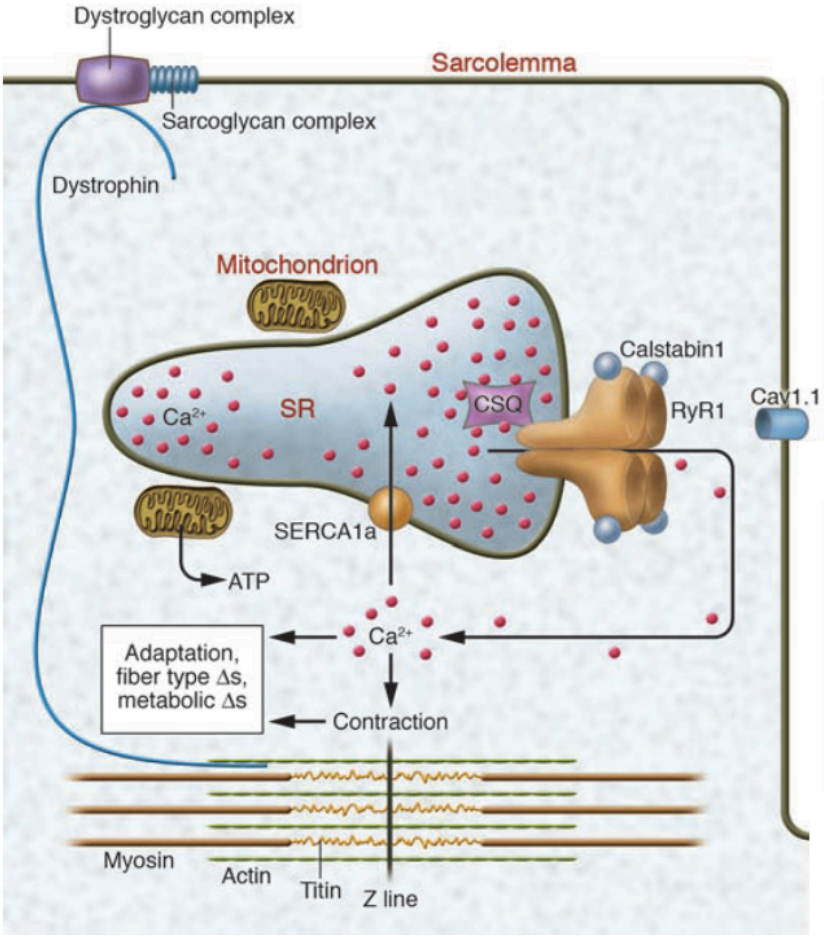

Figure 4. Representation of excitation contraction coupling process in skeletal muscle fibre. Adapted from Bellinger *et al* (2008)[25].

In the sarcoplasm, Ca^{2+} homeostasis is precisely regulated by cytosolic Ca^{2+} buffers. These Ca^{2+} binding proteins modulate Ca^{2+} diffusion through the cytoplasm much faster than Ca^{2+} sequestration into intracellular stores occur[8]. Some of those buffers are troponin C, ATP, parvalbumin, calmodulin or SERCA pumps (Figure 5).

Specifically, troponin C binds Ca^{2+} initiating contraction process[5], ATP acts as a mobile buffer for Ca^{2+} and Mg^{2+} and parvalbumin regulates relaxation speed in mouse muscle but it is expressed only at very low concentration in human muscles[26,27]. Finally, calmodulin regulates contractile function and activates signalling pathways involved in gene regulation[28,29].

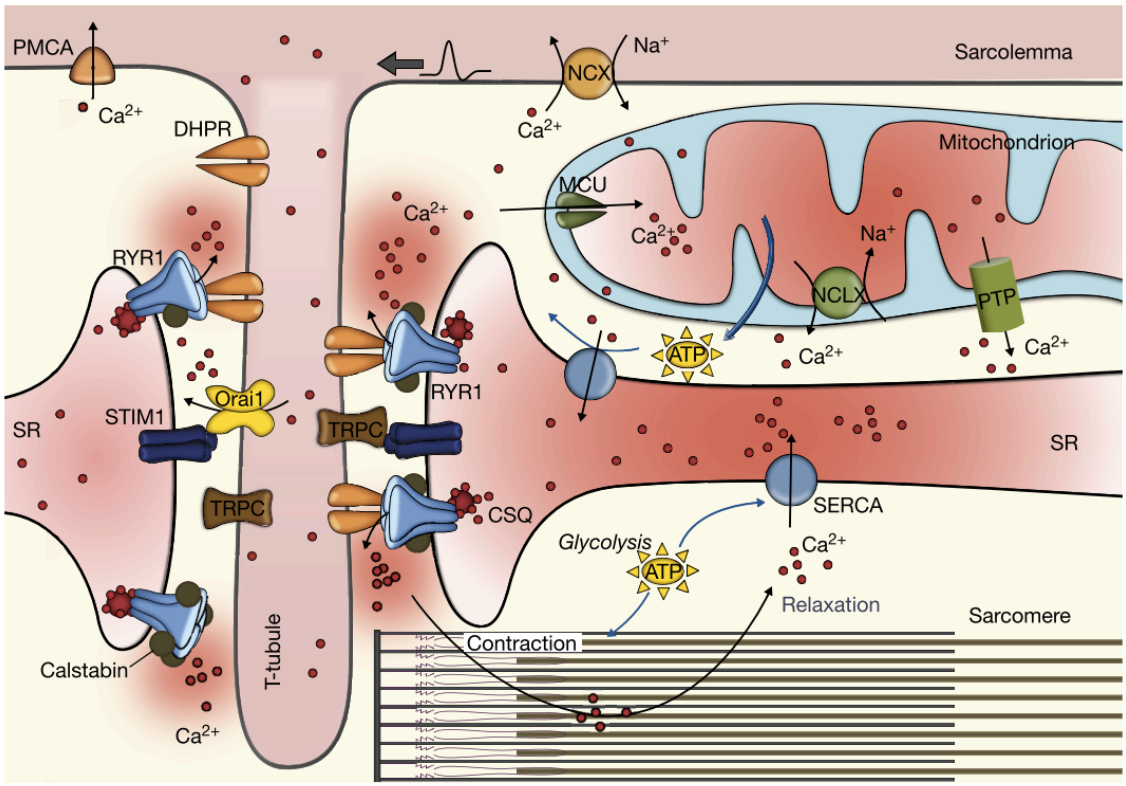

Figure 5. Representation of calcium signalling within the skeletal muscle. Calcium concentration is represented by red colour, being higher in more intense zones. From Vallejo-Illarramendi *et al.* (2014)[30].

The SR is a highly-specialised form of endoplasmic reticulum present in muscle. It is responsible for Ca^{2+} storage, release and uptake. In SR lumen, Ca^{2+}-binding proteins are distributed into the junctional SR, located in the triad proximal to the T-tubules, and the longitudinal SR, located surrounding myofibrils[31,32]. The longitudinal SR represent the Ca^{2+} storage area. It is localised around myofibrils in order to facilitate SERCA mediated Ca^{2+} reuptake and muscle relaxation[23]. The proteins that are present in this

area are mainly responsible for Ca^{2+} storage and the regulation of Ca^{2+} fluxes[33]. Intraluminal Ca^{2+}-binding proteins reduce free Ca^{2+} facilitating its reuptake to the SR[34,35]. The most significant proteins are calsequestrin (CSQ), histidine-rich Ca^{2+}-binding protein (HRC), sarcalumenin and calreticulin (Figure 5).

Ryanodine receptors

In the junctional SR Ca^{2+} release occur through two main channels, RyR and inositol 1,4,5-triphosphate receptors (IP3Rs)[36–38]. RyRs are the main calcium release channels of the SR in muscle and the endoplasmic reticulum (ER) in other cell types. In muscle, RyR is located in the triad in close proximity to DHPR. In mammals three RyR isoforms are defined (RyR 1-3) which share a 65 % of their sequence[39]. RyR1 and RyR2 are the predominant isoforms in skeletal muscle and heart, respectively, whereas RyR3 has been described to be present in immature skeletal muscle. Additionally, these three isoforms are present in neurons[36,40,41].

Several human diseases are associated with mutation in genes encoding for RyRs. Mutations affecting RyR2 lead to cardiac diseases[36,39], whereas mutations in the gene encoding RyR1 produce malignant hyperthermia (MH) and central core disease (CCD). MH is an autosomal dominant disorder. It is characterised by an excess Ca^{2+} release from the SR in response to volatile anaesthetics or stress, which produces muscle contraction and an uncontrollable increase in body temperature that is fatal unless treated[42]. Dantrolene is used to effectively treat MH and it acts blocking RyR1 activity in skeletal muscle[41,43]. CCD is a congenital myopathy that exhibits both autosomal dominant and recessive modes of inheritance. In CCD, mutations in RyR1 cause SR Ca^{2+} leak, defective EC coupling and increased mitochondrial oxidative stress leading to hypotonia and muscle weakness[21,44].

RyRs are the largest ion channels identified with a molecular mass of >2 MDa. Although the full structure of the channel has not been yet determined, cryo-electron microscopy (Cryo-EM) studies showed that RyRs are composed by four identical

subunits forming a “mushroom”-like structure. Three main domains are distinguished: a luminal, a transmembrane and a large cytoplasmic domain (Figure 6). Additionally, these studies found that each tetramer is in contact with its neighbouring RyRs through clamp region interactions forming RyR arrays[36,45].

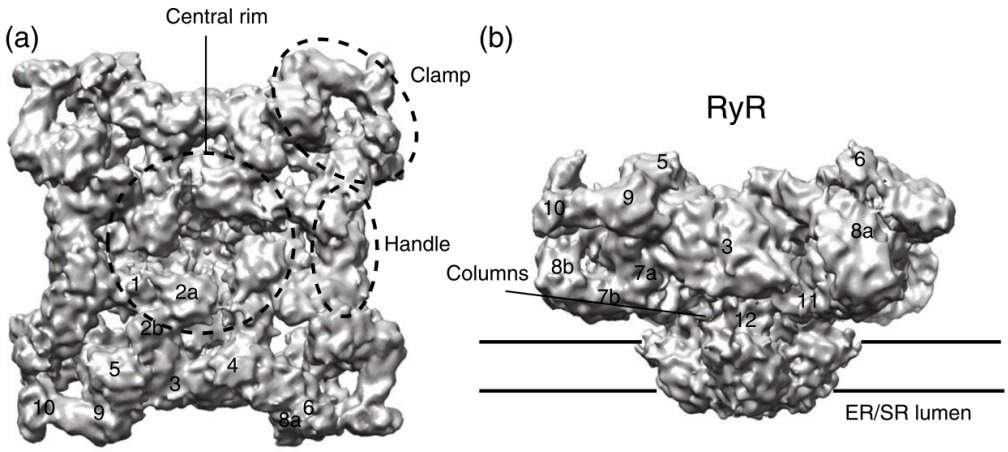

Figure 6. Cryo-EM structure of RyR. (a) top and (B) side view of RyR. Numbers indicate subregions. From Van Petegem (2015)[36].

In the triads, RyR and DHPR are located in close proximity both in skeletal and cardiac muscles, however the molecular mechanisms of E-C coupling considerably differ between these two muscle types[36,46]. In skeletal muscle, RyR1 activity is defined as voltage-induced Ca^{2+} release, where a direct physical interaction of the two channels is needed. Specifically, DHPR acts as a voltage sensor for RyR1 which is activated and changes it conformation opening the pore and releasing Ca^{2+} to the cytoplasm. It is being proposed that DHPR channels are grouped into tetrads and that each tetrad can interact with a RyR1. However, only every other RyR1 is associated with a DHPR tetrad[39,42]. On the other hand, in cardiac muscle RyR2 activity corresponds to a Ca^{2+}-induced Ca^{2+} release[39,46]. The influx of external Ca^{2+} through DHPR activates RyR2 producing SR Ca^{2+} release. Since direct physical interaction is not needed, the organisation of those channels is less regular in cardiac muscle and it is being proposed that four to six RyR2 can be activated for every DHPR[47].

RyR activity is regulated by several ligands including ions, small molecules and proteins. These ligands bind RyR near the cytosolic region, suggesting that channel gating is regulated by a long-range allosteric signalling[36,39,46]. RyR activity is regulated by cytosolic and luminal Ca^{2+}. Low cytosolic Ca^{2+} concentrations (~ 1 μM) activate RyR by binding high-affinity Ca^{2+} sites, while high cytosolic Ca^{2+} concentrations (~ 1 mM) inhibit channel activity by binding low-affinity Ca^{2+} sites. In addition, increased luminal Ca^{2+} is known to activate RyR in a process known as store-overload induced Ca^{2+} release[36]. Cytoplasmic Mg^{2+} and ATP have also been proposed to regulate RyR activity. Mg^{2+} inhibits RyR activity by binding low-affinity Ca^{2+} sites or by competing with Ca^{2+} to bind high affinity Ca^{2+} activation sites. On the other hand, ATP is a RyR activator.[21,39].

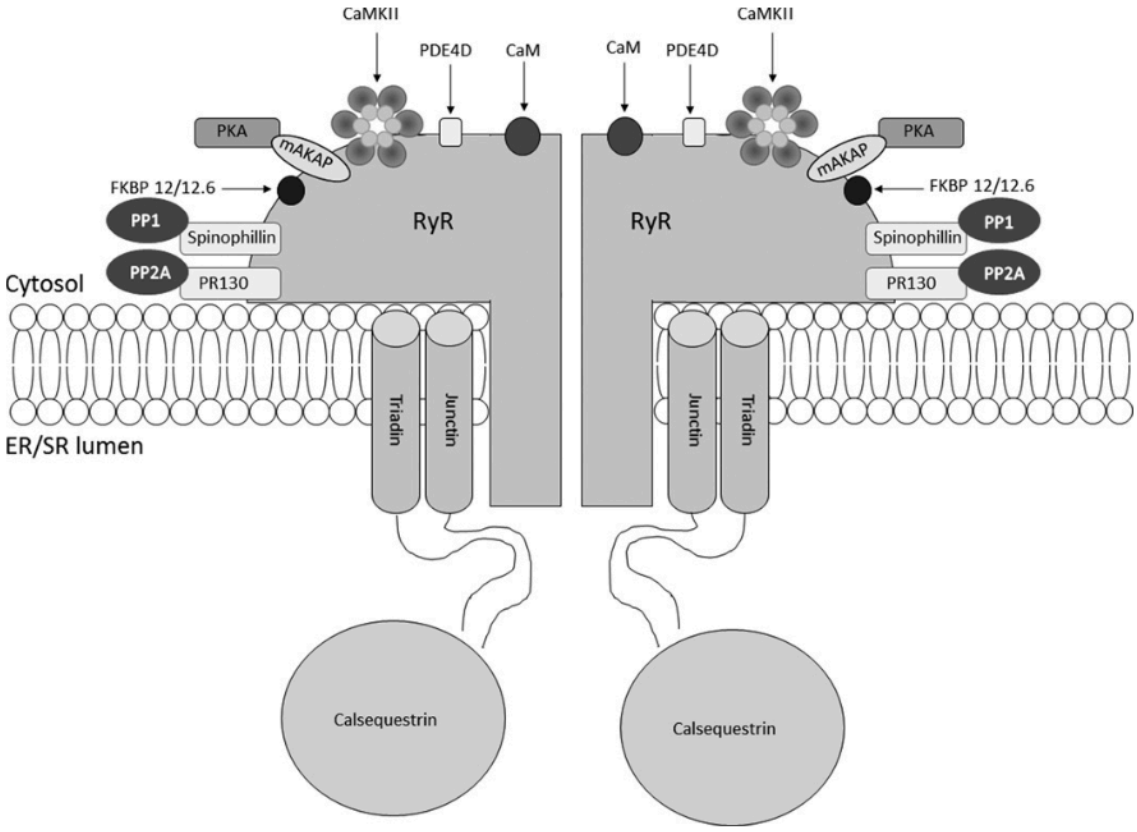

Figure 7. Illustration of RyR macromolecular complex containing several RyR activity modulators. Adapted from O´Brien *et al.* (2015)[48].

RyR macromolecular complex is constituted by several proteins that modulate channel activity (Figure 7). In SR lumen, RyR activity is regulated by CSQ alone or

through interaction with triadin and/or junctin. On the other hand, in the cytoplasmic domain several proteins contribute to regulate RyR activity. Calmodulin (CaM) is a 17 kDa Ca^{2+} binding protein that regulates RyR (1-3) by direct binding in a 4:1 stoichiometry (1 CaM per RyR subunit). At low cytosolic Ca^{2+} concentrations, Ca^{2+} free CaM (apoCaM) act like a partial agonist activating RyR. On the contrary, at high Ca^{2+} concentrations Ca^{2+} bound CaM (CaCaM) inhibits RyR activity. Phosphorylation of RyRs have shown to be important for channels physiological regulation but also to contribute to some pathogenic mechanisms. Several kinases (PKA, CaMKII) and phosphatases (PP1, PP2A and PDE3D) have been found to target RyRs. Some of them bind RyR via scaffolding proteins such as spinophilins or muscle A-kinase anchoring protein (mAKAP). RyR phosphorylation increases channel open probability facilitating SR Ca^{2+} release[48]. Similarly to phosphorylation, RyR activity can be regulated by other post-translational modifications such as S-nitrosylation, S-glutathionylation, S-oxidation or S-palmitoylation. Unless S-palmitoylation[49], these modifications increase RyR open probability facilitating Ca^{2+} release to the cytoplasm[21].

FKBP12 (Calstabin1 or Calst1) and FKBP12.6 (Calstabin 2 or Calst2) are small proteins member of the FK506 binding proteins family. These two isoforms share 85 % sequence homology and they are structurally very similar. Indeed, both isoforms bind and are inactivated by the immunosuppressant drug rapamycin[36,50]. Calst1 is highly expressed in all muscle types while Calst2 is expressed in many organs including brain, liver, thymus and heart[51]. Originally, Calst1 and Calst2 were thought to stabilise RyR1 and RyR2, respectively. However, recent studies suggest that dual modulation of RyRs by both Calst isoforms may occur[52]. Calst binds RyR in a 4:1 stoichiometry (one Calst per RyR subunit). Calst binding region in RyR1 has been localised within the N-terminal and the central domain of the channel, specifically at amino acids 619, 2157, 2341 and 2502[53]. Through this interaction, Calst1 regulates not only RyR1 channel activity but also its interactions with other channels. Furthermore, mutation in this region that disrupt Calst binding have been found in MH and CCD patients, where increased RyR activity induce increased Ca^{2+} concentration that contribute to disease phenotype[21].

Calst1 regulates RyR1 activity by stabilising the close state of the channel. Furthermore, it has been shown that disruption of RyR1 Calst1 binding increases channel open probability leading to leaky channels[50,54]. Calst depletion-induced RyR leakage has been proposed to be implicated in several pathologies such as muscular dystrophies[55,56], arrhythmias[57], myocardial infarcts[58] and stress-induced cognitive dysfunction[40]. RyR1 post-translational modifications can also regulate channel activity by affecting Calst binding to the channel. RyR phosphorylation by CaMKII or PKA reduce Calst binding and activate the channel whereas PP1 dephosphorylate and inactivate RyR by facilitating Calst binding[48]. Similarly, S-nitrosylation of cysteine residues reduce Calst binding affinity activating SR Ca^{2+} release[59,60]. Furthermore, abnormal RyR1 hyperphosphorylation at Ser2843 and hypernitrosylation at Cys3635 and 2327 dissociate Calst1 from RyR1 increasing channel open probability and leading to leaky channels, mechanism that has been involved in several pathologies[40,55,56,61]. On the contrary, S-palmitoylation eliminates palmitoyl residues from Calst binding site increasing Calst binding and closing RyR channel[49].

Calst1 coordinates RyR1 multi-protein group formation synchronising channel gating between adjacent RyR1 receptors[21]. This process in which more than one channel is opened and closed simultaneously, explains how RyR1s that do not bind DHPPR are regulated. In the same way, Calst modulates the interactions between RyR1 and DHPR. In one hand, Calst function as a gradient reader for RyR preventing subconductance state gating and reducing the channel open probability which reduces SR Ca^{2+} leak and aberrant Ca^{2+} release[62]. On the other hand, when RyR1 binds DHPR via its II-III loop during EC coupling, Calst1 potentiates RyR1 open state facilitating SR Ca^{2+} release. Furthermore, it has been shown that in absence of Calst1 RyR1 opening after DHPR activation is obliterated[63].

Calcium in mitochondria

In skeletal muscle, mitochondria are located in close proximity to SR. They play central roles regarding muscle metabolism, energy supply, reactive oxygen species

(ROS) and reactive nitrogen species (RNS) production/detoxification and calcium homeostasis among others[64]. The number of mitochondria in a muscle fibre is dependent of the fibre type being higher in slow, oxidative fibres and lower in fast glycolytic fibres[65]. In all of them, mitochondria are essential for muscle bioenergetics. Communication between SR and mitochondria is crucial for most of its functions and it occurs through the mitochondria-associated SR membrane (MAM)[66]. In muscle, mitochondrial and SR functions are not independent. Mitochondria uptakes SR-released Ca^{2+}, which regulates mitochondrial metabolism and ATP production. In addition, mitochondria produces and detoxifies ROS and RNS that regulate SR Ca^{2+} release and uptake[67]. In the same way, mitochondria are essential for muscle contraction. Specifically, they provide ATP for muscle physiological needs such as actin-myosin cross-bridge formation or SERCA mediated SR Ca^{2+} uptake[68]. Furthermore, mitochondria are important Ca^{2+} stores that have been implicated in the modulation of Ca^{2+} transients during EC coupling[69]. SR Ca^{2+} release for mitochondrial uptake occur in the MAM through IP3Rs, Ca^{2+} release channels that are highly expressed in these regions[66]. The outer membrane of the mitochondria is Ca^{2+} permeant. On the contrary, in the inner membrane negative potential mediated Ca^{2+} transport is needed. Specifically, Ca^{2+} uptake in the mitochondria is driven by the low-affinity mitochondria uniporter (MCU) or by the high affinity mitochondrial Ca^{2+}/H^{+} exchanger (LETM). At the same time, Ca^{2+} release from mitochondria can occur via the Na^{+}/Ca^{2+} exchanger protein (NCLX) or via Ca^{2+} induced Ca^{2+} release[70]. Additionally, at high Ca^{2+} concentration, Ca^{2+} release occur through the permeability transition pore (PTP)[71]. Mitochondria are considered one of the main ROS production sources. Although ROS and RNS were considered detrimental for the muscle, in the last years it is being suggested that they can induce reversible post-translational modifications that are necessary for normal muscle performance[72,73]. Specifically, ROS has been proposed to regulate the redox state of triad-associated proteins (such as RyR1) and the consequent susceptibility to Ca^{2+} induced Ca^{2+} release or Ca^{2+} sparks[73].

DUCHENNE MUSCULAR DYSTROPHY

Duchenne muscular dystrophy (DMD) is a severe and progressive disease that affects 1 in 3500-5000 live male births[74]. It is characterised by severe and progressive skeletal muscle degeneration and weakness that lead to premature death due to respiratory failure or cardiac dysfunction. DMD is caused by mutations in the *DMD* gene, the largest human gene containing 79 exons and positioned on the short arm of the X chromosome (Xp21). Recessive mutations in this gene lead to a complete loss of the dystrophin (DYST) protein, a structural protein that links the contractile machinery to muscle membrane[75]. Two-thirds of DMD cases are inherited whereas the rest is caused by spontaneous mutations affecting *DMD* gene. Up to now, more than 7000 mutation have been described in this gene[76]. The majority of them are large deletion (60-65 %) and large duplications (5-10 %) while the rest are due to small deletions or duplications, point mutations or splicing mutations[77]. Although out of frame mutations in *DMD* gene result in complete protein loss, in-frame mutations generate a truncated and partially functional protein resulting in a milder disease with later onset described as Becker muscular dystrophy (BMD)[77,78].

Clinical features and diagnosis

Progressive muscle weakness is the main feature of DMD. Starting in the legs and gradually affecting upper limbs and trunk muscles, it compromises patients' mobility and health. In DMD patients, muscle weakness is accompanied by motor development delay, calf hypertrophy, joint contractures and elevated serum creatine kinase (CK) levels[75,79]. In addition, some patients present a variable speech delay, learning disability and cognitive dysfunction[80,81].

As a consequence of proximal leg weakness, DMD patients present difficulties to arise from the floor to the standing position. Gowers´ sign describes this characteristic dystrophic sign in which patient push on the floor and climbing up his legs to complete this action (Figure 8)[74,82].

Due to the progressive weakness, patients loss independent ambulation and need a wheelchair usually by the age of 7-12[79]. In the teenage, muscle atrophy and muscle contractures become more prominent. When weakness occurs in postural muscles, spine curvature or scoliosis appear, which is one of the most prevalent cause of surgical interventions in DMD patients[83]. As the disease proceeds, muscle weakness affects respiratory and cardiac muscles producing respiratory dysfunction and cardiomyopathy. These complications that usually appear at late-teenage are the main cause that produce premature death in DMD patients[79,84].

Figure 8. Illustration showing Gowers´ sign in a DMD patient. From Mah *et al.* (2016)[74].

DMD diagnosis is mainly based on patient physical examination and clinical history[79,84]. It is commonly diagnosed between the ages of two and six years as a consequence of the observation of motor development delay or abnormal gait and muscle hypertrophy. The determination of serum CK levels is used as a screening tool in suspicious patients. In addition, magnetic resonance imaging (MRI) can be used as a biomarker of muscle degeneration as well as to assess disease progression and fibrotic and fat replacement (Figure 9)[85–88].

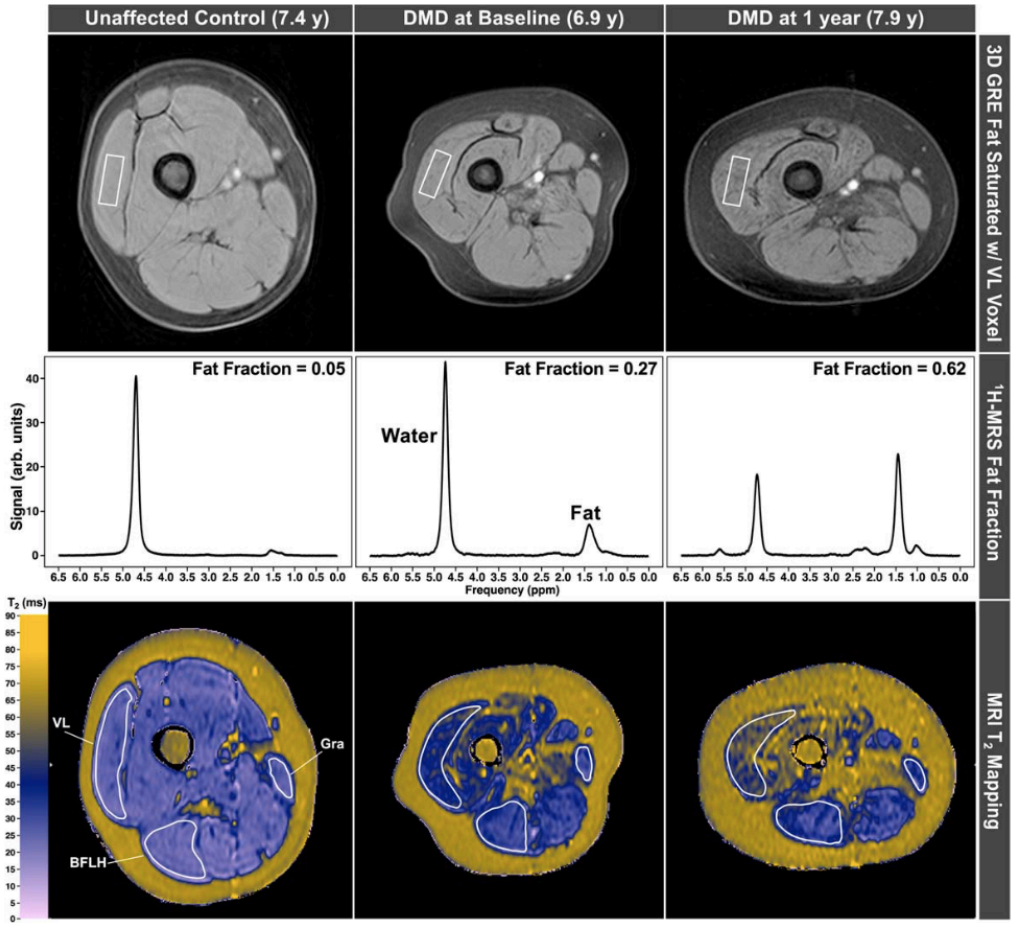

Figure 9. (Top) Three dimensional gradient eco images of the upper leg of an unaffected control (7.4-years-old) and a DMD boy at baseline (6.9-years-old) and the same DMD boy 12-months later (7.9-years-old) showing an increase of intramuscular fat infiltration. (Mid) ^{1}H-MRS spectra showing quantitative increase of fat fraction in DMD at baseline and after 12-months follow-up. (Bottom) MRI-T_2 maps showing increased T_2 fraction in DMD at baseline and after 12-months follow-up. 3D GRE = three-dimensional gradient refocused echo; ^{1}H-MRS = proton magnetic resonance spectroscopy; MRI = magnetic resonance imaging; VL = *vastus lateralis*; BFLH = long head of the *biceps femoris*; Gra = *gracilis*. From Willcocks *et al.* (2016)[87].

After physical examination, DMD can be confirmed by molecular genetic testing or dystrophin expression analysis in muscle biopsies[89]. The identification of the mutation that causes the disease is important to obtain accurate diagnosis and prognosis, to individualise treatments and for genetic counselling for families[90]. Mutation identification is commonly done using multiplex PCR of the most commonly deleted regions, studying the 79 exons of the *DMD* gene by MLPA or CGH microarrays or with

whole gene sequencing[91]. Finally, muscle biopsy could be used to study dystrophin expression at protein or RNA level. At histological level, DMD muscles show absent or reduced DYST staining which is accompanied by muscle necrosis, fibrosis, fatty tissue replacement and fibre size variation (Figure 10)[75].

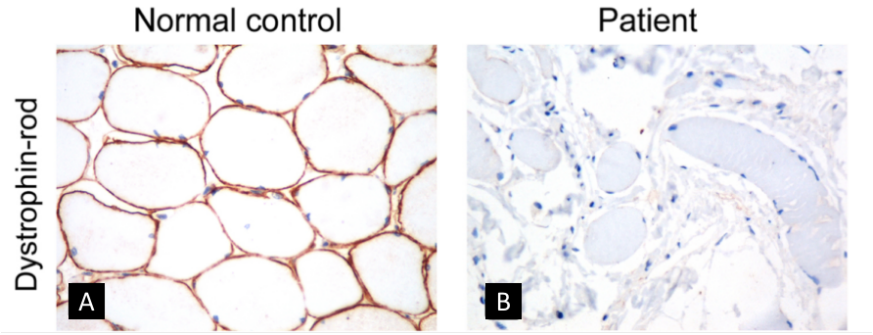

Figure 10. Muscle section from a healthy donor (Normal control) and a DMD patient (Patient) stained with an antibody against rod dystrophin. Adapted from Suriyonplengsaeng *et al.* (2017)[92].

Dystrophin

DMD gene is located in the X chromosome and contains 79 exons. It encodes for DYST, a 427 kDa rod-shaped protein which is part of the dystrophin glycoprotein complex (DGC) (Figure 11)[75].

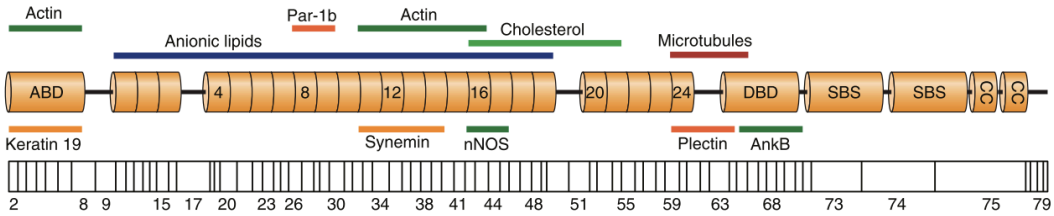

Figure 11. Dystrophin protein alignment with *DMD* gene exons. Top: Dystrophin protein domains and its binding sites with other molecules. Numbers identify spectrin-like repeats; ABD: actin binding domain; DBD: β-dystroglycan binding domain; SBS: syntrophin binding domain; CG: coiled-coiled region (binds α-dystrobrevin). Bottom: *DMD* gene exons correspondents with protein structure. From Allen *et al.* (2015)[75].

DYST is a large structural protein that connects the sarcolemma of the muscle fibre and the basal lamina of the extracellular matrix to the actin cytoskeleton providing

structural stability. Its central domain consists in 24 spectrin-like repeats. Each domain is composed by a triple-helical coiled-coil structure which is being suggest to act as a shock absorber and a force transducer during muscle contraction[74,75]. DYST binds F-actin via the N-terminal domain and other DGC components via the C-terminal domain (Figure 12). However, recent works demonstrated that not only DYST but also the whole DGC bind numerous signalling proteins that are essential for muscle function[75]. In this regard, DYST acts as a scaffold for several signalling proteins such as neuronal nitric oxide synthase (nNOS) or polarity regulating kinase partitioning-defective 1b (PAR-1b)[93].

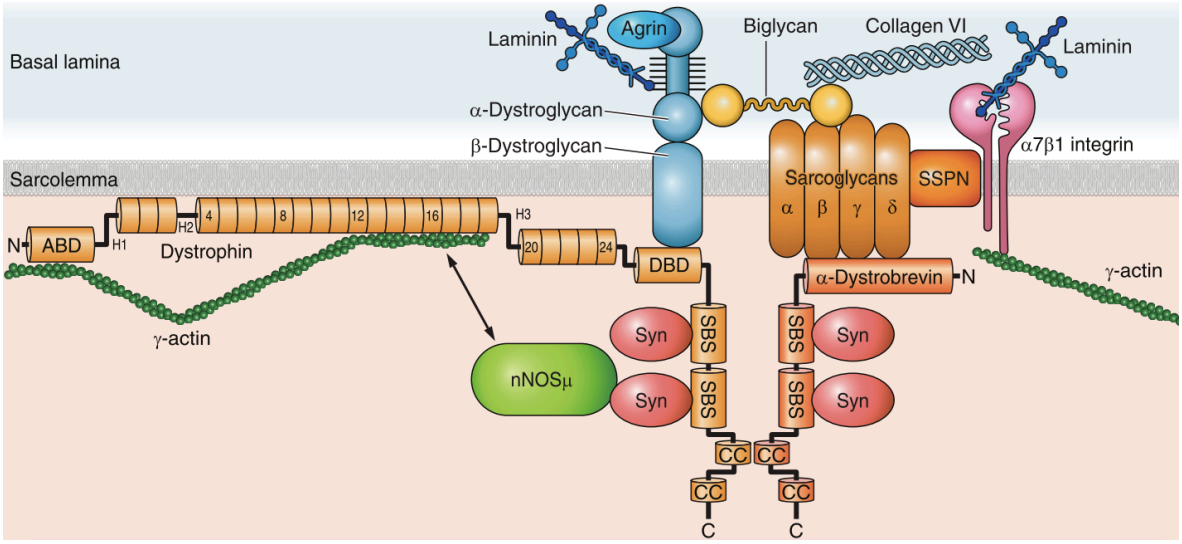

Figure 12. Illustration of the dystrophin glycoprotein complex (DGC). Dystrophin protein structure and connections with other proteins are shown. In DYST structure, N: N-terminal domain; C: C-terminal domain; ABD: actin binding domain; DBD: β-dystroglycan binding domain; SBS: syntrophin binding domain; CG: coiled-coiled region. Other interacting proteins, nNOS: neuronal nitric oxide synthase; Syn: syntrophin; SSPN: sarcospan. From Allen *et al.* (2015).[75]

In DMD, absence of DYST protein produces membrane fragility. As a consequence, Ca^{2+} influx into the sarcoplasm occur activating several proteases and proinflammatory cytokines that result in progressive muscle degeneration[75,94]. Furthermore, since nNOS requires intact DGC for sarcolemmal association, DYST deficiency produces nNOS displacement, which has been associated with increase of oxidative stress and ischemia[93–95]. Moreover, recent works suggest that nNOS

dysregulation increases NO production and enhances S-nitrosylation of proteins, leading to changes in protein activity and function[96]. Additionally, absence of the three DYST isoforms that are present in the brain, retina and Purkinje cerebellar neurons have been proposed to contribute to cognitive, behavioural and learning difficulties of DMD patients[80,97].

DYST is also expressed in satellite cells, where it has been proposed to regulate cell polarity and determine asymmetric division[98]. Asymmetric cell division is a process in which a satellite cell is divided generating both a stem cell and a progenitor cell. In DMD, absence of DYST has been proposed to impair cell polarity producing mitotic abnormalities that lead to a deficient generation of progenitor cells and a consequent reduction of muscle regenerative capacity[98,99].

Pathophysiology and calcium homeostasis

Duchenne muscular dystrophy is characterised by progressive muscle degeneration and weakness. The disease is caused by mutation in *DMD* gene that lead to a complete absence of DYST protein. DYST is a structural protein that provides stability to muscle fibre membrane[100]. As a consequence of DYST deficiency, dystrophic muscles show membrane fragility, which have been postulated to provoke an increase of extracellular Ca^{2+} influx producing calpain activation, protein degradation and mitochondrial overload and leading to fibre necrosis[75]. However, this mechanism has been postulated not to be strong enough to explain the muscle degeneration that DMD patients present[101,102]. Furthermore, evidence of increased intracellular Ca^{2+} concentrations have been found in pre-necrotic muscles from DMD patients, suggesting that a dysregulation of intracellular Ca^{2+} levels is one of the initial mechanisms that trigger dystrophic phenotype[101].

In this aspect, several mechanisms have been proposed to contribute to increased intracellular calcium levels in DMD patients or mouse models (Figure 5)[30,75]. Transient receptor potential canonical (TRPC) channels are mechanosensitive, voltage

independent Ca^{2+} channels that are located in the sarcolemma and show increased expression in mdx mouse model of DMD[24,103]. TRPC channels have been associated with store operated calcium entrance (SOCE), a mechanism that consists in an extracellular Ca^{2+} influx triggered by SR Ca^{2+} depletion, a mechanism that is also increased in dystrophic muscles[24,104]. Alteration of TRPC channels have been associated with several pathological mechanism and diseases such as respiratory and cardiac disorders, diabetes or central nervous system disorders. Interestingly, TRPC channels have also been proposed as promising therapeutic targets against most of those diaseases[105]. Additionally, other calcium handling proteins that present increased expression in DMD muscles, such as Orai1 and STIM1, have been associated with increased SOCE in dystrophic muscle[101,104]. Orai1 is a Ca^{2+} release-activated Ca^{2+} channel that is present in muscle sarcolemma. It interacts with the stromal interaction molecule1 (STIM1), a SR Ca^{2+} sensor that activates SOCE through interaction with Orai1 or TRPC channels.

The main SR Ca^{2+} release channel, RyR1, has also been involved in the increase of intracellular Ca^{2+} levels. Specifically, in mouse models of DMD, RyR1 receptor presents abnormal post-translational modifications that affect its binding to Calst and consequently its activity[25,55]. As a consequence of an increase of the inducible nitric oxide synthase (iNOS) and the increased of ROS, RyR1 undergoes hyperphosphorylation and hypernitrosylation, which reduce its binding affinity to the stabilising protein Calst1. Hence, leaky RyR1 channels are generated, which contributes to the increase of intracellular Ca^{2+} levels[55].

Similarly to what happens with RyR receptors, IP3R also present Ca^{2+} leak in DMD muscles. It has been shown that IP3R expression is increased in dystrophic muscle as well as increased IP3 levels and IP3 mediated Ca^{2+} transients were found in myotubes from both DMD patients and mouse model muscles[37]. Moreover, dysregulation of IP3R have been linked to mitochondrial dysfunction. IP3Rs are expressed in MAM, where Ca^{2+} uptake by the mitochondria occur[66]. Mitochondrial Ca^{2+} overload is present in dystrophic muscles leading to the activation of PTP and the induction of apoptosis.

Interestingly, inhibition of IP3R has demonstrated to prevent mitochondrial overload[68,106].

Defects in Ca^{2+} uptake have also been proposed to occur in DMD. Although controversial results can be found in literature, some works proposed that SERCA activity could be reduced in DMD[107–109]. In relation to that, a reduced Ca^{2+} buffering capacity that could negatively impact in SERCA activity has been found in mdx mice[16]. Furthermore, recent works demonstrated that the overexpression of SERCA in dystrophic muscle improves disease phenotype[108–110].

Animal models

Several animal models of DMD are available including naturally or laboratory generated models. Up to now, more than 60 models have been described including non-mammalian[111,112] and mammalian species[94,113]. Among them, canine DMD (cDMD) model is considered the best model owing to their similarity to DMD patients (Table 1). DMD dogs present elevated serum CK levels and a histological pattern of degeneration and regeneration that is similar to the one found in humans[94,114]. For these reasons, cDMD model constitutes the ideal model to test treatments response against DMD. However, cDMD pups present high mortality and the cost of colony maintenance is very high. Hence, the use of this model in research is very limited.

The mdx mouse is the most widely used model of DMD[115,116]. It presents a spontaneous stop codon mutation in exon 23 that produces complete absence of DYST protein. It has similar genotype to DMD patients and some characteristic dystrophic features, such as elevated CK or histological evidence of muscle damage, and compared to dogs, it has lower costs and easier maintenance. However, mdx mice present a much milder dystrophic phenotype than human patients (Table 1)[94,117,118]. Mdx mice present slightly reduced life spam compared to wild type animals. Muscle damage follows cycles of degeneration and regeneration starting at 4 weeks of age. Regeneration can be easily visualised as muscles showing central nucleation. In general, respiratory muscles

are most affected than limb muscles being diaphragm the muscle that is more similarly affected to humans[119–121]. Muscle performance is reduced in mdx mice. Furthermore, mdx mice show reduced specific force *in vivo* and *in vitro* in isolated muscle experiments[122]. In addition, intracellular calcium levels are elevated in muscle fibres from *flexor digitorum brevis* (FDB) muscles of dystrophic animals[123–125].

Table 1. Comparison of disease features in dystrophin deficient mice, dogs and humans. Adapted from McGreevy *et al.* (2015)[94].

	Mice	**Dogs**	**Humans**
Clinical			
Birth body weight	= normal	= normal	= normal
Grown-up body	≥ normal	< normal	< normal
Clinical course	Mild, non-progressive	Severe, progressive	Severe, progressive
Lifespan	= 75% of normal	= 25% of normal	= 25% of normal
Neonatal death	Rare	~ 25% of affected dogs	Rare
Age at first symptom	≥ 15 months	Birth to 3 months	2 to 4 years
Loss of ambulation	Rare	Uncommon	Common at early teenage
Muscle wasting	Minimal until ≥ 15 months	Progressive	Progressive
ECG abnormality	Frequent	Frequent	Frequent
Cardiomyopathy	≥ 20 months; dilated (female) and hypertrophic (male)	Detectable at 6 month by echocardiography	Evident at 16 years
Cognitive and CNS defects	Mild	No information available	One-third of affected individuals
Histopathology			
At birth	Minimal	Minimal	Minimal
Acute necrosis	2 to 6 weeks	None	None
Limb muscle fibrosis	Minimum in adult	Extensive and progressive	Extensive and progressive
Muscle regeneration	Robust	Poor	Poor

The milder dystrophic phenotype could be explained by several specie specific characteristics. In mdx mice, utrophin expression is increased in the sarcolemma. It has been shown that utrophin knocking down generates more severe phenotype, while utrophin overexpression is protective and ameliorates muscle disease in mdx mice[126,127]. Muscle regeneration is also more efficient in mice. It has been shown that satellite cells proliferation is increased in mice facilitating muscle repair, which could be associated with longer telomeres and shorter life spam[128]. The expression of cytidine monophosphate sialic acid hydroxylase gene (CMAH) is also specific of mice and is not present in humans. Moreover, the inhibition of this gene generates a more severe phenotype[129]. Finally, the small size of the mice could also be protective. Previous works suggested that small dog and humans are protected and show milder phenotype[75].

The dystrophic phenotype observed in mdx mice may be exacerbated using forced exercise protocols. Specifically, several works suggested that half an hour exercise in a treadmill twice a week is sufficient to generate progressive weakness in mdx mice[130,131]. Other alternative to obtain a more severe DMD phenotype in mice is to generate double knockout mice. Utrophin and dystrophin double knockout mice (dko) present a very severe phenotype, even more than the one present in humans[132]. As a consequence, this model is difficult to maintain, which limits its use for research. Another strategy that has been used is to generate more severe phenotype is to generate mdx mice with shorter telomeres. mTR mice lack the RNA component TERC of the telomerase and as a consequence present shorter telomeres. As a consequence, these mice present a severe phenotype, cardiomyopathy and reduced life spam[128]. Although these models present more severe phenotype, their physiological relevance is still on debate.

Human DMD models

In the last decades, mouse models of muscular dystrophies have been used to study the specific pathophysiological mechanism associated with disease progression and treatment response. However, these models do not often reproduce the severity of

human disorders, suggesting that pathogenic mechanisms could vary between species[133]. Hence, extrapolation of treatment response from mouse to humans is always challenging. Consequently, well-characterised and reproducible human *in vitro* models that recapitulate disease phenotype would be very useful in order to advance in the generation of specific therapies[134].

Human satellite cells and myotubes have been efficiently isolated from muscle biopsies of healthy or disease-affected donors[135,136]. After *in vitro* differentiation, human myotubes display high inter-individual heterogeneity regarding differentiation, morphology and survival[137,138]. As a consequence, when comparing healthy and dystrophic myotubes, it is usually difficult to discriminate between dystrophic features or differentiation stage-induced differences. Trying to solve this problem, several groups have worked in improving the potential and reproducibility of myotube differentiation. Different strategies include application of exogenous electrical pulse stimulation to cultures[139,140], co-culturing myotubes with embryonic rat spinal cord explants[141–143] or using different scaffolds to develop muscle-like functional structures[144,145]. However, primary human cultures present other important drawbacks that limit their use in research. In one hand, sample availability is limited, especially in dystrophic patients, due to scarcity of human biopsies. On the other hand, primary myoblasts present limited proliferation potential in culture and suffer senescent-induced changes which make impractical their use for high throughput screening, where high number of cells are needed[37,138,145,146]. In order to solve this problem, different strategies have been focused on increasing satellite cells proliferation potential such as pharmacological inhibition of p38 mitogen-activated protein kinase (MAPK)[147] or transient expression of Pax3[148]. In addition, dystrophic cell lines could be generated knocking-down disease causing genes in healthy myotubes using RNAi[149] or CRISPR/Cas9[150].

Immortalisation of primary myoblasts has also been use to overcome myoblast proliferation limitation[151]. The simultaneous expression of the human telomerase reverse transcriptase (hTERT) and cyclin-dependent kinase4 (CDK4) produce telomere

elongation and the inhibition of $p16^{INK4a}$-dependent stress pathway, respectively. As a consequence, myoblast proliferation is extended and differentiation potential is maintained over time[151,152]. Immortalised myoblasts maintain the main characteristics of their parental population[153], suggesting that their physiological relevance is not altered by the immortalisation process. Hence, immortalisation of myoblasts obtained from healthy or dystrophic donors could be a viable source of stable myoblast lines for high throughput drug screening[151].

Alternatively, several studies on neuromuscular disorders are based on myotubes obtained from sources different from muscle biopsies such as MyoD-converted fibroblasts or human inducible stem cells (iPSC) derived myoblasts. MyoD-converted fibroblast model has been used to generate myoblasts from skin biopsies of patients with neuromuscular disorders[154,155]. This transduction method is a simple and easy method to obtain functional myotubes that could be used for therapy testing. On the other hand, myoblasts can be differentiated from human iPSCs. They are generated over-expressing in somatic cells from healthy donors or patients a combination of pluripotency regulators (OCT4, SOX2, KLF4, NANOG, …)[156]. iPSC derived myogenic cells, have been proposed to be useful for studying disease phenotype or treatment efficacy as well as in cell transplantation therapy[157,158]. Furthermore, iPSC derived DMD myotubes showed impaired Ca^{2+} homeostasis[159]. However, the physiological relevance of these models is still under debate.

Current and experimental treatments for DMD

Currently there is not specific treatment for DMD. However, in clinical practice many forms of therapy are used to treat patients´ symptomatology and prolong survival. In this aspect, the involvement of a multidisciplinary team is essential to support patients and their families (Figure 13)[79,84].

Corticosteroids treatment is the most widely used pharmacologic intervention. They stabilise muscle function and prolong patients´ survival. Additionally, treated

patients show prolonged independent ambulation and delayed development of scoliosis and cardiomyopathy. However, they also present important side effects as short stature, obesity, cataracts and bone fractures[160–162].

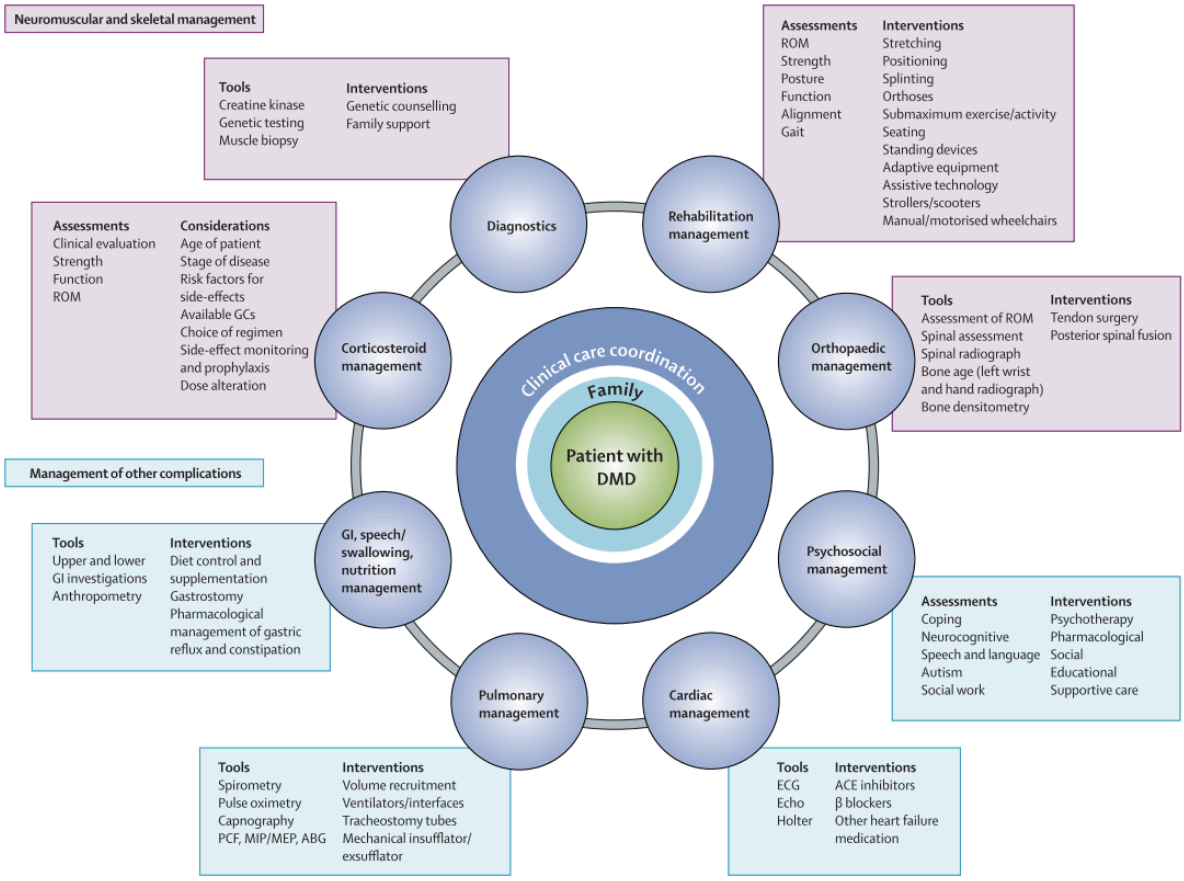

Figure 13. Interdisciplinary management of DMD patients. ABG: arterial blood gas. ACE: angiotensin converting enzyme. Echo: echocardiogram. ECG: electrocardiogram. GC: glucocorticoids. GI: gastrointestinal. MEP: maximum expiratory pressure. MIP: maximum inspiratory pressure. PCF: peak cough flow. ROM: range of motion. From Bushby *et al.* 2010[79].

As muscle weakness progress, cardiac and respiratory complications appear. Early detection of these pathologies is crucial to prolong patients´ survival. Cardiac pathologies are often asymptomatic due to patients' low physical capability. Conduction defects, arrhythmias and cardiac necrosis are usually present in DMD patients[163,164]. Early cardioprotective treatments (IACE, β-blockers, phosphodiesterase-5 inhibitors, …) can delay cardiac failure and prolong survival. Respiratory deficiency is another

feature of DMD. Prevention of respiratory complications consists of non-invasive positive pressure ventilation and chest physiotherapy[79,84].

Recent scientific advances have led to the development of new therapeutic strategies for DMD and other neuromuscular disorders[165–169]. Nowadays, the main strategies are focused on restoring dystrophin expression, increasing membrane stability by upregulating compensatory proteins, enhancing muscle regeneration, regulating intracellular calcium homeostasis or modulating the inflammatory cascade and fibrotic and ischemic responses (Table 2).

The ideal treatment for DMD patients would result in expression of fully functional dystrophin in muscle fibres. To achieve this, several approaches have been designed. Stop codon read-through agents are useful in patients with nonsense mutations (~ 10% of total DMD) in which a stop codon prevents *DMD* gene translation to protein. Aminoglycosides and Ataluren bind ribosomes allowing them to read through premature stop codons and leading to translation of a functional dystrophin protein[170,171]. The efficacy of Ataluren to induce full-length DYST production has been widely demonstrated in several *in vitro* and *in vivo* experimental DMD models such as mdx mice, sapje zebrafish or human myotube cultures[172–174]. Furthermore, in clinical trials with DMD patients, Ataluren treatment has demonstrated to delay the decline of walking ability in the six minutes walking test (6MWT). However, differences were not significant compared to placebo[175]. Based on these results, the U.S. Food and Drug Administration (FDA) decided not to authorised Ataluren commercialisation. Nonetheless, Ataluren obtained conditional commercialisation approval in the European Union (EU) in 2014, which was recently renewed in 2016 with an obligation to conduct a new long-term clinical trial.

Exon skipping technology is another strategy to restore dystrophin expression in DMD patients. It uses synthetic antisense oligonucleotides to skip over mutated exons in pre-mRNA and restore the reading frame, producing a truncated and partially functional dystrophin protein. As a result, the protein obtained would be similar to the

one found in Becker muscular dystrophy, in which patients presents milder phenotype than Duchenne patients[169]. Nowadays, several exon skipping therapies are under development but the ones targeting exon 51 are in the most advanced stage (14 % of patients could benefit from exon 51 therapy). Between them, eteplirsen (Sarepta Therapeutics) obtained FDA approval in 2016 becoming the first drug approved by the FDA for DMD[176,177]. It demonstrated to slow disease progression and significantly improve the 6MWT. However, drisapersen (Exon 51, BioMarin Pharmaceutical Inc) was recently rejected by the FDA due to lack of evidence that demonstrate drug´s effectiveness. Additionally, several clinical trials are ongoing with other exon skipping agents for exon 45 and 53[178,179].

Gene replacement therapy consists in introducing a functional dystrophin protein using adeno-associated viruses[94,180,181]. Owing to the enormous size of dystrophin gene, strategies have been focused in the generation of functional mini or micro-dystrophins[182,183]. Although microdystrophin gene injection was found to improve histopathology in canine DMD models, the therapy failed in DMD patients due to T-cell mediated immune response[184]. In any case, clinical trials using recombinant viruses and more efficient delivery systems are ongoing in DMD patients[74].

Compensatory proteins overexpression has been proposed to contribute to milder phenotype in mouse models of DMD. Similarly, in muscle biopsies from DMD and BMD patients, utrophin levels correlate with disease severity and muscle regeneration[185]. Furthermore, it has been shown that increasing utrophin or other cytoskeleton proteins such as alpha-7-beta-1 integrin, stabilise the sarcolemma ameliorating dystrophic symptoms[127,186]. Ezutromid is a utrophin modulator that is in phase II clinical trial and has shown to increase utrophin expression in skeletal and cardiac muscles of paediatric patients[187].

In order to accelerate muscle regeneration pharmacologic as well as cell transplantation therapies have been tested. Drugs targeting the inhibition of myostatin, a negative regulator of muscle mass, are being evaluated in several clinical trials[188,189].

On the other hand, cell transfer therapy is a promising therapy focused on increasing muscle regeneration using dystrophin expressing cells[168,190]. These cells could be obtained from the patient and re-implanted after *ex vivo* correction, or could be obtained from an unaffected donor[191–193]. Although promising, the efficiency of this therapy is still low and further optimisation is needed.

Dysregulation of calcium homeostasis has been proposed to trigger dystrophic pathogenesis in DMD[75,194]. Hence, drugs targeting Ca^{2+} handling proteins or processes would be potential treatments for dystrophic patients. Several strategies have been tested in mdx mice. Among them, RyR stabilisers and SERCA modulators are the most common strategies. RyR stabilisers, also named rycals, are small molecules designed to increase Calst binding affinity to hypernitrosylated RyR channels[55,56]. *In vivo* treatment with the rycal S107 stabilises the close conformation of the channel reducing RyR calcium leak. As a consequence, intracellular calcium levels are restored and muscle function is improved. S107 has shown to improve skeletal muscle defects in mdx and sarcoglycan deficient mice[55,56]. In addition, it has demonstrated to be useful for the treatment of cardiac arrhythmias[195,196], stress-induced cognitive dysfunction[40] and aging[197].

In humans, rycals (Armgo Pharma) are currently in pre-clinical development and clinical trials with the compound ARM210 are expected to start soon with the initial indication of DMD. Similarly, drugs targeting SERCA have demonstrated to improve muscle function in mdx mice. Alterations in SERCA expression and/or function have also been reported in other dystrophies[198], suggesting that it could constitute a novel therapeutic target. In addition, increasing SERCA expression and/or function lead to a reduction of intracellular Ca^{2+} levels, protecting muscle fibres and improving muscle performance[107,108,199]. Some of them such as enalapril or carvedilol have been tested in clinical trials and were found to delay cardiomyopathy in DMD patients[200].

Table 2. Emerging therapies for DMD.

- Dystrophin restoring therapies
  - Stop codon read-through agents
    - Gentamicin
    - Arbekacin *
    - Ataluren (Translarna) *
  - Exon skipping
    - Exon 51
      - AVI-4658 (Eteplirsen) *
      - GSK2402968 (Drisapersen)
    - Exon 53
      - SRP-4053 (Serapta) *
      - SRP-4045 (Prosensa) *
      - NS-065/NCNP-01 *
    - Exon 45
      - SRP-4045 *
    - Exon 44
      - PRO044
  - Gene replacement therapy
    - rAAV2.5-CMV-minidystrophin
    - rAAVrh74.MCK.micro-Dystrophin *
    - rAAV1.CMV.huFollistating344 *
- Membrane stabilization
  - Utrophin overexpression: SMT C1100 (Ezutromid) *
- Muscle regeneration
  - Myostatin inhibitors
    - BMS-986089 *
    - PF-06252616 *
  - GCSF analogues
    - Filgastrim *
- Cell therapy
  - Myoblasts *
  - Bone marrow derived mono nuclear stem cells
  - Umbilical cord mesenchymal stem cells *
  - Human induced pluripotent stem (iPS) cells *
- Calcium homeostasis: ARM210/S48168
- Anti-inflammatory
  - Idebenone *
  - Vamorolone *
  - Coenzime Q10 *
- Antifibrotic
  - FG-3019 *
  - Lisinopril *
  - Tamoxifen *
- Muscle ischemia: PDE-5 inhibitors
  - Tadalafil
  - Sildenafil

* Active or recruiting clinical trials, accessed on February 27, 2017 from www.clinicaltrials.gov

GCSF: granulocyte colony stimulating factor; PDE-5: phosphodiesterase type 5

Finally, other pharmacologic strategies have targeted inflammatory cascades or fibrotic and ischemic processes. Several of these drugs have been or are currently being tested in clinical trials with DMD patients[74]. Among them, tadalafil is a selective and reversible inhibitor of the PDE5. It is able to restore NO-mediated cGMP signalling, which is impaired due to the nNOS mislocalisation that occur as a consequence of DYST deficiency. Hence, tadalafil restores muscle hemodynamic response to exercise, reducing muscle ischemia and damage in mouse models of DMD[133,201,202]. Additionally, it delays the onset of dystrophic cardiomyopathy in mouse and canine DMD models[203]. In patients, tadalafil effects on muscle ischemia has been evaluated. In both DMD and BMD patients, it demonstrated to significantly alleviate muscle ischemia restoring normal blood flow[204,205].

OBJECTIVES

STRUCTURE OF THE THESIS

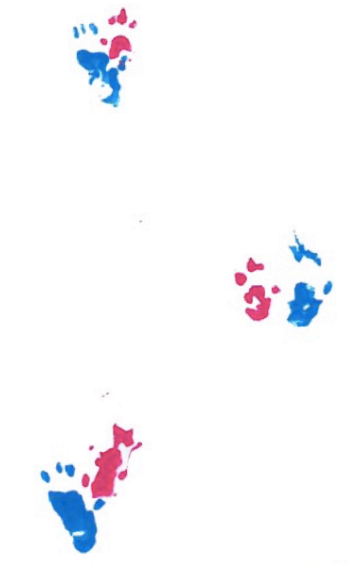

OBJECTIVES

The main objective of this thesis is to advance in the development of pharmacological therapies against Duchenne muscular dystrophy (DMD). This study arises from the hypothesis that drugs targeting ryanodine receptor 1 (RyR1) and calstabin 1 (Calst1) interaction could consolidate a therapeutic alternative for DMD patients. Specifically, this thesis studies the effect of novel ryanodine stabilisers, named as Ahulken (AHK) compounds, in mouse and human DMD models. The current lack of efficient therapies to treat dystrophic patients make this study particularly necessary.

The specific objectives can be summarised as follows:

1. To select two hit AHK compounds for *in vivo* studies.

    a. To determine the *in vitro* cytotoxicity of AHK compounds in mouse and human myotube cultures.

    b. To assess the effect of AHK compounds on RyR1-Calst1 interaction in myotubes under SIN-1-induced stress.

2. To test the effect of AHK compounds in mdx mouse model of DMD.

    a. AHK effect on calcium homeostasis in isolated fibres from mdx mice.

    b. AHK effect on muscle function.

    c. AHK effect on muscle degeneration.

3. To evaluate the effect of AHK compounds in a human cellular DMD model.

    a. To validate a human *in vitro* DMD model for therapy testing.

    b. To study the effect of AHK compounds on RyR1-Calst1 binding and calcium homeostasis in a human DMD model.

STRUCTURE OF THE THESIS

The structure of thesis follows the order of the previously described objectives. As such, the text has been arranged in three main sections:

The first study (**Chapter 1**) aims to select two hit candidates from a family of novel compounds designed to increase RyR1-Calst1 binding affinity as a treatment against Duchenne muscular dystrophy. For this purpose, compounds cytotoxicity and action mechanism is evaluated in mouse and human myotube cultures.

In a further study (**Chapter 2**), the effect of the selected compounds and a reference compound (S107) are tested in mdx mouse model of Duchenne muscular dystrophy. The compounds effect is based on their ability to enhance RyR1-Calst1 binding in disease conditions where RyR1 suffers hypernitrosylation and hyperphosphorylation leading to Calst1 depletion and calcium leaky channels. This calcium leak has been proposed to contribute to the increased intracellular calcium levels that trigger dystrophic pathogenesis in DMD patients. The effect of these novel compounds on calcium homeostasis, muscle function and muscle degeneration is studied.

In a final work (**Chapter 3**), compounds efficacy is studied in a human DMD model. The effects on RyR1-Calst1 binding and calcium homeostasis are analysed as indicators of the potential utility of the compounds in DMD patients. In order to select the optimum human model to test the compounds, two different approaches are evaluated, both of them based on immortalised human myoblasts. Within them, the model generated using DYST-shRNA mediated dystrophin knocking down is fully characterised to evaluate it accuracy to recapitulate dystrophic features of DMD.

CHAPTER 1:

Toxicity and mechanism of Ahulken compounds in mouse and human cellular models

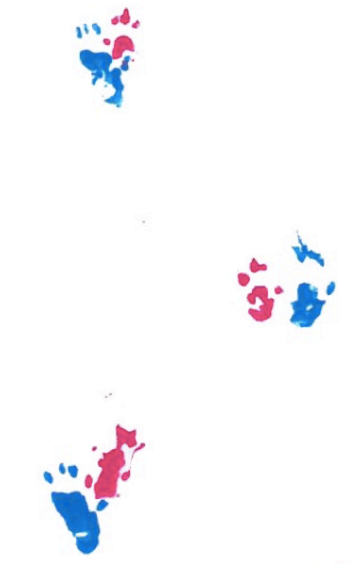

INTRODUCTION

Ahulken (AHK) is a novel family of small molecules (triazoles) specifically designed to stabilise the interaction between ryanodine receptor 1 (RyR1) and calstabin 1 (Calst1) in order to regulate intracellular calcium levels in the muscle fibre. These molecules have a low molecular weight, they follow Lipinski's rule of five for druglikeness and they are very stable and water soluble. They have been designed in collaboration with Dr. Jesús María Aizpurua (Faculty of Chemistry, University of the Basque Country, Spain) by *in silico* molecular docking and they have been synthesised using a "click" synthesis approach. Up to now, more than 15 AHK compounds with large structural variability have been synthesised (named as A5, A6, A7, etc.) (Figure 1). AHK compounds have been recently protected by a patent application (P201630670, 24/05/16).

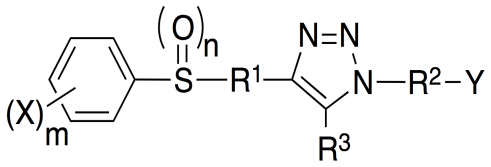

Figure 1. General structure of AHK compounds. R^1, R^2, R^3, X and Y have been substituted to generate the different AHK compounds.

Ryanodine receptors are the main calcium release channels in skeletal muscle and heart[36,41]. RyR activity can be regulated *in vivo* by post-translational modifications (PTM), such as phosphorylation, S-nitrosylation, S-glutathionylation and S-palmitoylation[25,48,49,206]. In particular, RyR phosphorylation and S-nitrosylation have been associated with changes in channel activity through reduction of its binding affinity to calstabin[55,207]. Calst is a small protein that binds RyR in a 4:1 stoichiometry (one Calst per RyR subunit) and stabilises the close state of channel[36]. Therefore, a reduction of Calst binding leads to leaky RyR channels and increased intracellular calcium

concentrations[25,41].

Calst depletion-induced RyR leakage has been observed in several physio-pathological conditions, such as chronic exercise, aging, muscular dystrophies, heart failure or cognitive dysfunction[40,55,56,58,197,207]. Accordingly, in those conditions, RyR phosphorylation and S-nitrosylation have been found to be increased, leading to a reduction of Calst binding affinity. Overall, this mechanism has been proposed to contribute to disease phenotype by affecting intracellular calcium homeostasis and activating several cell damage and death pathways[25]. Interestingly, recent studies have reported that pharmacologic modulation of RyR-Calst binding with RyR stabilisers, such as S107 (Armgo Pharma), reduce pathological calcium leakage, preventing muscle degeneration and improving muscle function[40,55,56,58,197,207]. These works constituted the first evidence of RyR-Calst as a useful therapeutic target for drug development against muscle disorders and the rational for the recent development of AHK compounds.

During initial stages of drug development process, it is essential to determine the safety profiles of novel molecules in order to identify potential hazardous compounds and select safe candidates for *in vivo* studies. In this context, *in vitro* cytotoxicity studies constitute a cost-effective alternative that allow the screening of high number of candidates and a consequent selection of the safest molecules[208]. In general, a compound is considered cytotoxic when it interferes with cellular attachment or proliferation, provokes dramatic changes in cell morphology or reduces cell viability. Among the techniques described to assess cytotoxicity *in vitro,* the most extended cytotoxicity biomarkers are constitutive enzymes that are released into the cell culture medium as a consequence of membrane integrity loss. In particular, lactate dehydrogenase (LDH) measurement in culture media is a robust and cost-effective technique that is commonly used to easily determine *in vitro* cytotoxicity of novel drug candidates[208].

Specific *in vitro* models that recapitulate disease phenotype are also needed in order to prove the action mechanism of novel RyR stabilisers. In this aspect, the peroxynitrite donor SIN-1, could be potentially used to induce post-translational

modifications of RyR1 *in vitro* and generate cellular models of calstabin1 depletion that would be useful to test treatments targeting these processes.

SIN-1 is a biochemical tool that has been used to study the effects of NO in physiological and pathological conditions. Aerobic decomposition of SIN-1 produces $O_2^{\bullet-}$ and $NO^{\bullet}$, which react forming peroxynitrites (Figure 2)[209].It has also been shown that SIN-1 derived peroxynitrites have a direct effect in protein phosphorylation through PKA activation in a cAMP-independent manner[210]. Furthermore, NO and peroxynitrites directly induce protein nitrosylation, leading to alterations in intracellular calcium homeostasis[206,211]. All together, these works suggest that SIN-1 could be used to study peroxynitrite-induced protein post-translational modifications *in vitro.*

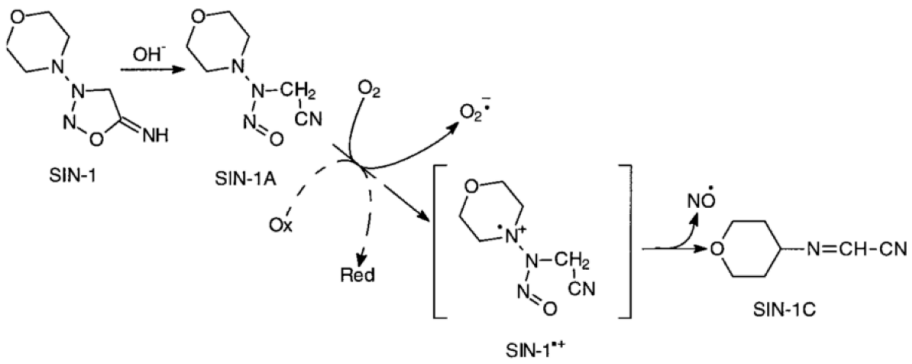

Figure 2. SIN-1 oxidation to $NO^{\bullet}$ and SIN-1C. The broken line represents the reaction that would happened in the presence of oxidising agents, others than molecular oxygen, where intermediate product would be formed without releasing superoxide.

The main goal of the present study was to select the most appropriate AHK compounds for the *in vivo* studies based on their toxicity and mechanism. To this end, 1) the toxicity profiles of AHK compounds and S107 reference compound were analysed in mouse and human myotube cultures; 2) an *in vitro* model was generated using SIN-1 and human myotubes in order to study RyR1 post-translational modifications and Calst1 binding and 3) the effect of AHK compounds on RyR1-Calst1 interaction was tested.

METHODS

Cell cultures

C2C12 myoblasts were obtained from the American Type Culture Collection (ATCC). Myoblasts were grown in DMEM supplemented with 10% FBS and 1% penicillin/streptomycin (P/S). Cells were seeded onto 0.5% gelatin coated dishes, and, after reaching confluence, medium was replaced with differentiation medium (DMEM 2% horse serum (HS) and P/S). Cells were differentiated for 6-7 days until contractile myotubes were obtained.

On the other hand, LHCN-M2 immortalised human myoblasts were kindly provided by Dr. Vincent Mouly (Myology Institute, Paris). These cells were generated by the Platform for Immortalisation of Human Cells (Myology Institute, Paris). Human myoblasts were grown in Skeletal Growth Medium (SGM, PromoCell) supplemented with 10% fetal bovine serum (FBS), 1X Glutamax and 50 μg/mL gentamicin in 0.5% gelatin coated dishes. At confluence, cells were washed with DPBS and the appropriate volume of 2.6 mg/mL extracellular matrix (ECM, Sigma), diluted in DMEM, was added. Cultures were incubated at 37 ºC for 30 min to allow ECM polymerisation, forming thin overlays of approximately 1 mm, and then, basic differentiation medium (dMD: DMEM 10 μg/mL insulin, 100 μg/mL aprotransferrin and 50 μg/mL gentamicin) was added. Once fusion started, medium was replaced by complete differentiation medium (cDM: Neurobasal A medium supplemented with 1X B27, 1X Glutamax, 20 ng/mL BDNF, 50 ng/mL IGF-1, 5 ng/mL CNTF, 20 ng/mL NT-3, 4 μg/mL laminin, 100 ng/mL agrin and 50 μg/mL gentamicin.) and half volume of the medium was changed every 3 days. After 8 days of differentiation, highly mature myotubes were obtained.

Cytotoxicity assay

In vitro cytotoxicity of AHK compounds was assessed in mouse and human myotube cultures. For this purpose, C2C12 and LHCN-M2 myoblasts were seed in 96-well plates and were cultured as previously described. After 6-7 days of differentiation, cultures were exposed to seven different concentrations of AHK compounds for 24 hours. The toxicity of S107 reference compound and the following AHK compounds (A5, A6, A7, A8, A9R, A9S, A10R, A10S, A11R, A11S, A12 and A13) was analysed at different concentrations (10 nM, 150 nM, 1 μM, 10 μM, 100 μM, 1 mM and 2 mM), using quadruplicates for each condition. After 24 hours, supernatants were collected and the amount of lactate dehydrogenase (LDH) was measured using Cytotox 96® kit. Briefly, 50 μl of cell supernatants were incubated with reaction solution for 30 min at room temperature in the dark. Then, the reaction was stopped and absorbance was measured at 492 nm. The absorbance was normalised to the total LDH content in the remaining cells, which was obtained by incubating cells with 1X lysis solution for 30 min.

RyR1-Calst1 complex dissociation by SIN-1

LHCN-M2 human myotube cultures were used in order to study the action mechanism of Ahulken compounds. In LHCN-M2 myotubes, the dissociation of the RyR1-Calst1 complex was induced using the peroxynitrite donor SIN-1. For that LHCN-M2 myotubes were seeded onto 12 mm coverslips, and at 7 days of differentiation, myotubes were treated overnight with 150 nM of A6, A7 or S107 compounds. Next day, myotubes were exposed to 5 mM SIN-1 for 30 min at 37 ºC, and afterwards, they were fixed with 4% paraformaldehyde. Some myotubes were treated with 15 μM rapamycin for 30 min at 37ºC. This condition was considered a positive control for RyR1-Calst1 dissociation control, since rapamycin is a well-characterised agent that binds Calst1 and dissociates it from RyR1.

In situ Proximity Ligation Assay (PLA)

In situ PLA is a novel technique that allows direct detection of protein interactions and modifications with high specificity and sensitivity. Two interacting proteins located in close proximity (30-40-nm) can be readily detected, localised and quantified in unmodified cells and tissues[212,213]. This is achieved by using species-specific secondary antibodies linked to complementary oligonucleotides that, in close proximity, hybridise. Upon subsequent addition of a ligase, a polymerase and a labelled complementary oligonucleotide, distinct bright spots are obtained, and can be imaged and quantified by fluorescence microscopy.

Paraformaldehyde fixed myotubes were incubated with blocking solution (2% BSA, 1% GS, 0.5% triton X-100 and 0.02 NaN_3 in PBS) for 1 hour at room temperature. Afterwards, coverslips were transfer into a humidity chamber and they were incubated overnight with the following primary antibodies: anti-RyR1 mouse mAb (1:200, Thermo Scientific), anti-Calst1 rabbit pAb (1:100, Novus Biologicals), anti-PKA rabbit pAb (1:100, Cell Signalling) and anti-CysNO rabbit pAb (1:500, Sigma-Aldrich). PLA assay was performed using the Duolink® In situ Orange kit (Sigma). For counterstaining, cells were incubated with FITC-conjugated Myosin Heavy Chain-CFS mAb (1:50, R&D) for 30 min and they were mounted with ProLong® Gold antifade reagent with DAPI (Life Technologies). High resolution images were acquired using an ECLIPSE Ti-S/L100 microscope (Nikon) equipped with a 20X S-Fluor objective and attached to a lambda-DG4 illumination system and an Orca-Flash2.8 camera (Hammamatsu) with NisElements software.

Image quantification was made using ImageJ (NIH) and the "Batch spot analysis macro" from Dr. Henry Wellcome lab (https://www.uea.ac.uk/biological-sciences/research/facilities/henry-wellcome-lab/macros). This macro allows the analysis of several images at the same time, applying the same parameters in all of them. After setting several parameters to discriminate the specific PLA signal, the macro generates a file with the areas of the detected spots. The spot areas were then divided

into the smallest detected area (2.43 μm), which corresponds to the individual spot size. Finally, the total number of spots per image was normalised to the MyHC area, which corresponds to the total myotube area. At least 4 images per condition were analysed with an average of 8-9 myotubes per image.

Statistical analysis

Data are presented as mean ± SEM. Normal distribution of samples was ensured by Kolmogorov-Smirnov and Shapiro-Wilk tests. Student's *t*- test was performed for paired comparisons and $P < 0.05$ was considered statistically significant.

RESULTS

In vitro cytotoxicity of AHK compounds

In vitro cytotoxicity of S107 and AHK compounds in C2C12 mouse myotube cultures is shown in Figure 3. S107 was found to be extremely toxic at 1-2 mM concentrations, resulting in 100% cell death after 24 hours in culture (Figure 3A). In contrast, most AHK compounds did not shown toxicity, even at higher concentrations (Figure 3B). However, A8, A12 and A13 compounds showed some toxicity (around 10-20%) at 2 mM concentration and A5 displayed toxicity of around 10-20%, starting at 10 μM concentration (Figure 3C).

LHCN-M2 myotube were used to assess the *in vitro* cytotoxicity of S107 and some AHK compounds in human cultures. Similarly to that observed in C2C12 myotubes, S107 resulted in a 100% cell death at 1-2 mM concentrations after 24 hours treatment in human cultures (Figure 4A). Likewise, A6 and A7 were non-toxic, even at higher concentrations. However, two compounds (A9S and A11R) showed mild toxicity (< 30%) at 2 mM concentration (Figure 4B).

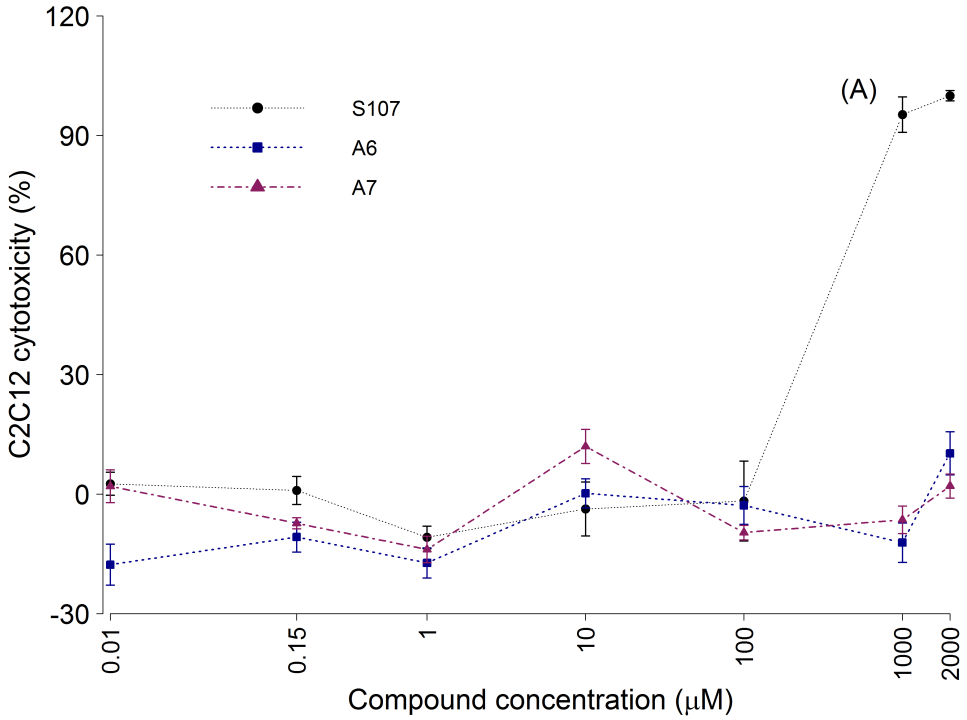
(A)
S107
A6
A7
C2C12 cytotoxicity (%)
120
90
60
30
0
-30
0.01
0.15
1
10
100
1000
2000
Compound concentration (μM)

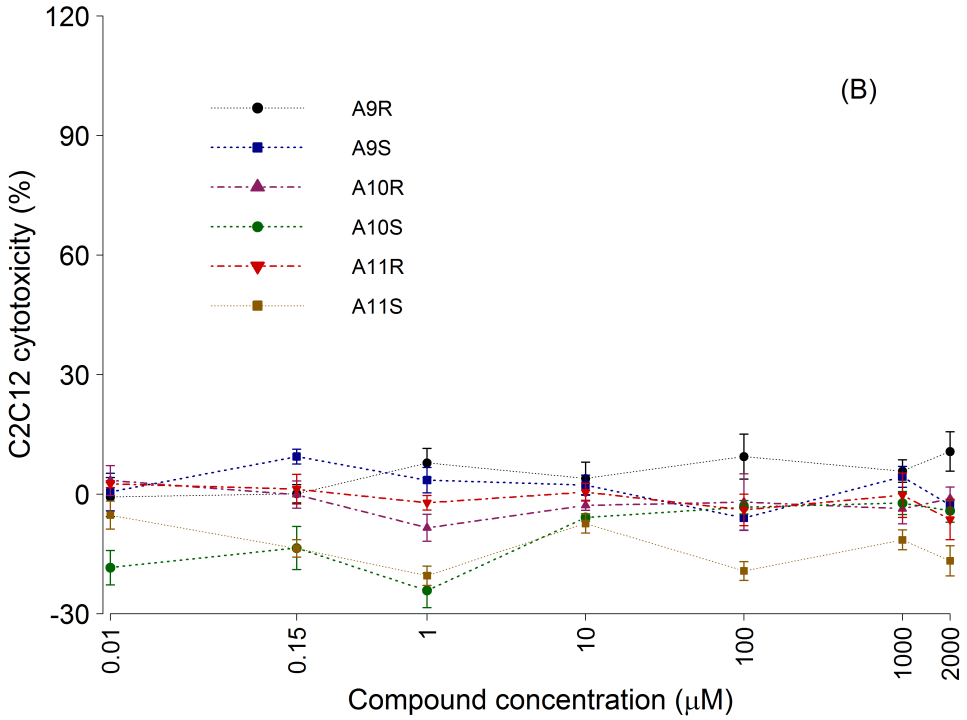
(B)
A9R
A9S
A10R
A10S
A11R
A11S
C2C12 cytotoxicity (%)
120
90
60
30
0
-30
0.01
0.15
1
10
100
1000
2000
Compound concentration (μM)

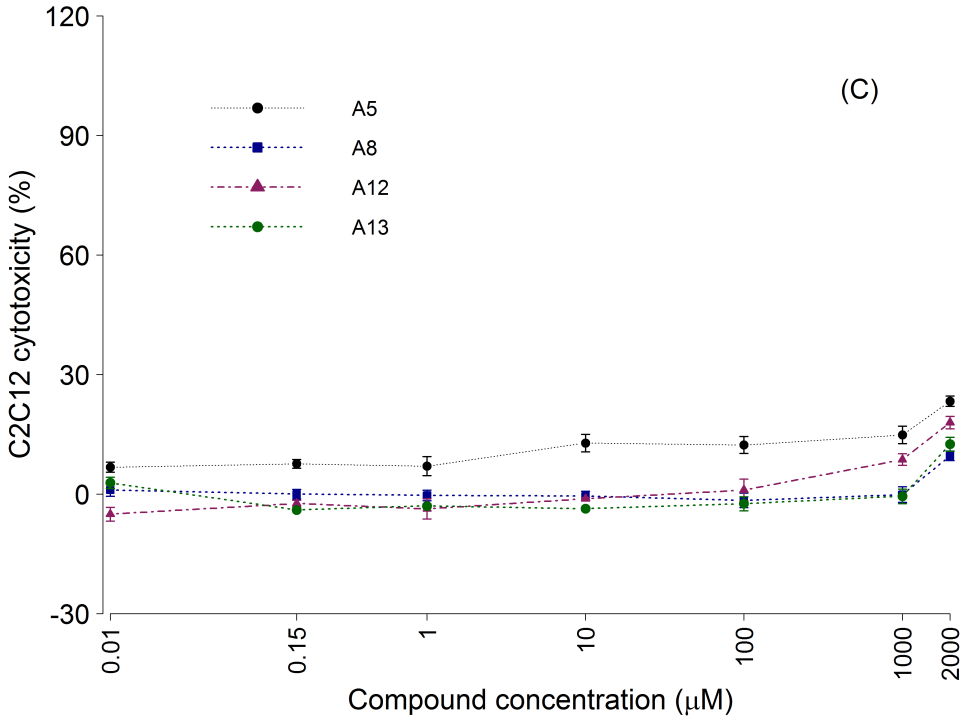

Figure 3. Concentration dependent 24 hours *in vitro* cytotoxicity of (A) S107, A6 and A7, (B) A9R, A9S, A10R, A10S, A11R and A11S and (C) A5, A8, A12 and A13 AHK compounds in 7-days-old C2C12 myotubes. Data are represented as average of the percentage of cell death ± SEM, n = quadruplicates per condition in 3 independent cultures.

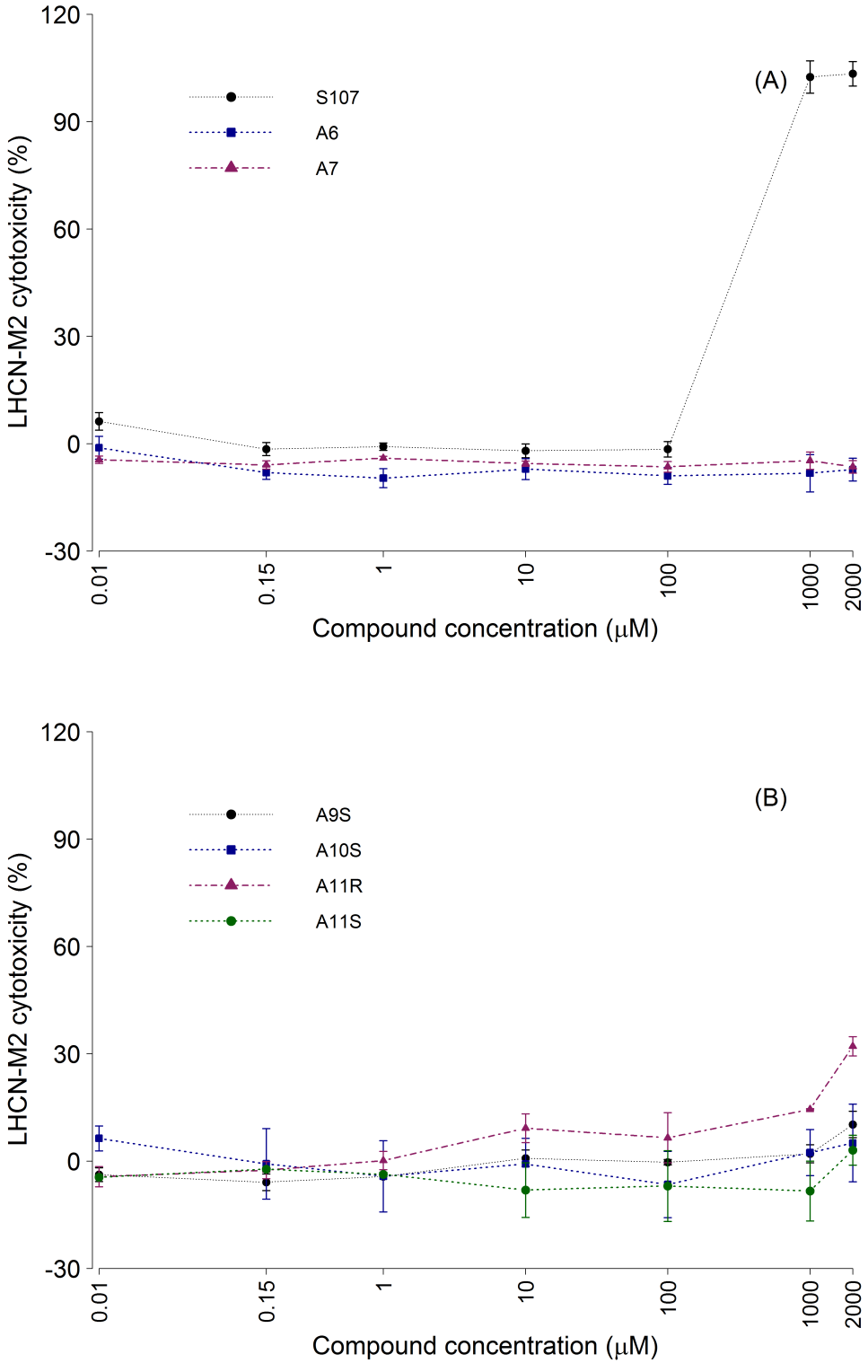

Figure 4. Concentration dependent 24 hours *in vitro* cytotoxicity of (A) S107, A6 and A7 and (B) A9S, A10S, A11R and A11S AHK compounds in 7-days-old myotubes. Data are represented as average of the percentage of cell death ± SEM, n = quadruplicates per condition in 3 independent cultures.

RyR1-Calst1 binding and AHK compounds

In situ proximity ligation assay (PLA) was used to assess RyR1 PKA-phosphorylation and CysNO-nitrosylation in LCHN-M2 myotubes. Using this technique, SIN-1 was found to induce RyR1 phosphorylation and nitrosylation *in vitro* in LHCN-M2 myotubes (Figure 5). In the presence of the peroxynitrite donor, RyR1 phosphorylation was significantly increased 2-folds compared to the non-treated myotubes (100 ± 19.89% in non-treated vs 200.35 ± 22.19% in SIN-1 treated myotubes; paired *t*-test, $P < 0.05$). Likewise, SIN-1 treated myotubes showed a significant increase (17%) of RyR1 nitrosylation (117.49 ± 2.22%) compared to non-treated myotubes (100 ± 3.94%; paired *t*-test, $P < 0.05$).

RyR1-Calst1 interaction was specifically quantified by *in situ* PLA (Figure 6A). In LHCN-M2 myotubes, SIN-1 treatment induced a 60% reduction of RyR1-Calst1 binding (39.87 ± 8.46%) compared to non-treated myotubes (100 ± 9.80%) (paired *t*-test, $P < 0.01$). This reduction was similar to that observed in rapamycin treated myotubes (46.63 ± 2.96%) (Figure 6B).

In relation to pre-treatment of LHCN-M2 myotubes with 150 nM S107, a partial prevention of calstabin1 depletion was observed (Figure 7A). in the presence of S107 Calst1 binding to RyR1 increased in a 33% (39.87 ± 8.46 to 73.29 ± 7.48) (paired *t*-test, $P < 0.05$). Similarly, 150 nM A6 and A7 pre-treatments significantly enhance RyR1-Calst1 binding to 67.45 ± 2.97% and 75.17 ± 10.64% respectively compared to non-treated SIN-1 stressed myotubes (39.87 ± 8.46%) (paired *t*-test, $P < 0.05$) (Figure 7B). However, in absence of SIN-1, the compounds did not change RyR1-Calst1 binding (paired *t*-test, $P > 0.05$) (Figure 8).

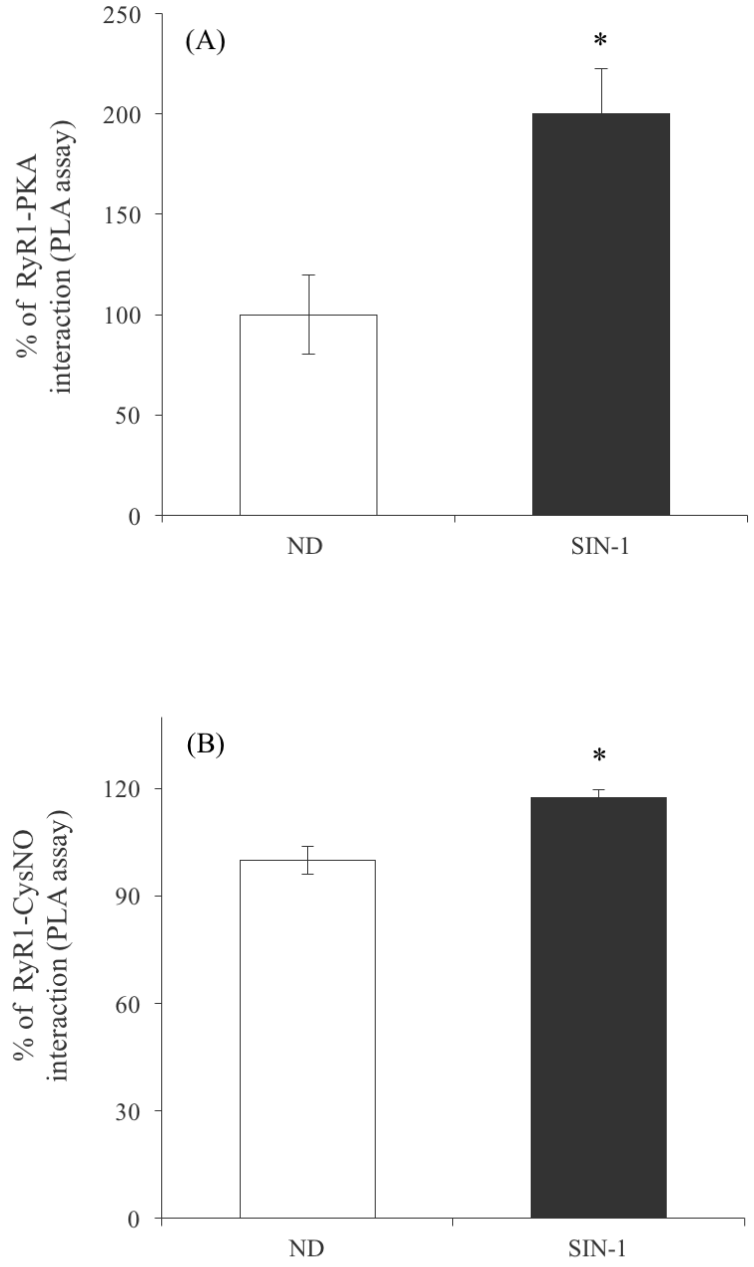

Figure 5. *In situ* proximity ligation assay (PLA) analysis of (A) RyR1 phosphorylation and (B) RyR1 nitrosylation in non-treated (ND) and SIN-1 stressed (SIN-1) LHCN-M2 myotubes. Data are represented as percentage of colocalisation. The unstressed (ND) control was taken as 100%. All data are mean ± SEM, n = 4, * P <0.05 (paired t-test).

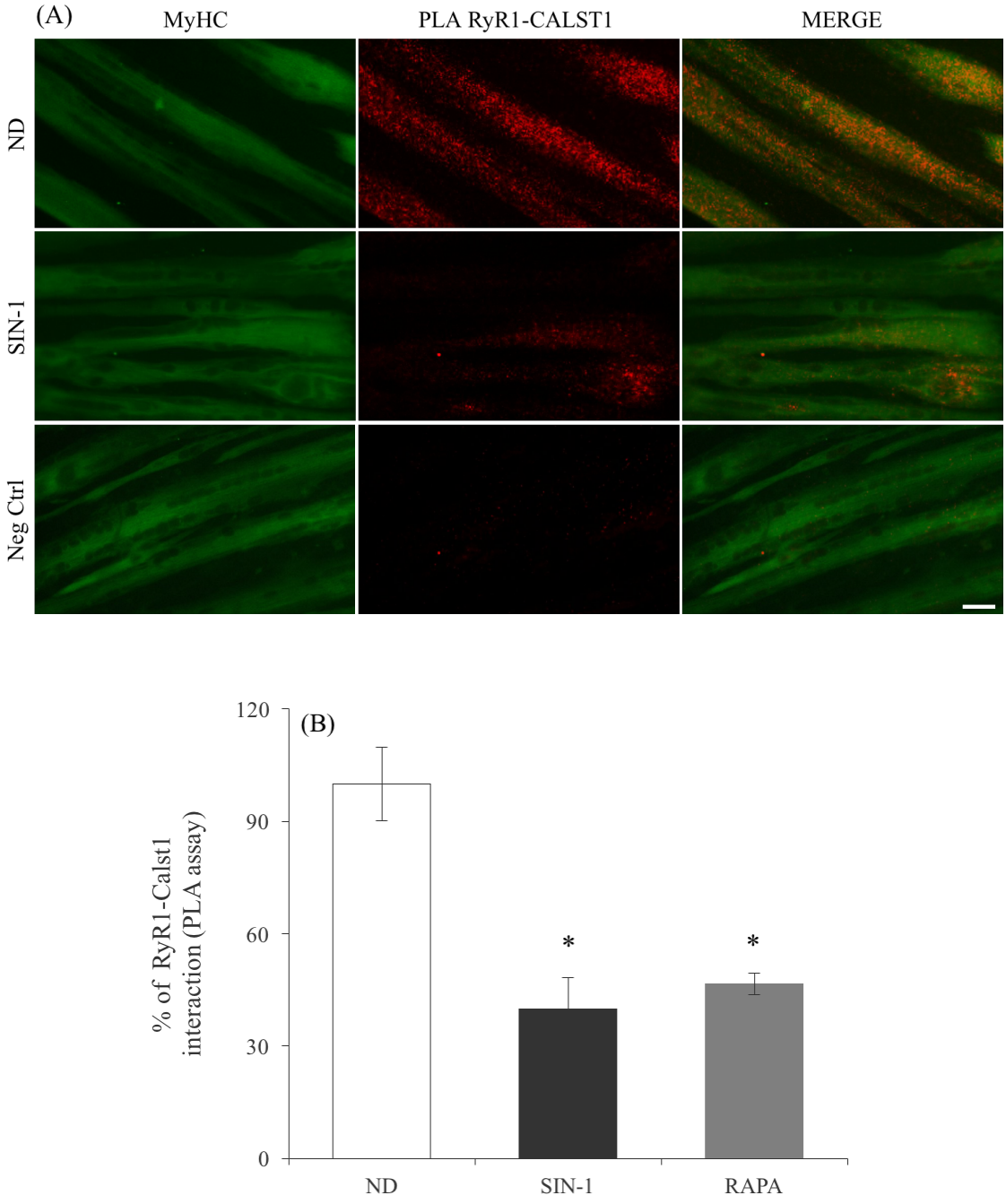

Figure 6. (A) Representative *in situ* proximity ligation assay (PLA) images showing RyR1-Calst1 PLA assay (red) and MyHC (green) in non-stressed (ND) and SIN-1 stressed (SIN-1) LHCN-M2 myotubes. Neg Ctrl corresponds to negative control made with just one primary antibody. Scale bar 25 μm. (B) *In situ* proximity ligation assay (PLA) quantification of RyR1-Calst1 in non-treated (ND), SIN-1 treated (SIN-1) and Rapamycin treated (RAPA) LHCN-M2 myotubes. Data are represented as percentage of colocalisation. The unstressed (ND) control was taken as 100%. All data are mean ± SEM, n = 11-15 from 4 independent cultures, * P <0.05 (paired t-test).

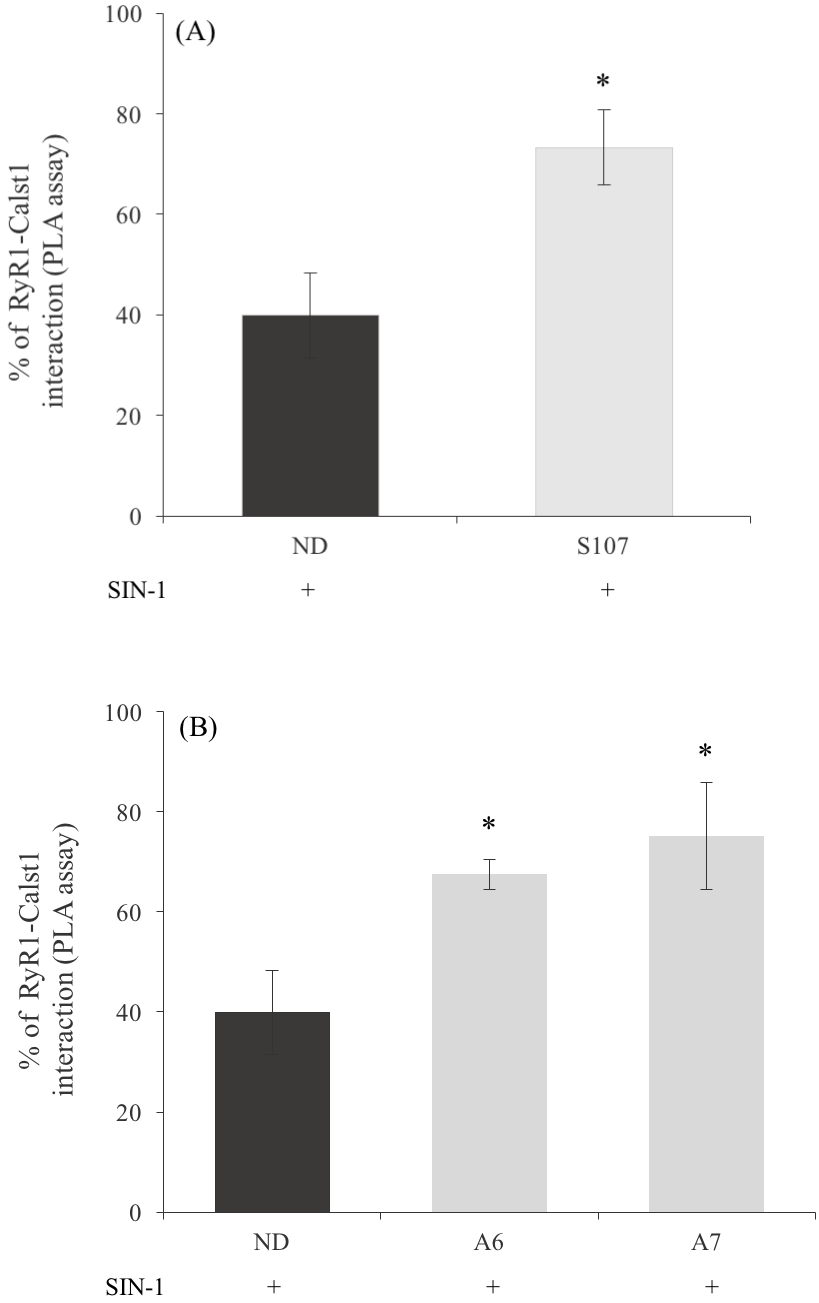

Figure 7. *In situ* proximity ligation assay (PLA) analysis of RyR1-Calst1 in (A) non-treated (ND) and S107 treated (S107) and in (B) non-treated (ND), A6 treated (A6) and A7 treated (A7), SIN-1 stressed LHCN-M2 myotubes. Data are represented as percentage of colocalisation. The unstressed and non-treated control was taken as 100%. All data are mean ± SEM, n = 11-15 from 4 independent cultures, **P* <0.05 (paired *t*-test).

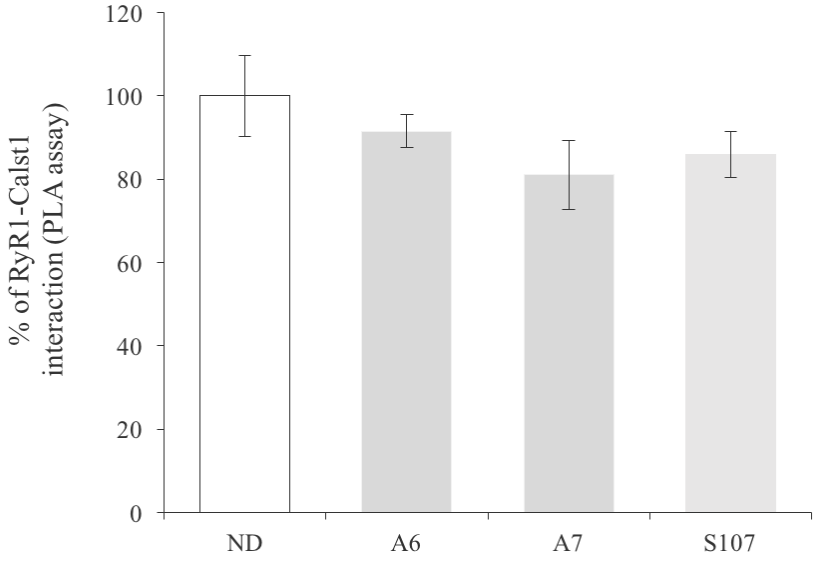

Figure 8. *In situ* proximity ligation assay (PLA) analysis of RyR1-Calst1 in non-treated (ND), A6 treated (A6), A7 treated (A7) and S107 treated (S107) LHCN-M2 myotubes. Data are represented as percentage of colocalisation. The unstressed and non-treated (ND) control was taken as 100%. All data are mean ± SEM, n = 11-15 from 4 independent cultures.

DISCUSSION

In skeletal muscle, RyR1 undergoes post-translational modifications that regulate its physiological function. However, these mechanisms also contribute to the pathogenic mechanism of some diseases via Calst1 depletion and calcium leakage[55,56]. In the present work, a family of novel compounds (AHK compounds) has been presented. These compounds have been designed to specifically interact with this promising target, preventing Calst1 depletion from RyR channel.

In order to elucidate the toxicity profile of AHK compounds, mouse and human myotube cultures were used and LDH release was measured as a cytotoxicity indicator. It should be noted that, LDH measurement in cell culture media is a very extended, cost-effective technique that is used to study the *in vitro* cytotoxicity of a compound during initial drug development stages[208]. This technique allows the simultaneous testing of

high number of compounds easily and in a timely manner, providing a prediction of human toxicity.

The rycal S107 was non-toxic *in vitro* at 150 nM, which was the concentration that was found by previous studies in the plasma of several mouse models after *in vivo* treatment, without any obvious toxicity[55,56]. Remarkably, the results of the present study showed that at higher concentrations (1-2 mM), S107 was extremely toxic inducing the death of all the cells in both mouse and human myotube cultures. Interestingly, AHK compounds (and especially A6 and A7 compounds) presented very low cytotoxicity levels in mouse and human myotubes, even at the higher concentrations (Figures 3 and 4). This finding suggests that these compounds could constitute a safer alternative to the S107 compound.

Up to now, RyR immunoprecipitation from muscle homogenates and the consequent immunoblot study of its binding partners has been the most extended technique to study RyR-Calst interaction and the effect of RyR stabilisers on it[214]. Since, RyR1 immunoprecipitation is a tricky technique, this study proposes that the proximity ligation assay (PLA) could be used as a quantitative and easy technique[212] to study RyR1-Calst1 interaction in heathy human myotubes.

Previous works proposed that SIN-1 treatment could induce RyR1 phosphorylation and S-nitrosylation[206,210]. Accordingly, in the present study, treating healthy human myotubes with SIN-1 significantly increased RyR1 phosphorylation and S-nitrosylation *in vitro*. Several works have found a correlation between these RyR1 post-translational modifications and Calst1 dissociation from the channel[21,48]. Using SIN-1 treated human myotubes model, we confirmed that RyR1 phosphorylation and S-nitrosylation led to a subsequent Calst1 depletion from the channel similar to that produced by rapamycin, a well-known pharmacological Calst1 inhibitor[36]. Additionally, this effect was partially recovered with S107 treatment, as previously reported in mouse models of several muscular diseases and some physiological conditions such as chronic exercise and aging[55,56,197,207].

AHK compounds are small molecules that have been designed *in silico* using molecular docking to interact with RyR1-Calst1 complex and enhance its binding affinity (unpublished data). In this work, we have demonstrated that A6 and A7 compounds partially recover RyR1-Calst1 binding, similarly to that observed with S107 treatment (Figure 7). In contrast, in the absence of SIN-1, none of the compounds changed the amount of RyR1-Calst1 interaction, suggesting that the compounds act specifically by preventing calstabin depletion from abnormally modified ryanodine channels.

In summary, these results indicate that proximity ligation assay (PLA) technique in combination with SIN-1 treated healthy human myotubes model could be used to easily study RyR1 post-translational modifications and Calst1 binding. Hence, this technique could be used to test the effect of novel RyR stabilisers on this interaction. Additionally, it has been demonstrated that AHK compounds efficiently enhance RyR1-Calst1 binding *in vitro* in human myotube cultures without showing any toxicity, suggesting that they could constitute a safer alternative to the previously reported S107 (Armgo Pharma).

In conclusion. based on the results obtained in this work, A6 and A7 AHK compounds were selected for the *in vivo* experiments owing to their low toxicity profiles in mouse and human cellular models and their ability to enhance RyR1-Cals1 binding.

CHAPTER 2:

Effect of Ahulken compounds in mdx mouse model of Duchenne muscular dystrophy

INTRODUCTION

Duchenne muscular dystrophy (DMD) is an inherited X-linked genetic disorder caused by mutations in *DMD* gene. This gene encodes for dystrophin, an intracellular protein that forms part of the dystrophin glycoprotein complex (DGC). This complex connects the extracellular matrix to the actin cytoskeleton, stabilising the myofibre membrane during repeated muscle contractions. In addition, the DGC serves as a scaffold for several signalling proteins that are essential for muscle function[75]. Thus, absence of dystrophin leads to membrane damage and a consequent uncontrolled calcium influx, which activates several pathological pathways and produces muscle wasting and premature death. Unfortunately, no efficient therapies are available to treat these patients.

Up to now, more than 60 animal models of DMD have been described[94]. The mdx mouse (C57BL/10ScSn-Dmdmdx/J) is the most widely used model. This mouse line presents a spontaneous nonsense point mutation in exon 23, which results in absence of dystrophin (DYST) protein. Although mild, mdx mice recapitulate several dystrophic features present in Duchenne patients, such as elevated serum CK levels, muscle degeneration, cardiac damage and cognitive dysfunction[94,115,215]. For these reasons, mdx mice represent an essential model to further investigate molecular mechanisms underlying DMD and test novel therapeutic agents against this disease.

It is also known that, defects in calcium homeostasis are implicated in DMD pathophysiology[30]. Biopsies from DMD patients showed calcium accumulation evidences and hypercontracted fibres[102,216]. In addition, pre-necrotic DMD fibres from foetuses and premature infants showed calcium accumulation[217], suggesting that the dysregulation of calcium homeostasis is an early event that triggers muscle degeneration in DMD. Accordingly, increased intracellular calcium levels have also been observed in mouse models of DMD (mdx mice) [30,104]. In this context, several mechanisms have been proposed to explain the increased calcium levels in dystrophin deficient muscles,

including increased calcium influx through the myofibre membrane, abnormal SR calcium levels or leaky calcium channels[30].

Specifically, in mdx mouse model, ryanodine receptor type 1 (RyR1) has been found to be abnormally nitrosylated and phosphorylated. These post-translational modifications lead to a reduction of its binding, affinity to calstabin 1 (Calst1) and a subsequent calcium leak through the channel[55]. RyR stabilisers (rycals) have demonstrated to efficiently increase RyR1-Calst1 binding reducing calcium leak and improving dystrophic phenotype[55,56]. Based on this mechanism, a novel family of compounds, named as Ahulken (AHK), has been specifically designed as a safer alternative to the pre-existing rycals to treat Duchenne patients (unpublished data; Chapter 1). However, studies showing the *in vivo* effects of AHK compounds in dystrophic models are needed in order to validate their efficacy.

Therefore, the aim of the current study was to test the effect of the AHK compounds A6 and A7, and the rycal S107 (Armgo Pharma) in mdx mice *in vivo* and *ex vivo* using isolated fibres from *flexor digitorum brevis* muscles.

METHODS

Mouse lines and treatment administration

C57BL/10ScSn-Dmd/J mice (hereafter mdx) and C57BL/10ScSnJ mice (hereafter wild type), were obtained from The Jackson Laboratory (Bar Harbor, ME, USA). Aged-matched 1-moth-old male mice were randomly assigned to treatments with S107, A6, A7 or vehicle (H_2O). Treatments were administered in drinking water for 5 weeks at 0.25 mg/mL concentration and water consumption and mice weight were daily monitored. All experiments were conducted in accordance with protocols approved by the Institutional Animal Care Ethical Board Committee of the Donostia University Hospital.

Treadmill exercise

In order to exacerbate dystrophic phenotype, mice were exercised in a treadmill once per week during the first two weeks of treatment and twice per week during the rest of the experiment. The exercise protocol consisted in acclimation with gentle walking for 2 min at 7 cm/s speed, followed by 8 min at 13 cm/s. The main exercise session involved 30 min running at 20 cm/s speed. Mice were forced to finish the exercise by application of low-intensity electric shock.

Calcium imaging in FDB muscle fibres

Calcium imaging experiments were performed *ex vivo* in isolated *flexor digitorum brevis* (FDB) muscle fibres from wild type (wt) and mdx mice. Briefly, FDB muscles were dissected and placed in Mammalian Ringer buffer (145 mM NaCl, 1 mM $MgSO_4$, 2,5 mM KCl, 10 mM HEPES, 10 mM Glucose and 1 mM $CaCl_2$) with 2 mg/mL collagenase 1A. After 2 hours in agitation at 37 ºC, collagenase was neutralised with 3 volumes of FDB medium (DMEM, 2% FBS and 5 mg/mL Gentamicin). Thereafter, fibres were allowed to set and upper medium was discarded to remove debris. Finally, fibres were centrifuged at 1000 rpm for 1 min and they were seeded in ECM coated 12 mm dishes in FDB medium. For *in vitro* studies, fibres were treated overnight with the RyR modulators (A6, A7 or S107) at 150 nM concentration.

Ratiometric calcium dye Fura-2AM was used to measure resting intracellular calcium levels in isolated muscle fibres. First, fibres were loaded with 4 μM Fura-2AM and 0.02 % pluronic acid for 30 min at 37ºC in culture medium. After, fibres were placed in Ringer solution (125 mM NaCl, 5 mM KCl, 1.2 mM $MgSO_4$, 6 mM glucose, 2 mM $CaCl_2$ and 25 mM HEPES, pH 7.4) for other 30 min at 37 ºC to remove extracellular dye and allow to de-esterification. Experiments were performed under continuous perfusion (2 mL/min; 37 ºC) with Ringer buffer using an ECLIPSE Ti/L100 microscope (Nikon) equipped with a 20X S-Fluor objective and attached to a lambda-DG4 illumination system. Image acquisition was performed using an Orca-Flash 2.8 camera

(Hamamatsu) and the NisElemments-Advanced Research software (Nikon). Intracellular calcium concentration was estimated by the ratio of Fura-2AM fluorescence intensities at 340 and 380 nm after background correction.

Serum creatine kinase

Blood was collected by intracardiac puncture in isoflurane anesthetised mice. Samples were centrifuged at 6000 *g* for 10 min at 4ºC and serum was kept at -80ºC until analysis. Creatine kinase determination was performed in Biochemistry Service of the Donostia University Hospital following a standardised photometric technique. Haemolysed samples were discarded.

Grip Strength test

Forelimb grip strength was weekly determined using a grip strength meter (Bioseb) in exercised mice following standard procedures (TREAT-NMD SOP ID: SMA_M.2.1.002). Mice were lifted by the tail and left to grasp the grid with the forelimbs. Five consecutive measurements were done leaving mice to rest 1 min between them and only the three highest measurements were considered. Data were normalised to the mice weight.

Ex vivo force measurement in isolated muscle

Ex vivo force measurement experiments were performed in collaboration with Dr Thomas Rando lab at Stanford University (USA). Specific force was measured in isolated *tibialis anterior* muscle (TA) from mdx mice treated for 6 weeks with A6.

Force experiments were performed in an 800A *in vivo* apparatus attached to a 701C stimulator (Aurora Scientific). The testing chamber was filled with Kreb solution (Sigma) and kept at 25 ºC using an external water heater. Additionally, chamber was oxygenated with a 95% O_2, 5% CO_2 mixture to ensure tissue viability. Calibrated Dynamic Muscle Control and Analysis Software (Aurora Scientific) was used to acquire muscle force measurements.

After sacrificing the mice, *tibialis anterior* (TA) muscle was excised and attached to the force transducer lever around the top of the patellar tendon and the TA tendon. First, supramaximal stimulation conditions were established to ensure the recruitment of all fibres from the muscle. After selecting the voltage that produced the most powerful twitches, the optimum muscle length was selected. For this purpose, twitch forces produced after 6 electrical pulses of 1 ms each at 1 Hz were measured at different TA lengths and the stretched length at which the highest force was obtained was selected. Muscles were allowed to rest one minute between each electric pulse. After determining the optimal voltage and length, a 500 ms tetanic stimulation was performed at 100 Hz and muscle maximum tetanic force was measured. Finally, muscle was weighted and specific force was calculated.

Histology

Mice were sacrificed by cervical dislocation at the end of the treatment and diaphragm and *tibialis anterior* muscles were dissected for histological studies. Diaphragms were first placed in a relaxing solution (100 mM KCl, 2 mM EGTA, 4 mM ATP and 7 mM $MgCl_2$, pH 7). Next, right hemi-diaphragms were embedded in OCT and snap-frozen in liquid nitrogen-cooled isopentane. On the other hand, *tibialis anterior* muscles were mounted onto a cork slice with OCT and they were snap frozen in liquid nitrogen-cooled isopentane. All muscles were stored at -80 ºC until sectioning.

Cross-sections of 7 μm were performed in a Leica CM1950 cryostat. Sections were fixed with pre-cooled acetone and blocked (2% BSA, 1% GS, 0.5% Triton X100 and 0.02% NaN_3 in PBS) for 1 hour. Afterwards, sections were incubated with primary antibodies collagen IV (Sigma; 1:1000) and dystrophin (Mandra1, Sigma; 1:100) overnight at 4 ºC. After washing, samples were incubated with Alexa Fluor 488 or 555-conjugated secondary antibodies for 1 hour at room temperature. Finally, slides were mounted with ProLong® Gold antifade reagent with DAPI (Life technologies) and images were acquired using an ECLIPSE 80i microscope (Nikon) equipped with a 10X objective and a DS-U2 camera (Nikon).

Collagen IV and DAPI stained sections were used for central nucleation quantification. Central nucleation was defined as the percentage of fibres presenting at least one central nucleus. At least four (10X) images per mice were analysed.

RESULTS

AHK consumption and tolerance

AHK compound are well tolerated orally. Mice drank around 2.5-3 mL per day, which constitutes a dose of 31.5-37.5 mg $kg^{-1}day^{-1}$ (Figure 1). No significant differences were detected between the different groups of treatments during the 5 weeks of experiment (One-way ANOVA, Tukey´s Post hoc test, $P > 0.05$). Similarly, no significant differences in body weight were found between wild type, mdx and treatment groups (Figure 2).

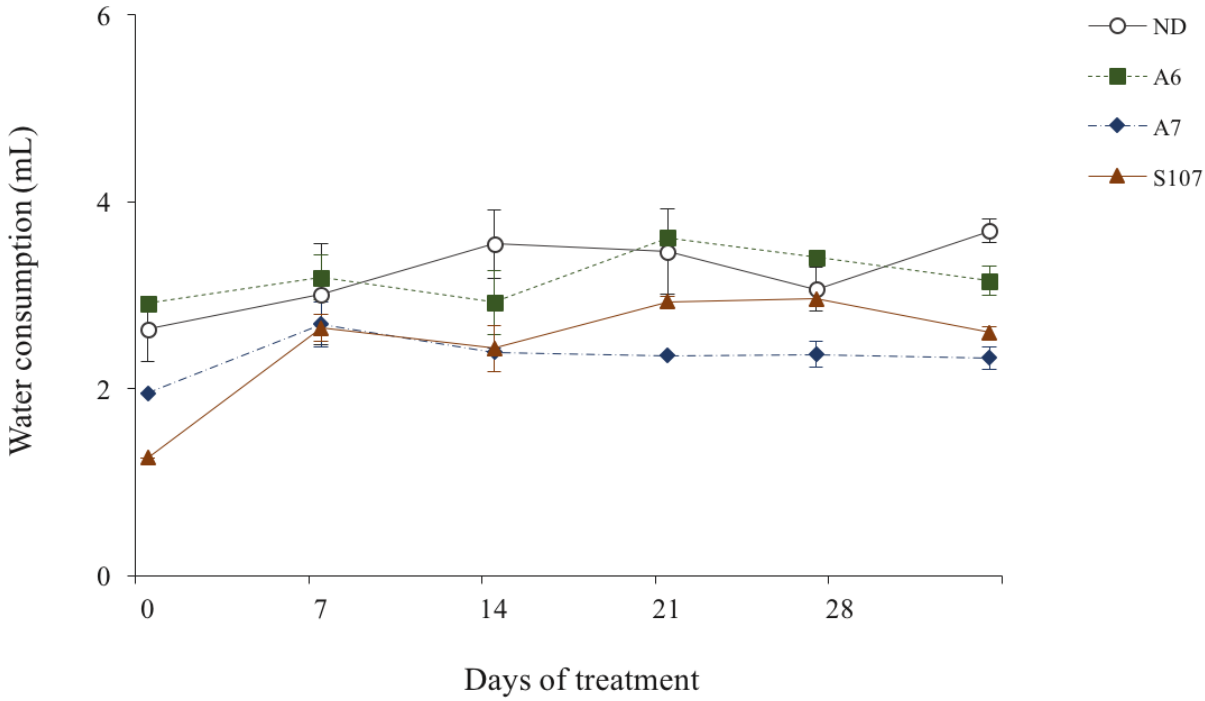

Figure 1. Water consumption per mice in vehicle treated (ND), A6 treated (A6), A7 treated (A7) and S107 treated (S107) mice. Data are represented as average ± SEM, n = 11 ND; n = 10 A6; n = 6 A7; n = 6 S107.

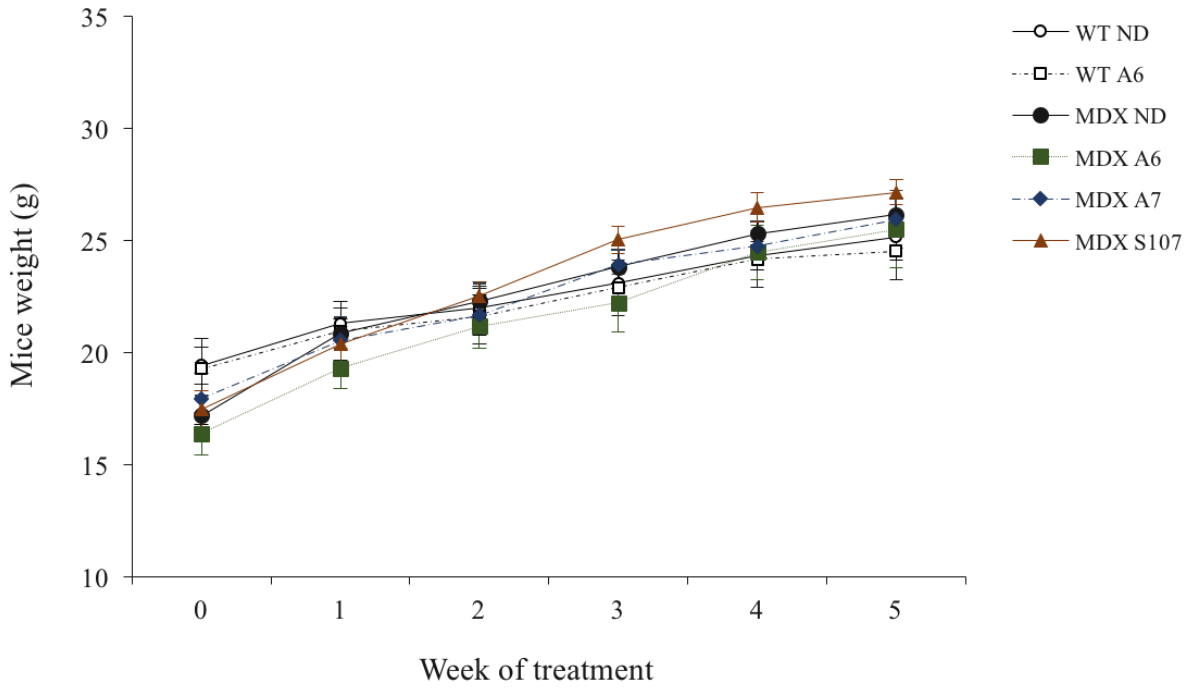

Figure 2. Body weight changes during treatment in vehicle treated wild type (WT ND), A6 treated wild type (WT A6), vehicle treated mdx (MDX ND), A6 treated mdx (MDX A6), A7 treated mdx (MDX A7) and S107 treated mdx (MDX S107) mice. Data are represented as average ± SEM, n = 10 WT ND; n = 6 WT A6; n = 11 MDX ND; n = 10 MDX A6; n = 6 MDX A7; n = 6 MDX S107.

AHK and calcium homeostasis

Single fibres from mdx mice showed significantly higher resting intracellular calcium levels compared to wild type fibres (0.60 ± 0.01 vs 0.54 ±0.07, $P<0.001$) (Figure 3A-C). In mdx fibres, overnight *in vitro* treatment with RyR modulators (AHK and S107) at 150 nM concentration significantly reduced resting intracellular calcium to wild type levels (Kruskal–Wallis, $P < 0.05$) (Figure 3C). In contrast, single fibres from *in vivo* treated mdx mice showed a significant reduction of calcium levels only with AHK treatment, but not with S107 (Kruskal–Wallis, $P < 0.05$) (Figure 3D).

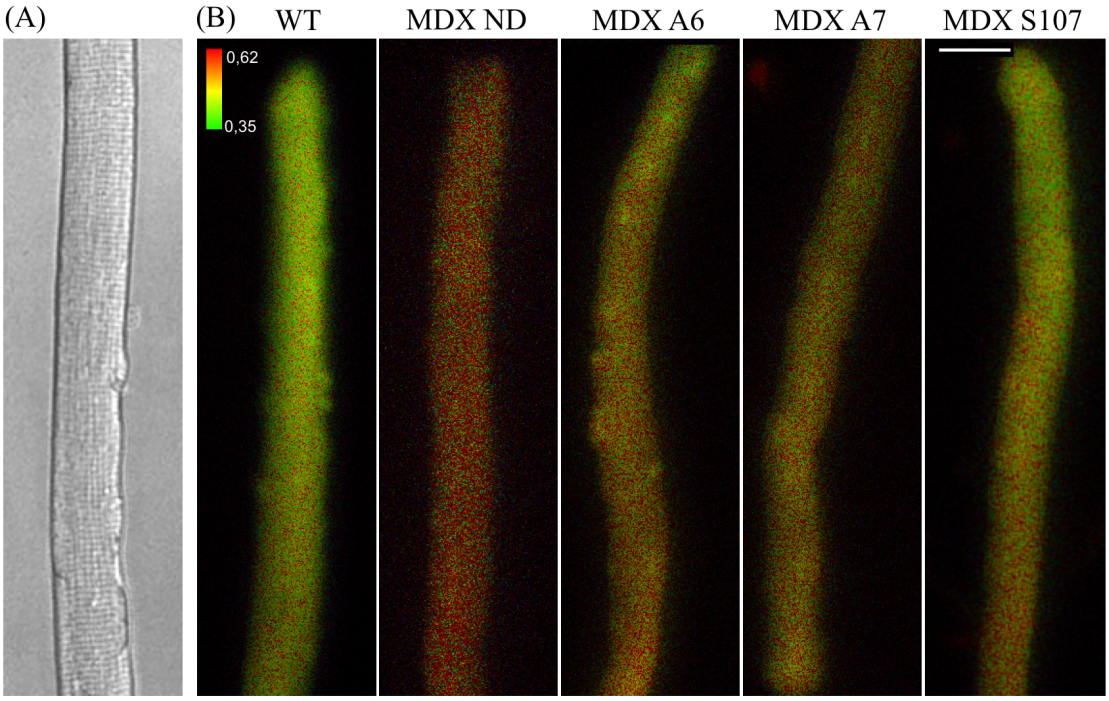
(A)
(B)
WT
MDX ND
MDX A6
MDX A7
MDX S107
0,62
0,35

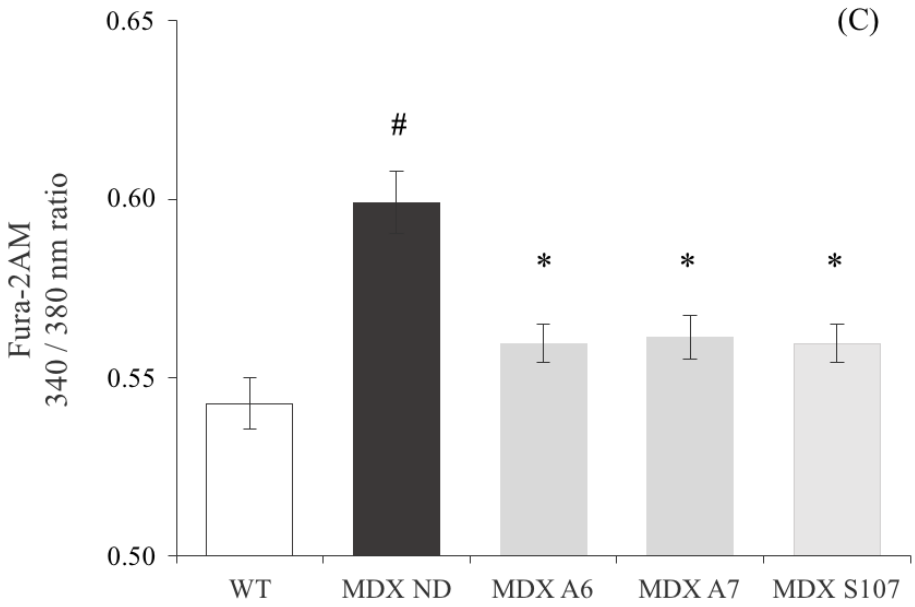
(C)
Fura-2AM
340 / 380 nm ratio
0.65
0.60
0.55
0.50
#
*
*
*
WT
MDX ND
MDX A6
MDX A7
MDX S107

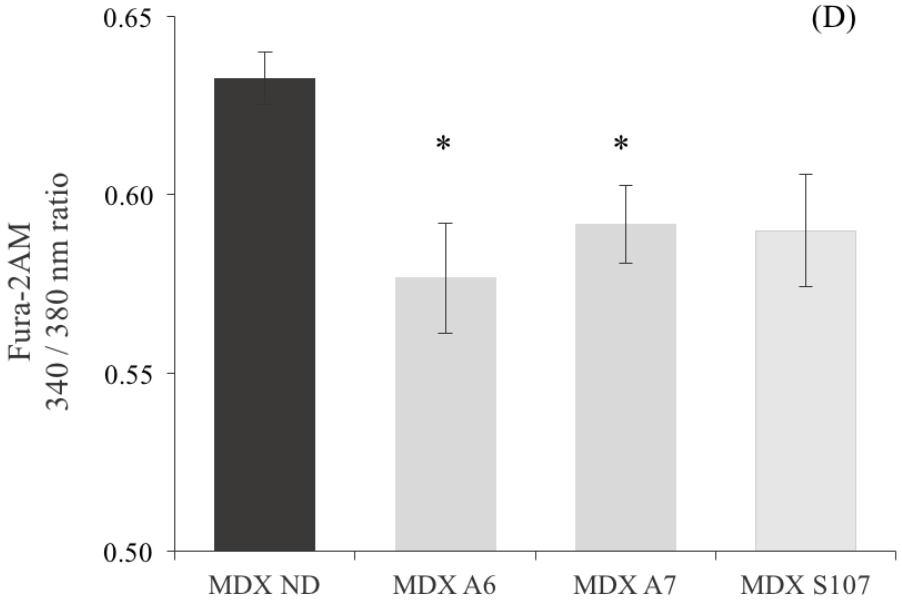

Figure 3. (A) Single fibre isolated from FDB muscle showing characteristic striation pattern. (B) Representative pseudocolor images of Fura-2AM loaded fibres from wild type (WT), non-treated mdx (ND MDX), A6 treated mdx (MDX A6), A7 treated mdx (A7 MDX) and S107 treated mdx (MDX S107) mice. Scale bar 25µm. (C) Resting intracellular calcium levels of FDB-isolated fibres from wild type (WT), non-treated mdx (MDX ND) mice after overnight *in vitro* treatment with A6 (MDX A6), A7 (MDX A7) and S107 (MDX S107). Data are represented as average ± SEM, n = 53 WT; n = 97 MDX ND; n = 78 MDX A6; n = 83 MDX A7; n = 78 MDX S107 fibres analysed. # vs WT and * vs non-treated (ND) P <0.05 (Kruskal-Wallis). (D) Resting intracellular calcium levels of FDB-isolated fibres from *in vivo* treated vehicle treated mdx (MDX ND), A6 treated mdx (MDX A6), A7 treated mdx (MDX A7) and S107 treated mdx (MDX S107) mice after 5 weeks of treatment. Data are represented as average ± SEM, n = 133 MDX ND; n = 135 MDX A6; n = 145 MDX A7; n = 78 MDX S107 fibres analysed from at least 3 mice per condition. * P <0.05 (Kruskal-Wallis).

Serum CK levels

Dystrophic mice (mdx) showed a significant increase in serum creatine kinase levels compared to wild type (wt) mice (16065.70 ± 2527.61 vs 3524.77 ± 709.05 U/L; One-way ANOVA Tukey´s Post hoc test, $P < 0.05$). After 5-weeks treatment, A6 significantly reduced serum CK levels in mdx mice (8505.82 ± 1291.41 U/L; One-way ANOVA Tukey´s Post hoc test, $P < 0.05$). On the other hand, A7 and S107 showed a

tendency to reduce serum CK levels (10183 ± 716.94 U/L and 7914 ± 1514.89 U/L, respectively; One-way ANOVA Tukey´s Post hoc test, $P > 0.05$) (Figure 4).

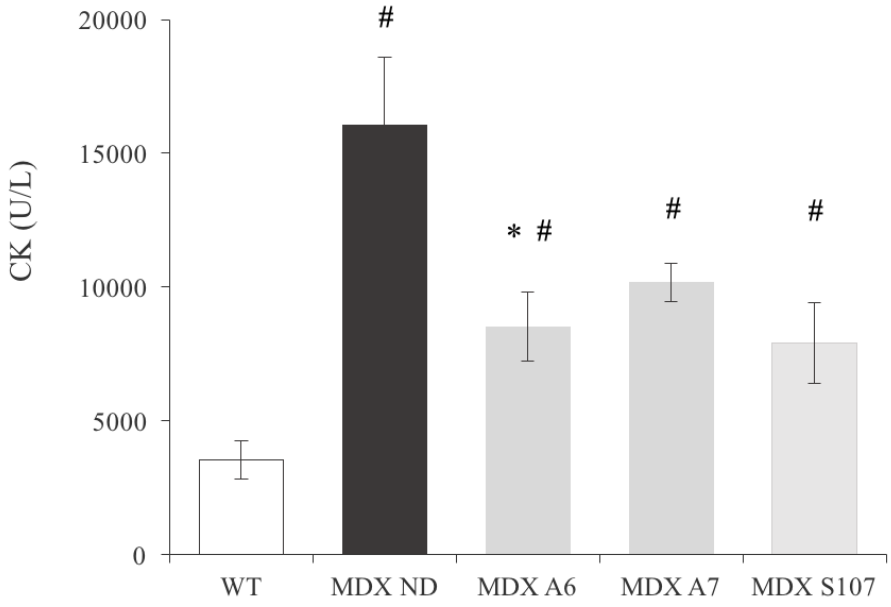

Figure 4. Serum creatine kinase (CK) levels of wild type (WT), non-treated mdx (MDX ND), A6 treated mdx (MDX A6), A7 treated mdx (MDX A7) and S107 treated mdx (MDX S107) mice after 5 weeks of treatment. Data are represented as average ± SEM, n = 4 WT; n = 3 MDX ND; n = 4 MDX A6; n = 3 MDX A7; n = 4 MDX S107. # vs WT and * vs non-treated (ND) $P < 0.05$ (One-way ANOVA Tukey´s Post hoc test).

AHK effect in muscle strength

Grip strength test results showed that mdx mice present a significant 35% reduction in forelimb strength compared to wt mice (4.66 ± 0.14 in wt vs 3.04 ± 0.11 in mdx) (Figure 5A). Treatment with AHK or S107, significantly increased grip strength of mdx mice in a 30-40% (One-way ANOVA Tukey´s Post hoc test; $P < 0.05$) without having any detectable effect in wild type mice (Figure 5B).

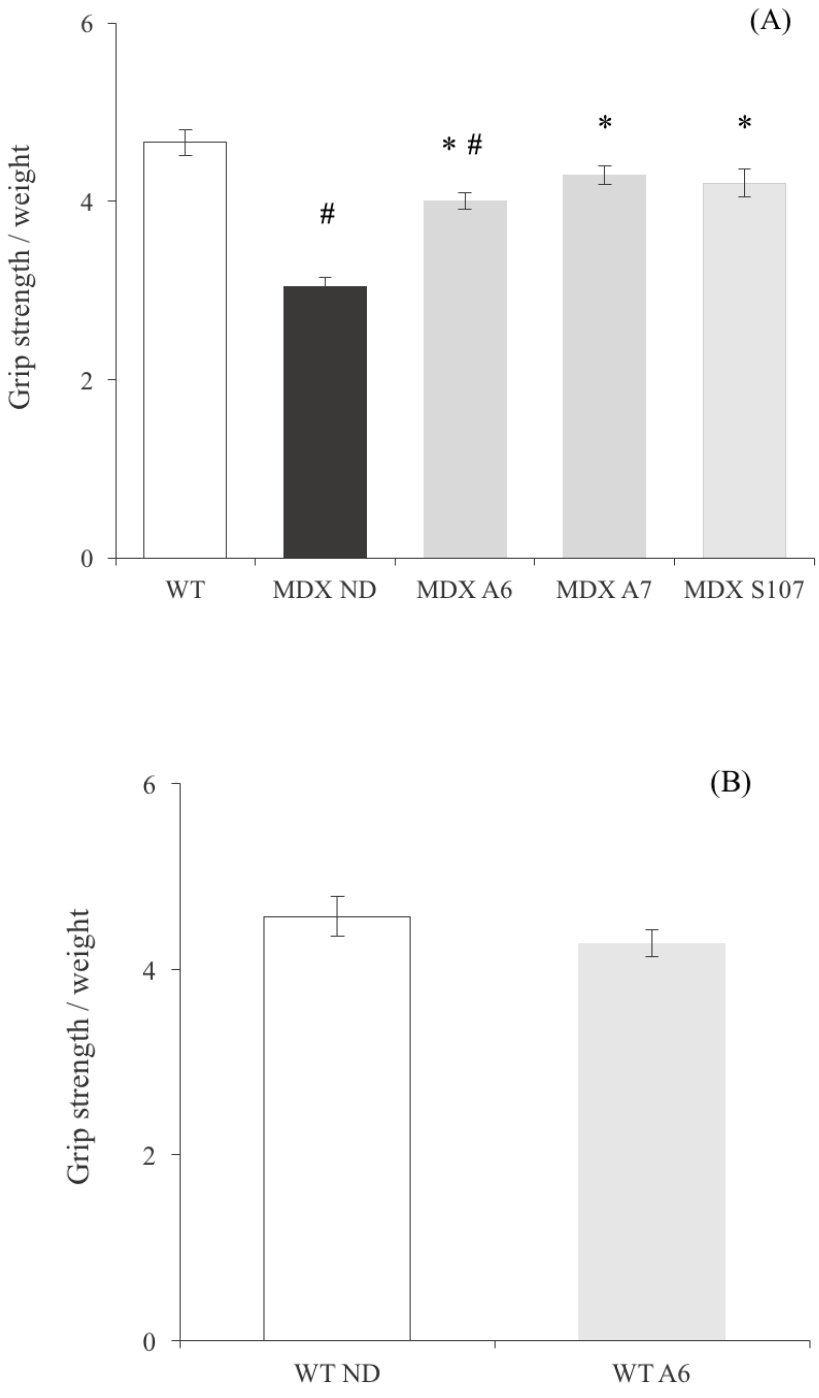

Figure 5. Forelimb grip strength of (A) wild type (WT), non-treated mdx (MDX ND), A6 treated mdx (MDX A6), A7 treated mdx (MDX A7) and S107 treated mdx (MDX S107) mice and (B) non-treated wild type (WT) and A6 treated wild type (WT A6) mice after 5-weeks of treatment. Data are represented as average ± SEM, n = 10 WT; n = 11 MDX ND; n = 10 MDX A6; n = 6 MDX A7; n = 6 MDX S107; n = 6 WT A6. # vs WT and * vs non-treated (ND) P <0.05 (One-way ANOVA Tukey´s Post hoc test).

In order to validate grip strength results, muscle specific force was measured *ex vivo* in *tibialis anterior* muscle of wt and mdx mice. Similarly to that observed using the grip test, dystrophic mice also showed a significant reduction in TA muscle specific force (18.79 ± 0.24 in wt vs 9.59 ± 0.18 in mdx; One-way ANOVA Tukey´s Post hoc test, $P < 0.05$), while A6 treatment resulted in a 16% increase of dystrophic TA specific force (One-way ANOVA Tukey´s Post hoc test, $P < 0.05$) (Figure 6).

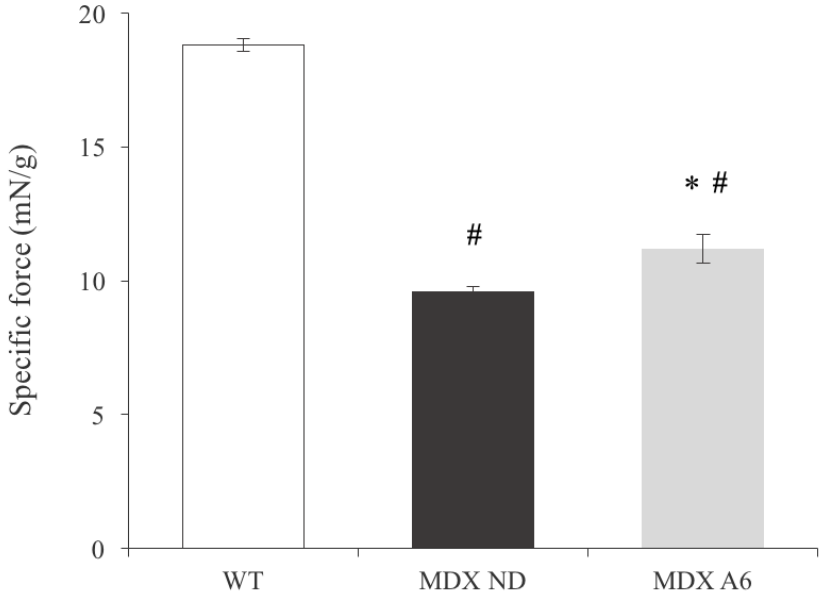

Figure 6. Tibilis anterior force measurements in wild type (WT), non-treated mdx (MDX ND) and A6 treated mdx (MDX A6) mice after 6-weeks of treatment. Data are represented as average ± SEM, n = 9 WT; n = 9 MDX ND; n = 9MDX A6. # vs WT and * vs non-treated (ND) $P < 0.05$ (One-way ANOVA Tukey´s Post hoc test).

In non-treated mice, the results obtained with grip strength test strongly correlated with the ones from the *ex vivo* force measurement experiments (Rs = 0.901; $p < 0.01$) (Figure 7A). In contrast, the simultaneous analysis of the non-treated and the treated mice, showed a weaker correlation between both tests (Rs = 0.635; $p < 0.01$) (Figure 7B).

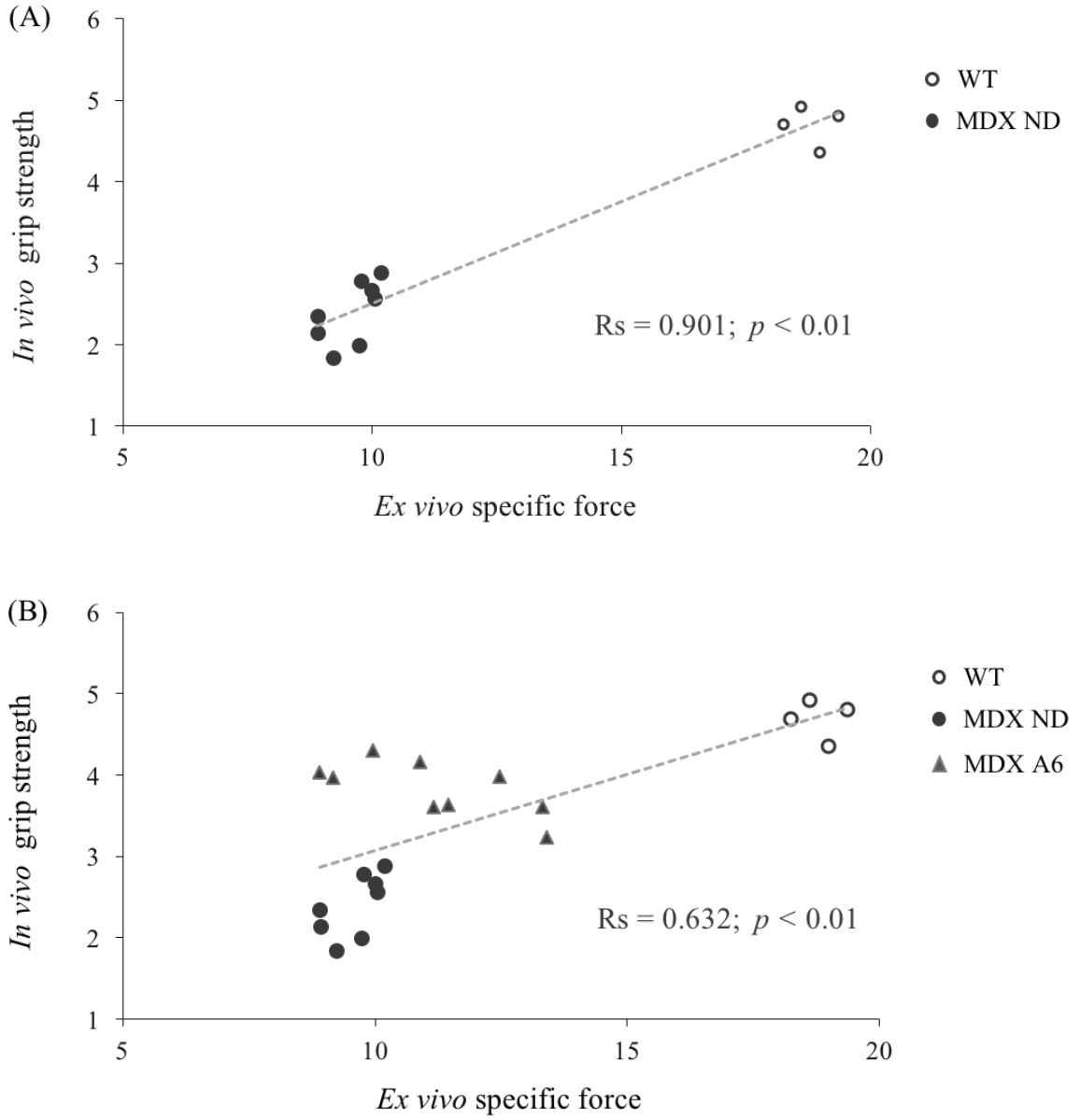

Figure 7. Relationship between grip strength and ex vivo force measurement data. (A) wild-type (WT) and non-treated mdx (MDX ND) mice. (B) wild-type (WT), non-treated mdx (MDX ND) and A6-treated mdx (MDX A6) mice. Rs = Spearman´s rank correlation coefficient.

Histological evidence of muscle damage

Diaphragm muscles from mdx mice showed a 45.09 ± 1.96% of centrally nucleated fibres which was significantly higher than the one found in wild type mice (5.05% ± 0.67) (One-way ANOVA Tukey´s Post hoc test, $P < 0.05$) (Figure 8). 5-weeks treatment with the compounds A6 and A7, as well as with S107, significantly reduced

the percentage of fibres with central nuclei in a 28%, 20% and 19% respectively (Figure 8B).

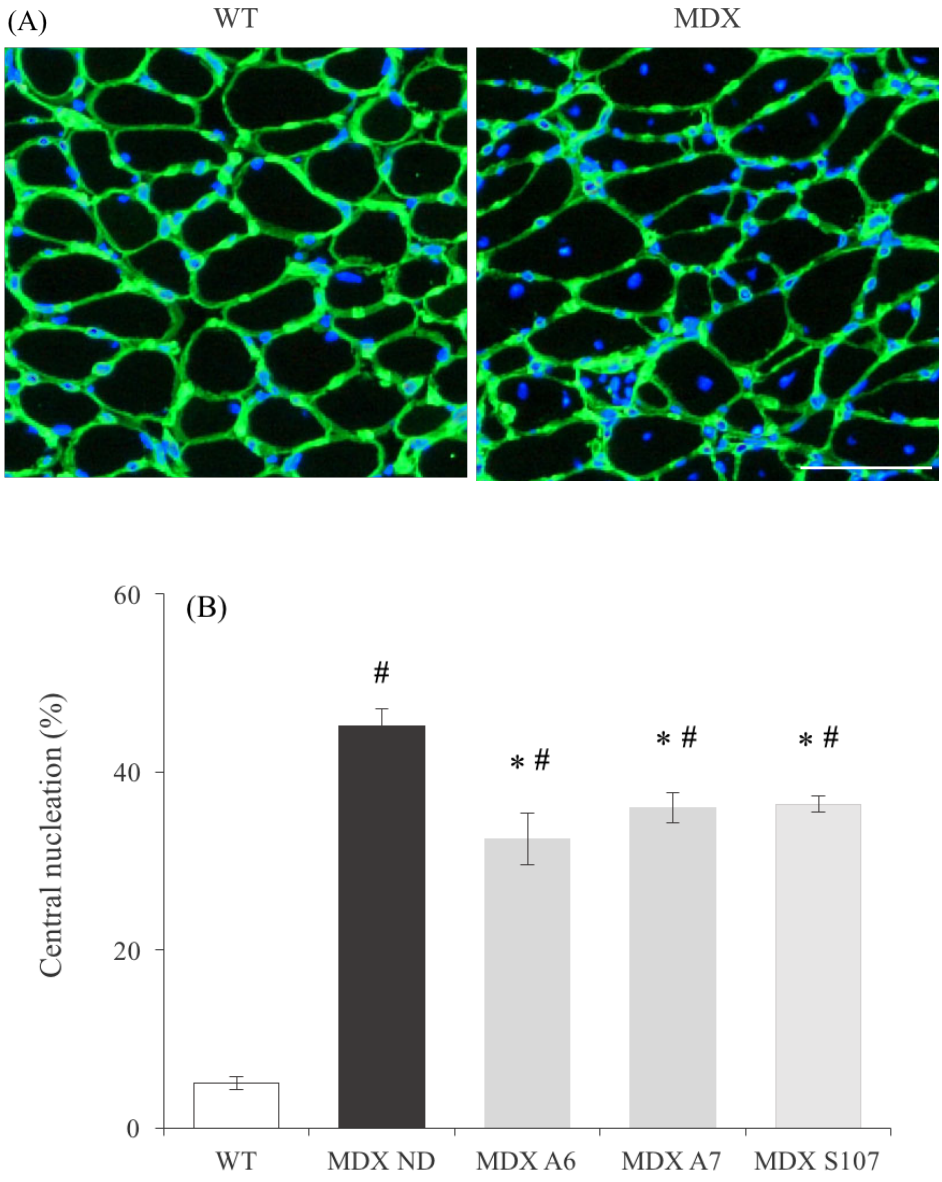

Figure 8. (A) Diaphragm cryostat sections from wild type (WT) and mdx (MDX) mice stained for collagen IV (green) and nuclei (blue) showing central nucleation in dystrophic muscle. Scale bar 100 µm. (B) Quantification of myofibre central nucleation in diaphragm muscles from wild type (WT), non-treated mdx (MDX ND), A6 treated mdx (MDX A6), A7 treated mdx (MDX A7) and S107 treated mdx (MDX S107) mice after 5-weeks of treatment. Data are represented as average ± SEM, n = 3 WT; n = 9 MDX ND; n = 7 MDX A6; n = 6 MDX A7; n = 6 MDX S107. # vs WT and * vs non-treated (ND) P <0.05 (One-way ANOVA Tukey´s Post hoc test).

A similar effect was observed in TA muscle, were mdx mice showed a 57.66 ± 1.89% of central nucleation. In TA muscle A6 and A7 significantly reduced central nucleation to 44.56 ± 1.21% and 45.25 ± 3.98% respectively. In addition, S107 significantly reduced central nucleation to 46.12 ± 3.21% (Figure 9).

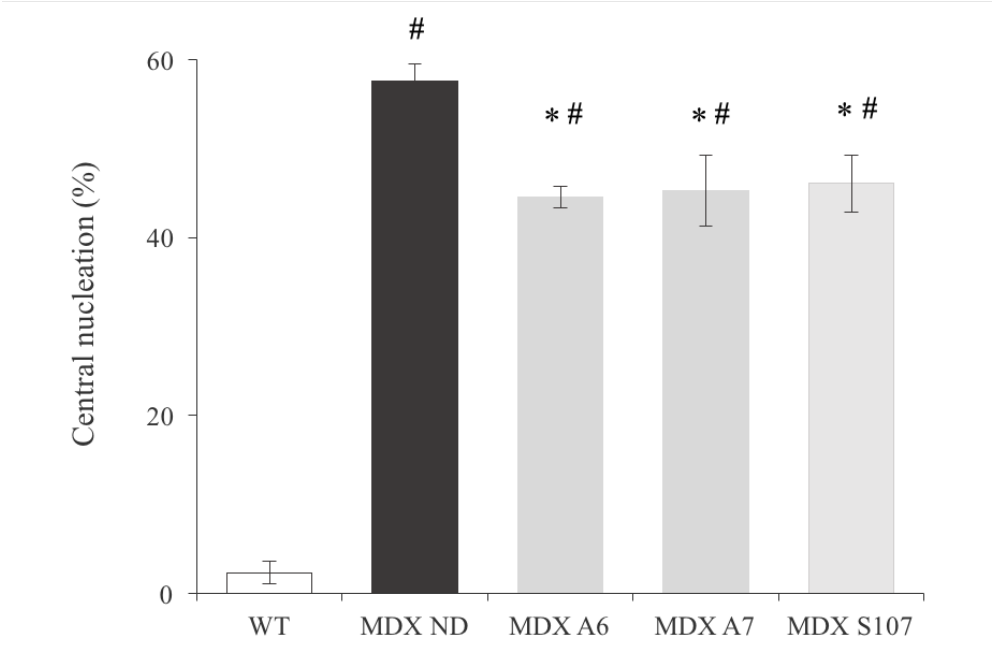

Figure 9. Quantification of myofibre central nucleation in *tibialis anterior* muscles from wild type (WT), non-treated mdx (MDX ND), A6 treated mdx (MDX A6), A7 treated mdx (MDX A7) and S107 treated mdx (MDX S107) mice after 5-weeks of treatment. Data are represented as average ± SEM, n = 3 WT; n = 9 MDX ND; n = 7 MDX A6; n = 4 MDX A7; n = 4 MDX S107. # vs WT and * vs non-treated (ND) P <0.05 (One-way ANOVA Tukey´s Post hoc test).

DISCUSSION

Duchenne muscular dystrophy is a devastating genetic disease characterised by progressive muscle degeneration and weakness that result in premature death. Currently, only palliative treatments are available to treat DMD patients, so the development of specific treatments is needed[74]. Although gene therapy seems to be a very promising approach [74,162], it presents several difficulties that would make the way long, so novel pharmacological tools that would allow a better management of symptoms and would

improve patient's quality of life are needed. RyR stabilisers are one of those emerging therapeutic alternatives that have demonstrated efficacy in several mouse models of muscular dystrophy[55,56]. Here, the effect of two novel RyR stabilisers, A6 and A7, was tested in the mdx mouse model of Duchenne muscular dystrophy. In parallel, the rycal S107 (Armgo Pharma) was used as a reference treatment in these experiments, since it shares the same mechanism of action with AHK compounds.

A6, A7 and S107 compounds were administered in drinking water in order to reduce administration-induced stress in the mdx mice[116]. Treatments were started at the age of 1-month, coinciding with the initial phase of degeneration-regeneration and necrosis[215]. After 5-weeks of treatment, no evident sign of toxicity was detected in any of the treatment groups. Likewise, water consumption was similar in all the conditions suggesting that the administered dose was equivalent within the different groups.

Several studies have already reported that resting intracellular calcium levels are significantly higher in mdx muscle fibres[123–125]. Hence, in the present work resting intracellular calcium levels were measured in isolated FDB muscle fibres, in order to assess whether RyR modulators are able to rescue alterations in calcium homeostasis that occur in dystrophic skeletal muscles. Indeed, overnight *in vitro* treatment with A6, A7 or S107 reduced intracellular calcium to wild type levels, suggesting a reduction of SR calcium leak (Figure 3). Interestingly, a similar effect was observed when analysing fibres obtained from mdx mice treated with AHK compounds during 5 weeks. In addition, although no significant S107 treated mdx mice also showed a reduction of intracellular calcium levels. The difference observed between *in vitro* and *in vivo* treated fibres and S107 treatment could reflect that AHK compounds have better *in vivo* bioavailability than S107 after oral administration.

Dysregulation of calcium homeostasis has been involved in the pathophysiology of muscular dystrophies[30]. Furthermore, treatments targeting calcium related processes have demonstrated efficacy in improving dystrophic features in mouse models of DMD[55,107]. In order to prove whether RyR modulation with AHK compounds improved

muscle performance and reduced muscle degeneration, mice were analysed after 5-weeks of treatment. Mdx mice shows a mild phenotype, so forced exercise in a treadmill was used in order to exacerbate muscle pathology and evaluate treatment efficacy[130,215,218].

Measurement of serum creatine kinase levels is a validated method to detect muscle damage and screen dystrophic patients[219]. Furthermore, several studies reported increased CK levels also in mdx mice[107,116,218]. A previous study reported that treatment with the RyR stabiliser S107, reduced serum CK levels in mdx mice[55]. Although in the present work serum CK levels were reduced with all the tested treatments, only the reduction observed with the novel compound A6 was significant in mdx mice (Figure 4). Interestingly, treatment with the new rycal lead candidate from Armgo Pharma, Arm210, has not shown any effect on serum CK levels in mdx mice[220].

Another reliable outcome that is commonly used to assess the efficacy of novel treatments against DMD is the forelimb grip strength[116]. Several works have reported force deficits in mdx mice[130,215,221,222]. Furthermore, a variety of experimental therapeutic strategies have shown a positive effect in increasing force production in several mouse models of DMD[112,115,223–227]. In the present work, AHK treated mice presented a significant increase in forelimb grip strength after 5-weeks of treatment, demonstrating that AHK compounds could be beneficial for DMD patients (Figure 5). As expected[55], S107 treatment also improved force deficit in mdx mice. On the contrary, A6 treatment did not alter force production in wild-type mice, which supports that AHK compounds specifically act through abnormally modified RyR receptors.

Next, in order to validate grip strength results, *ex vivo* force measurement experiments in TA muscle were performed in collaboration with Rando lab at Stanford University. In these studies, TA muscles from mdx mice showed a significant reduction of specific force, which was significantly increased with A6 treatment. However, the magnitude of the effect showed using these two different approaches was slightly different. Using grip strength technique A6 treatment increased mdx force in a 30%,

whereas in isolated TA experiments the increase was around 16%. Accordingly, *ex vivo* force measurement and *in vivo* forelimb grip strength data presented a strong correlation when analysing wild type and non-treated mdx mice. Interestingly, when adding A6 treated mice to the analysis the correlation between both techniques was weaker, although it remained significant (Figure 7). The observed differences between both tests could be indicating muscle independent effects of the drug, such as effects on mice motivation or learning ability, effect on other non-muscle tissue or changes in metabolism[228]. Undoubtedly, further experiment would be needed in order to elucidate other possible effects of A6.

Next, muscle damage was quantified in order to determine whether the improvement detected in functional assays correlated with a reduction in muscle damage. For this purpose, central nucleation was quantified in diaphragm and *tibialis anterior* muscles of mdx mice as an indicator of degeneration-induced muscle regeneration[117]. Limb muscles of mdx mice, such as *tibialis anterior* muscle (TA), display similar disease progression than DMD patients, showing cycles of degeneration and regeneration; however, severity of damage in these muscles is much lower than in dystrophic patients. Diaphragms from mdx mice recapitulate more closely human disease progression, and thus it has become a fundamental muscle in the evaluation of therapeutic interventions in mdx mice[115,215,228]. As previously described in several works[115–117,215], in the present study dystrophic mice showed centrally nucleated fibres of around 45.09% in diaphragm and 57.66% in TA muscles. Furthermore, AHK compounds significantly reduced central nucleation in mdx muscles in a 24-20% (Figure 8 and 9) similarly to what was previously reported in S107 treated mice[55], displaying their efficiency in preventing muscle degeneration. All together, these results show that AHK compounds normalise resting intracellular calcium levels in mdx mice, ameliorating muscle damage and improving muscle function. Thus, we conclude that AHK compound could be considered a novel therapeutic alternative to treat muscular dystrophies.

The principal limitation of this study is that mice were treated with the compounds in drinking water *ad libitum*, so the exact amount of compound consumed per mouse is unknown. Serum determination of the compounds could help to clarify the results and diminish the high variability found in several tests. For future experiments, a controlled administration per mice that would allow dose-effect assessment will help to elucidate the benefits of these compounds for the treatment of DMD patients.

CHAPTER 3:

Development of a human cellular model of Duchenne muscular dystrophy for testing the therapeutic effect of AHK compounds

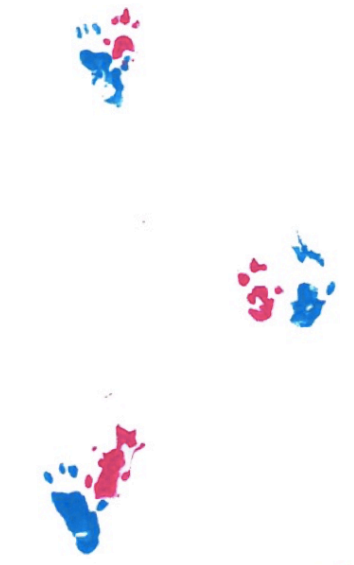

INTRODUCTION

Muscular dystrophies are a heterogeneous group of genetic disorders characterised by skeletal muscle degeneration and weakness. Duchenne muscular dystrophy (DMD) is the most common childhood form of muscular dystrophy affecting 1 in 3500-5000 boys[79,229]. This disease is caused by mutations in the *DMD* gene that lead to absence of dystrophin (DYST) protein[102] and provokes muscle degeneration and premature death. Unfortunately, no specific therapies are available to treat these patients[74].

In the last decades, animal models of DMD have been used to better understand DMD pathophysiology and develop novel therapeutic strategies[94].In mdx mouse model, dystrophin deficiency is accompanied by an increased phosphorylation and nitrosylation of the ryanodine receptor 1 (RyR1) which is the main calcium release channel of the muscle. These post-translational modifications reduce RyR1 binding affinity to calstabin 1 (Calst1), a small protein that stabilises the close state of the channel. As a consequence, RyR1 leak calcium to the cytoplasm, contributing to the increased intracellular calcium levels that are a hallmark of dystrophic muscles[25,55]. Interestingly, Ahulken compounds (AHK), which are RyR1 stabilisers that have been designed to act through this novel molecular target, increase RyR1-Calst1 binding improving dystrophic phenotype and reducing intracellular calcium leak in mdx mouse (unpublished data; Chapter 2). However, little is known about RyR1 post-translational modifications and the effect of AHK compounds in DMD patients or human models of the disease.

Although animal models have been essential to study muscle physiology and pathology *in vivo* and *in vitro*[144,230], they usually present a mild dystrophic phenotype that makes results extrapolation to patients challenging[115,133,222]. Additionally, disease mechanisms as well as treatment responses can vary between species, thus the development of human models would be of great interest to predict patients' response to experimental treatments.

Within the human *in vitro* systems, patient-derived primary myoblast cultures are the preferred model due to their high physiological relevance. However, this model presents some important drawbacks that make difficult to use it as a screening tool. Specifically, primary myotubes present limited proliferation potential, suffer senescence-induced changes and display high inter-individual heterogeneity[137,138,231,232]. In addition, it has been reported that dystrophic myoblasts show alterations in proliferation and differentiation, compared to healthy myoblasts[37,145,146]. For these reasons, comparison of cells from different donors and/or pathologies could be challenging.

Alternatively, several work have been focused on generating myotubes from non-muscular sources, such as fibroblasts (MyoD-converted)[154,155,233] or inducible pluripotent stem cells (hiPSCs)[156,159,234]. Although these models overcome sample availability limitations, their physiological relevance is still on debate. On the other hand, immortalisation of patient-derived primary myoblasts has become a very interesting strategy. Since immortalisation of myoblasts solves sample availability and limited proliferation troubles without compromising the physiological relevance of the model[151–153], they constitute a reproducible model that could be used for drug testing.

The main objectives of this work were to 1) develop a reliable and reproducible human *in vitro* model of DMD based on immortalised myoblasts, 2) study RyR1-Calst1 binding and calcium homeostasis in a human model of DMD and 3) test the effect of AHK compounds in a human model of DMD.

METHODS

Cell cultures

LHCN-M2[152] and KM155C25 (healthy control) and NH10-637A (DMD patient, deletion 44-50) human immortalised myoblasts were generated by the Platform for Immortalisation of Human Cells (Myology Institute, Paris) and they were kindly

provided by Dr Vincent Mouly. LHCN-M2, KM155C25 and NH10-637A cells were referred to as CTRL1, CTRL2 and DMD, respectively. Human myoblasts were cultured as previously described in Chapter 1. Briefly, myoblasts were grown in SGM medium on 0.5% gelatin coated dishes. At confluence, ECM was added to generate a thin overlay and cells were incubated with basic differentiation medium (bDM) until they started to fuse. Then, medium was replaced by complete differentiation medium (cDM) and half volume was changed every three days. Highly mature myotubes were obtained after eight days of differentiation and they were used in the rest of experiments.

Silencing of dystrophin with shRNA

Lentiviral particles containing short hairpin RNA (shRNA) were used to knock down dystrophin in LHCN-M2 myotubes. Lentiviral particles were produced by the Viral Vectors Platform at Inbiomed (Spain) from the following plasmid DNAs: TRCN0000053243 (DYST-shRNA) and SHC002 (NS-shRNA) (Sigma-Aldrich). Human myoblasts were infected with DYST-shRNA or NS-shRNA containing lentivirus at a multiplicity of infection (MOI) of 5 in proliferation medium supplemented with 4 μg/mL polybrene for 24 hours. Finally, infected myoblasts were selected during seven days with puromycin containing proliferation medium.

Morphologic characterisation

To characterise myotube morphology, the width of fully mature myotubes was measured at 10X magnification. A minimum of four images and 20 myotubes from three independent cultures were analysed per condition. Image quantification was performed using ImageJ software (NIH).

Creatine kinase assay

Creatine kinase activity was measured in cell culture homogenates from CTRL1, CTRL2, DMD and shRNA infected LHCN-M2 myotubes as a maturity marker[235,236]. Myotubes were lysed with a 0.1% Triton X-100 in 2M Tris solution and CK activity

was determine using CK-NAC colorimetric kit (Thermo Fisher). Measurements were made in a NanoDrop® ND-1000 apparatus. Homogenates from at least 3 independent cultures were analysed.

Quantitative real-time PCR

Total RNA was extracted from cell culture homogenates using the MiniRNeasy kit and RNase-Free DNase Set (Qiagen). After quantification, cDNA was obtained from 1 µg RNA using SuperScript® Vilo cDNA Synthesis kit (Thermo Fisher). Finally, qPCR reaction was carried out in a 7900HT Real-Time PCR System apparatus (Applied Biosystems).

cDNAs from CTRL1, CTRL2, DMD and DYST-shRNA and NS-shRNA myotubes were used to study the mRNA expression of the following genes: *ACTN1*, *CAPN3*, *CK*, *DHPRα1*, *HPRT1* and *DYST*. qPCRs were carried out with 10 ng of cDNA and 300 nM of forward and reverse primers diluted in Power SYBR® Green PCR master mix (Thermo Fisher). The amount of cDNA was calculated from the appropriate standard curve. The following forward and reverse primer sequences were used: *ACTN1*, 5′-TTCAACGTGCCTGCCATGT -3′ and 5′-CAACACGATGCCGGTGG TA-3′; *CAPN3*, 5′-GAAAAGAGGAACCTCTCTGAGGAA-3′ and 5′-CGAAGAT GATGGGCTTG GTT-3′; *CK*, 5′-GAAGCTCTCTGTGGAAGCTCTCA-3′ and 5′-CCTTCTCCGTCATGCTCTTCA-3′; *DHPRα1*, 5′-GCCATCTCCGTGGTGAAGAT-3′ and 5′-CACTGC ACCACGTGCTTCA-3′; *HPRT1* 5′-CATGGACTAATTATG GACAGGACTGA-3′ and 5′-TGAGCACACAGAGGGCTACAA-3′; and *DYST* 5′-ACAGGGCAAAAACT GCCAAA-3′ and 5′-CGCAGTGCCTTGTTGACATT -3′. Primers were designed using Primer Express® software (Thermo Fisher) and specificity was ensured with Reverse e-PCR online software (http://www.ncbi.nlm.nih.gov/projects/e-pcr/reverse.cgi).

Western blotting

CTRL1, CTRL2, DMD and DYST-shRNA and NS-shRNA myotubes were homogenised in modified RIPA assay buffer (10 nM Tris, 100 mM NaCl, 1 mM EDTA, 1 mM EGTA, 20 mM $Na_4P_2O_7$, 1% Triton X-100, 0.5% sodium deoxycolate, 0.1% SDS, 10% glycerol, 1X Halt Protease & Phosphatase Inhibitor Cocktail EDTA-Free, pH 7.5) for total protein extraction. Then, total protein amounts were quantified using the Bio-Rad Protein Assay dye reagent and 4X Sample Buffer was added to the samples (250 mM Tris pH 7.5, 20% glycerol, 8% SDS, 20% β-mercaptoethanol and 5 mg/mL bromophenol blue). Finally, samples were boiled for five minutes and stored at -20 ºC until analysis.

Protein extracts were solved in Min-PROTEAN® TGX™ 4-20% gradient SDS-PAGE precast gels (Bio-Rad). Next, proteins were transferred onto low fluorescence PVDF membranes and blocked with TBS-tween and 5% skim milk powder. After that, membranes were incubated with primary antibodies overnight at 4 ºC. The following antibodies were used: anti-DHPRα2 mouse mAb (1:1000, Abcam), anti-ACTN rabbit pAb (1:1000, Sigma), anti-CK rabbit (1:1000, Sigma), FITC-conjugated Myosin Heavy Chain-CFS mAb (1:50, R&D), anti-DYST mouse mAb (1:500, DSHB) and anti-α-sarcoglycan mouse mAb (1:500, Santa Cruz). After washing, membranes were incubated with Alexa Fluor 647 or 488-conjugated secondary antibodies and fluorescence images were acquired with a Typhoon Trio Imager (GE Healthcare). For image quantification Image Studio Lite 4.0 software was used.

Proximity ligation assay

DYST-shRNA and NS-shRNA myotubes were treated overnight with 150 nM A6 or A7 and *in situ* proximity ligation assay (PLA) was performed as previously described in Chapter 1. Briefly, myotubes were fixed with paraformaldehyde and incubated with blocking solution for 1 hour at room temperature. Next, coverslips were incubated with anti-RyR1 mouse mAb (1:200, Thermo Scientific), anti-Calst1 rabbit

pAb (1:100, Novus Biologicals), anti-PKA rabbit pAb (1:100, Cell Signalling) and anti-CysNO rabbit pAb (1:500, Sigma-Aldrich) primary antibodies and PLA assay was made using Duolink *In situ* Orange kit. After that myotubes were stained with FITC-conjugated Myosin Heavy Chain-CFS mAb (1:50, R&D) and they were mounted with ProLong® Gold antifade reagent with DAPI (Life technologies). High resolution images were quantified using ImageJ software (NIH) and the "Batch spot analysis macro" from Dr. Henry Wellcome lab. PLA signal was normalised by total myotube area, obtained by quantification of MyHC stained area.

Calcium imaging

For intracellular calcium imaging studies DYST-shRNA and NS-shRNA myotubes were treated overnight with A6 and A7 at 50 nM and 150 nM concentrations. Then, experiments were performed as previously described in Chapter 2. In short, myotubes were incubated with 4 μM Fura-2AM and 0,02% pluronic acid in culture medium for 30 min at 37ºC. Then, they were placed in Ringer solution for 30 min at 37ºC and image acquisition was done under continuous perfusion. Intracellular calcium concentration was estimated by the ratio of Fura-2AM fluorescence intensities at 340 nm and 380 nm after applying background correction.

RESULTS

Characterisation of CTRL1, CTRL2 and DMD myoblasts

After eight days in differentiation medium, highly mature myotubes were obtained from immortalised patient-derived primary myotubes (Figure 1A). Myotube width analysis revealed significant differences between CTRL2 and DMD myotubes (paired *t*-test, $P < 0.05$). CTRL2 myotubes showed an average width of 21.17 ± 2.31 μm, whereas DMD myotubes width was 27.75 ± 2.93 μm.

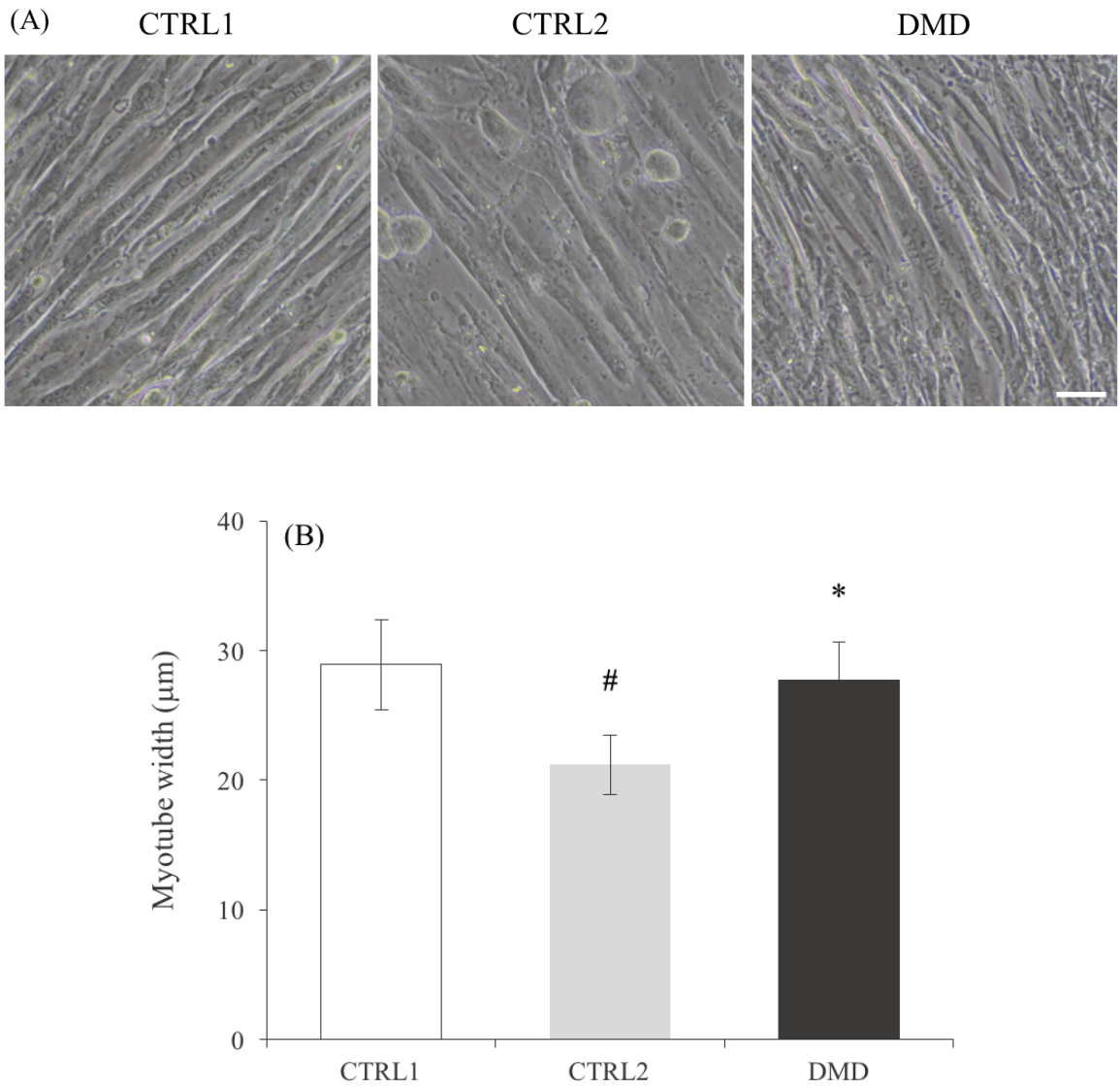

Figure 14. (A) Representative bright field images of CTRL1, CTRL2 and DMD myotubes after 8 days of differentiation. Scale bar 50 µm (B) Quantification of myotube width in CTRL1, CTRL2 and DMD myotubes after 8 days of differentiation. Data are represented as average ± SEM, n = 20-40 myotubes per 3-5 independent cultures. # compared to CTRL1 and * compared to CTRL2 $P < 0.05$ (non-paired *t*-test).

In contrast, no significant differences were found between DMD and CTRL1 myotubes (Figure 1B). In relation to culture maturity, no significant differences were found in CK activity in culture homogenates from any of the three cell lines (Figure 2).

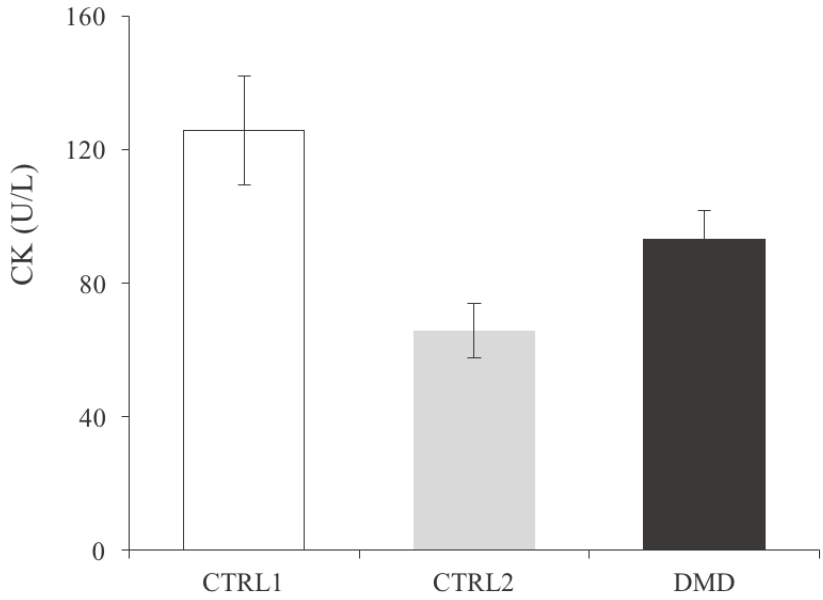

Figure 15. Creatine kinase (CK) activity in CTRL1, CTRL2 and DMD myotubes after 8 days of differentiation. Data are represented as average ± SEM, n =3-5 independent cultures.

When analysing mRNA expression of maturity related genes, significant differences in *ACTN 1, CAPN3*, *CK* and *DHPRα1* expression were found between CTRL1 and DMD myotubes (Figure 3). DMD myotubes showed 2.42-fold increase in *ACTN1* expression, 0.62-fold reduction of *CAPN3* expression, 0.35-fold reduction in *CK* expression and a 1.34-fold increase in *DHPRα1* expression compared to CTRL1 myotubes (paired *t*-test, $P < 0.05$). In contrast, only significant differences in *CAPN3* expression were found between CTRL2 and DMD, where *CAPN3* expression was 2-folds higher in dystrophic myotubes (paired *t*-test, $P < 0.05$).

Finally, western blot analysis revealed that the expression of DHPR, ACTN1, CK and MyHC was similar between CTRL1 and DMD myotubes (Figure 4). In the same way, no significant differences were found among CTRL2 and DMD myotubes (paired *t*-test, $P > 0.05$).

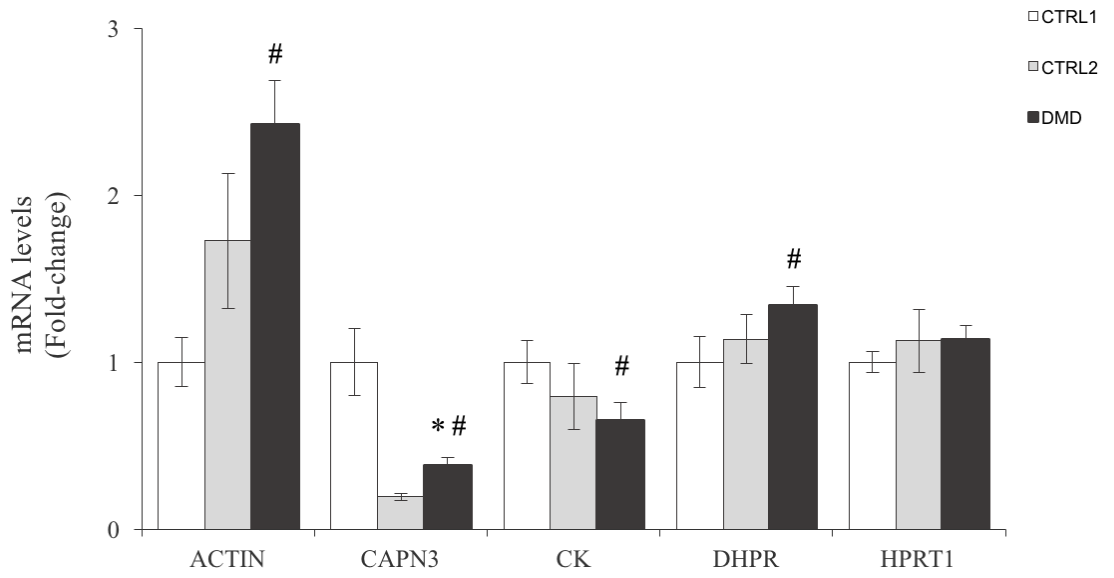

Figure 3. mRNA expression of *ACTN1*, *CAPN3*, *CK*, *DHPRα1* and *HPRT1* in CTRL1, CTRL2 and DMD myotubes after 8 days of differentiation. CTRL1 myotube value was taken as 1. Data are represented as average ± SEM, n =3-5 independent cultures. # compared to CTRL1 and * compared to CTRL2, P <0.05 (paired t-test).

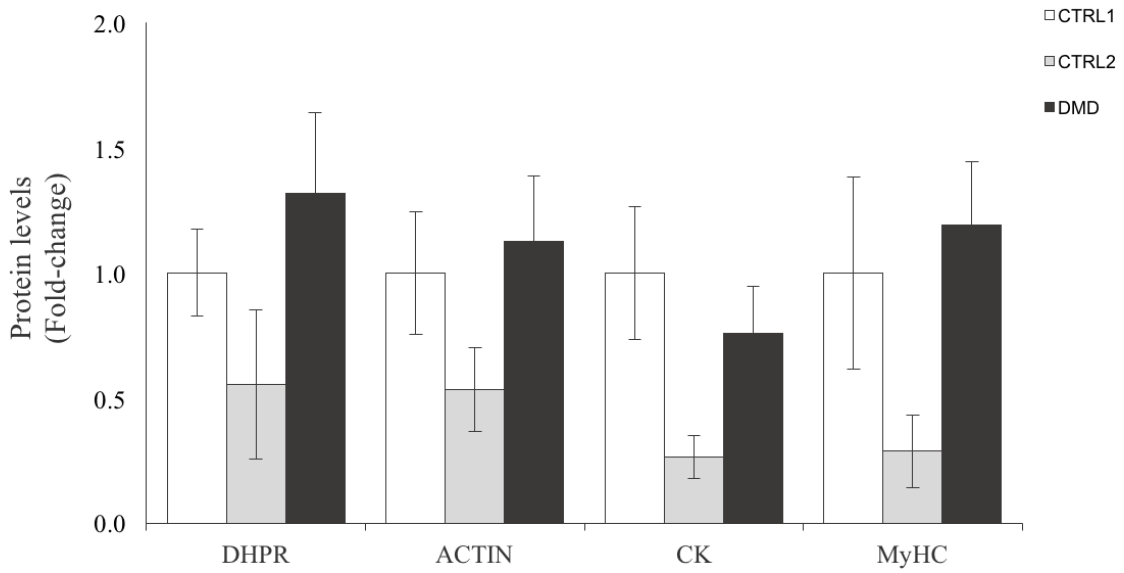

Figure 4. Protein levels of DHPRα2, ACTN, CK and MyHC in CTRL1, CTRL2 and DMD myotubes after 8 days of differentiation. CTRL1 myotube value was taken as 1. Data are represented as average ± SEM, n =3-5 independent cultures.

Characterisation of DYST-shRNA and NS-shRNA myoblasts

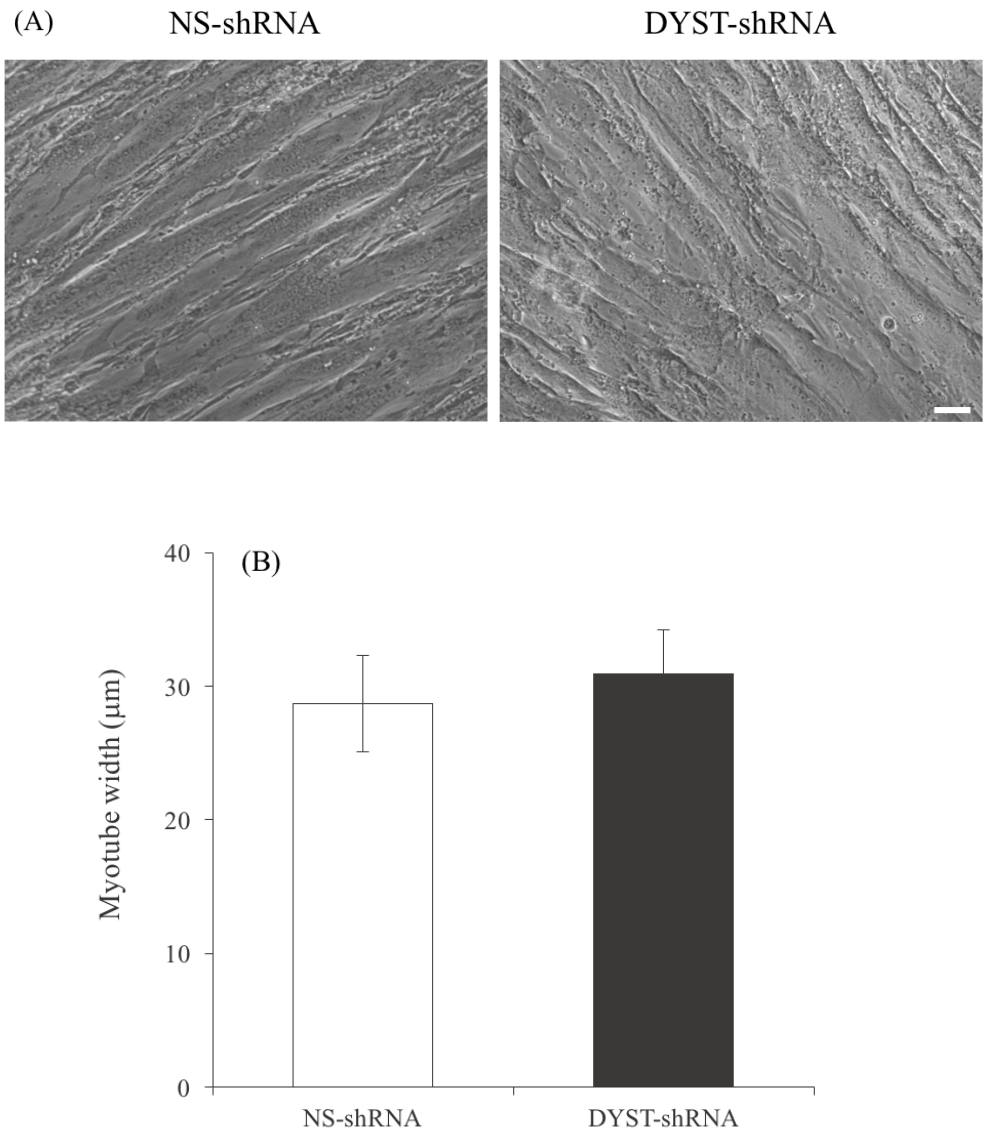

Figure 5. (A) Representative bright field images of NS-shRNA and DYST-shRNA infected LHCN-M2 myotubes after 8 days of differentiation. Scale bar 25 µm. (B) Quantification of myotube width in NS-shRNA and DYST-shRNA myotubes after 8 days of differentiation. Data are represented as average ± SEM, n = 20-25 myotubes per 3 independent cultures.

NS-shRNA and DYST-shRNA infected LHCN-M2 myotubes showed very similar morphology and maturation (Figure 5A). When analysing myotube width, no significant differences were observed between control and dystrophic myotubes, which

width was around 28.71 ± 3.62 μm (Figure 5B). In relation to maturity, NS-shRNA myotubes showed 132.67 ± 3.62 U/L CK activity which did not change after DYST knocking down (paired *t*-test, $P > 0.05$) (Figure 6).

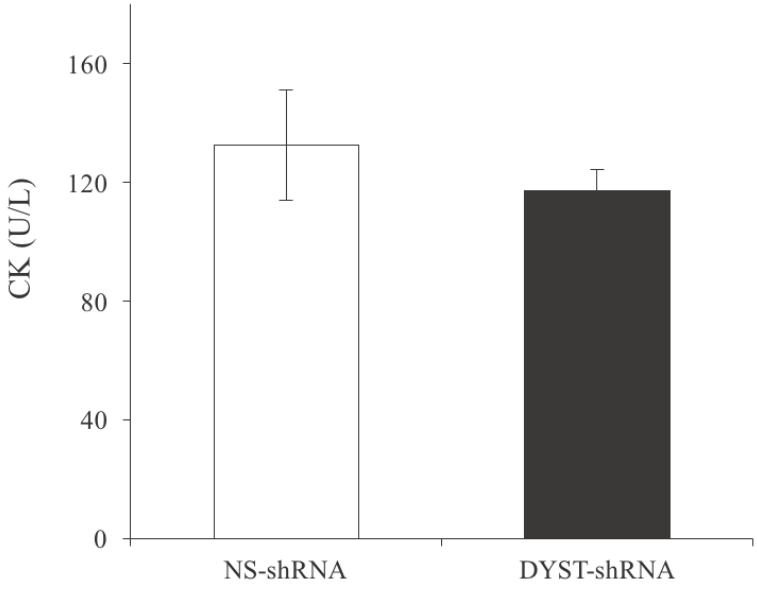

Figure 6. Creatine kinase (CK) activity in NS-shRNA and DYST-shRNA myotubes after 8 days of differentiation. Data are represented as average ± SEM, n =3 independent cultures.

In the same way, mRNA expression of *ACTN 1, CAPN3*, *CK* and *DHPRα1* did not change with dystrophin silencing (paired *t*-test, $P > 0.05$) (Figure 7). Consistently, no significant differences were found in protein levels of DHPR, ACTN1, CK and MyHC between NS-shRNA and DYST-shRNA myotubes (paired *t*-test, $P > 0.05$) (Figure 8).

However, it was observed that the infection efficiently reduced *DYST* mRNA levels in a 38.24%, being protein levels undetectable in DYST-shRNA myotubes (paired *t*-test, $P < 0.05$) (Figure 9). Additionally, α-sarcoglycan expression was significantly reduced in DYST-shRNA myotubes (0.55 ± 0.11) when compared to NS-shRNA myotubes (1 ± 0.12) (paired *t*-test, $P < 0.05$) (Figure 10).

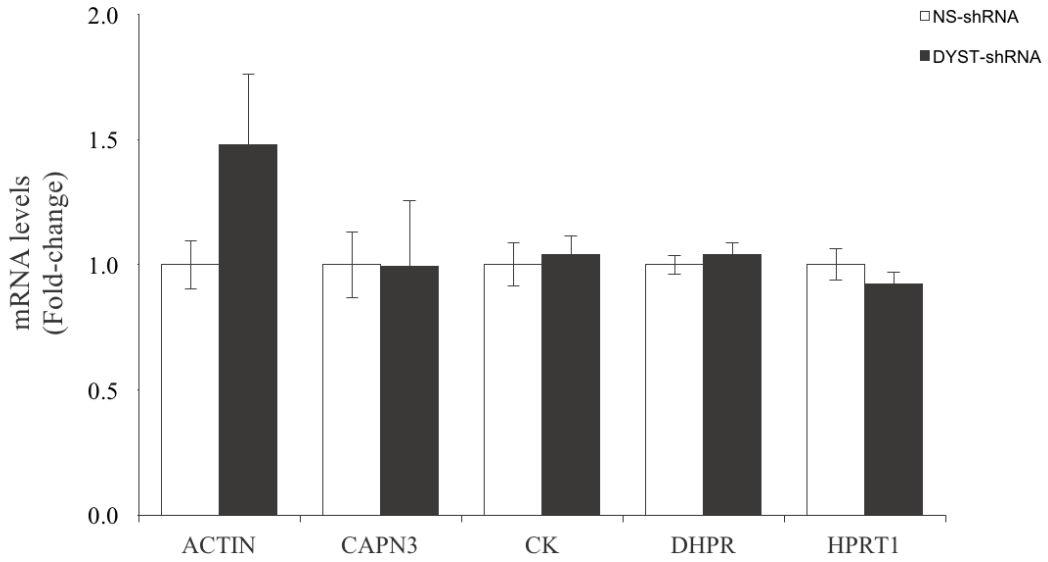

Figure 7. mRNA expression of *ACTN1*, *CAPN3*, *CK*, *DHPRα1* and *HPRT1* in NS-shRNA and DYST-shRNA infected LHCN-M2 myotubes after 8 days of differentiation. NS-shRNA value was taken as 1. Data are represented as average ± SEM, n =3 independent cultures.

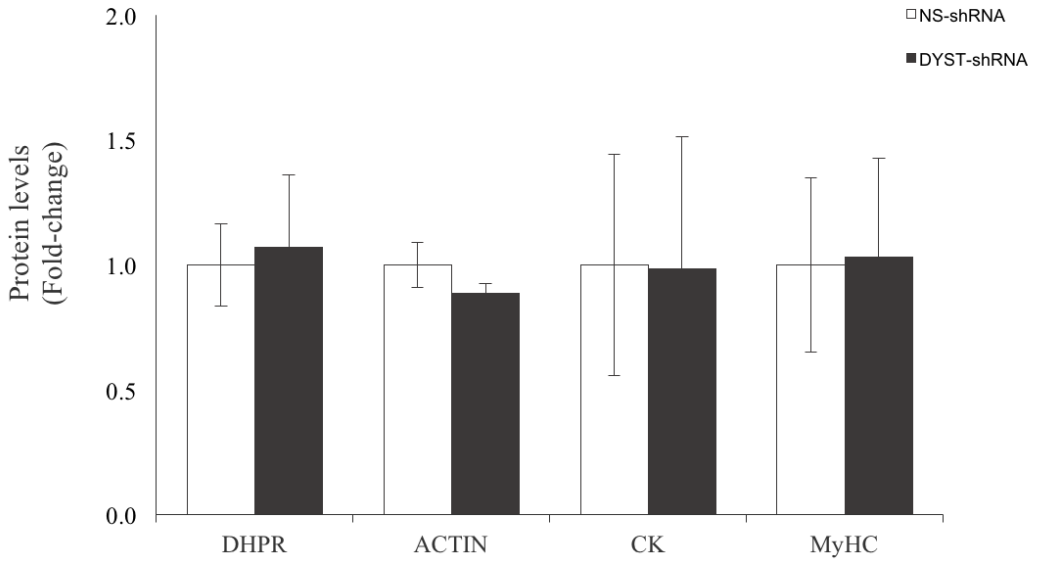

Figure 8. Protein levels of DHPRα2, ACTN, CK and MyHC in NS-shRNA and DYST-shRNA myotubes after 8 days of differentiation. NS-shRNA value was taken as 1. Data are represented as average ± SEM, n =3 independent cultures.

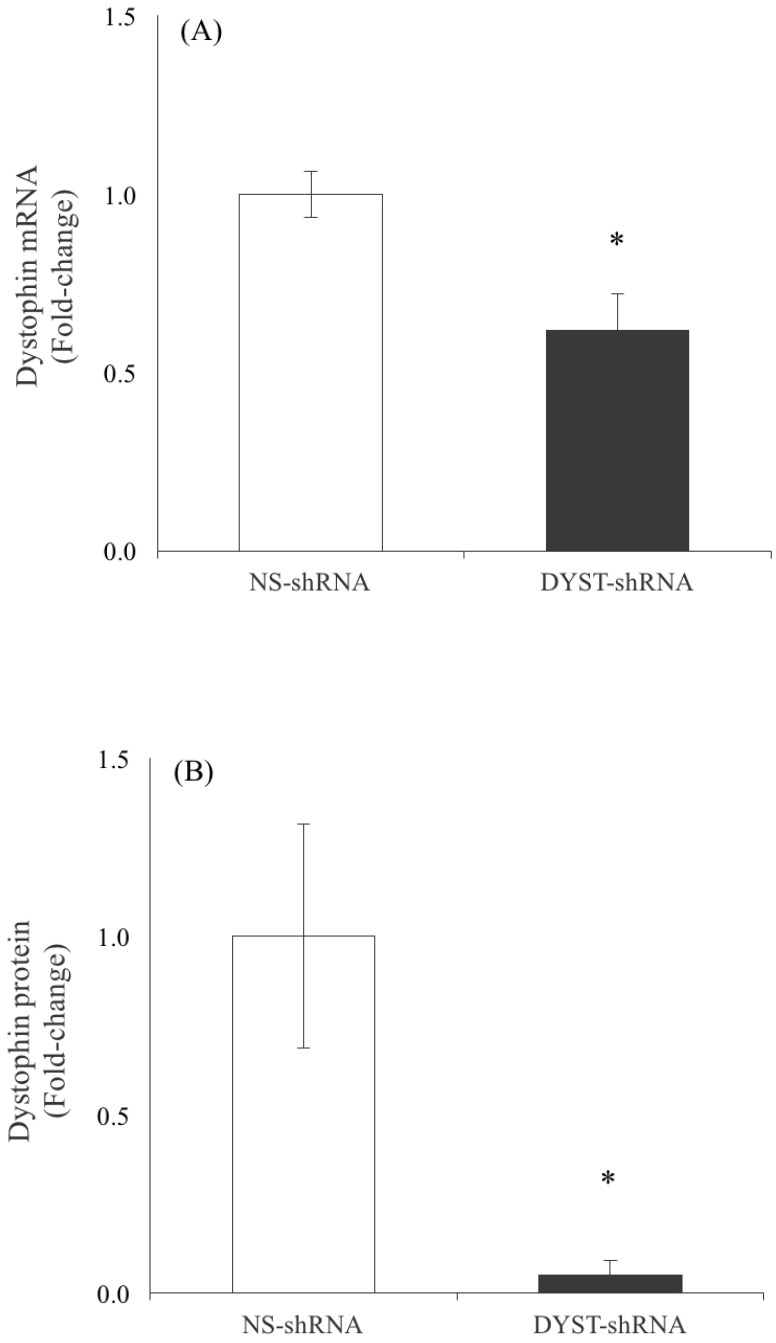

Figure 9. (A) mRNA and (B) protein levels of DYST in NS-shRNA and DYST-shRNA myotubes after 8 days of differentiation. NS-shRNA value was taken as 1. Data are represented as average ± SEM, n =3 independent cultures. * P <0.05 (paired t-test).

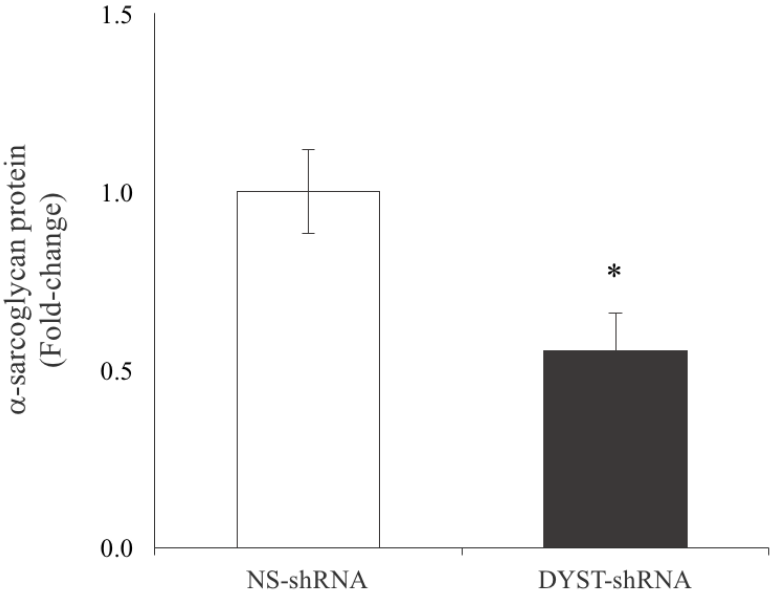

Figure 10. Protein levels of α-sarcoglycan in NS-shRNA and DYST-shRNA myotubes after 8 days of differentiation. NS-shRNA value was taken as 1. Data are represented as average ± SEM, n =3 independent cultures. * P <0.05 (paired t-test).

RyR1-Calst1 and calcium homeostasis in DYST-shRNA and NS-shRNA myotubes

At 8 days of differentiation, dystrophin knock down myotubes (DYST-shRNA) showed significant changes in RyR1 post-translational modifications and Calst1 binding (paired t-test, $P < 0.05$). First, RyR1 was found to be hypernitrosylated and hyperphosphorylated in dystrophin deficient myotubes (Figure 11). RyR1 phosphorylation was increased in a 62.20 ± 18.20% whereas nitrosylation was 97.90 ± 19.50% higher. Consequently, DYST-shRNA infected myotubes showed a 48.24% reduction in RyR1-Calst1 interaction compared to the NS-shRNA infected myotubes (Figure 12A).

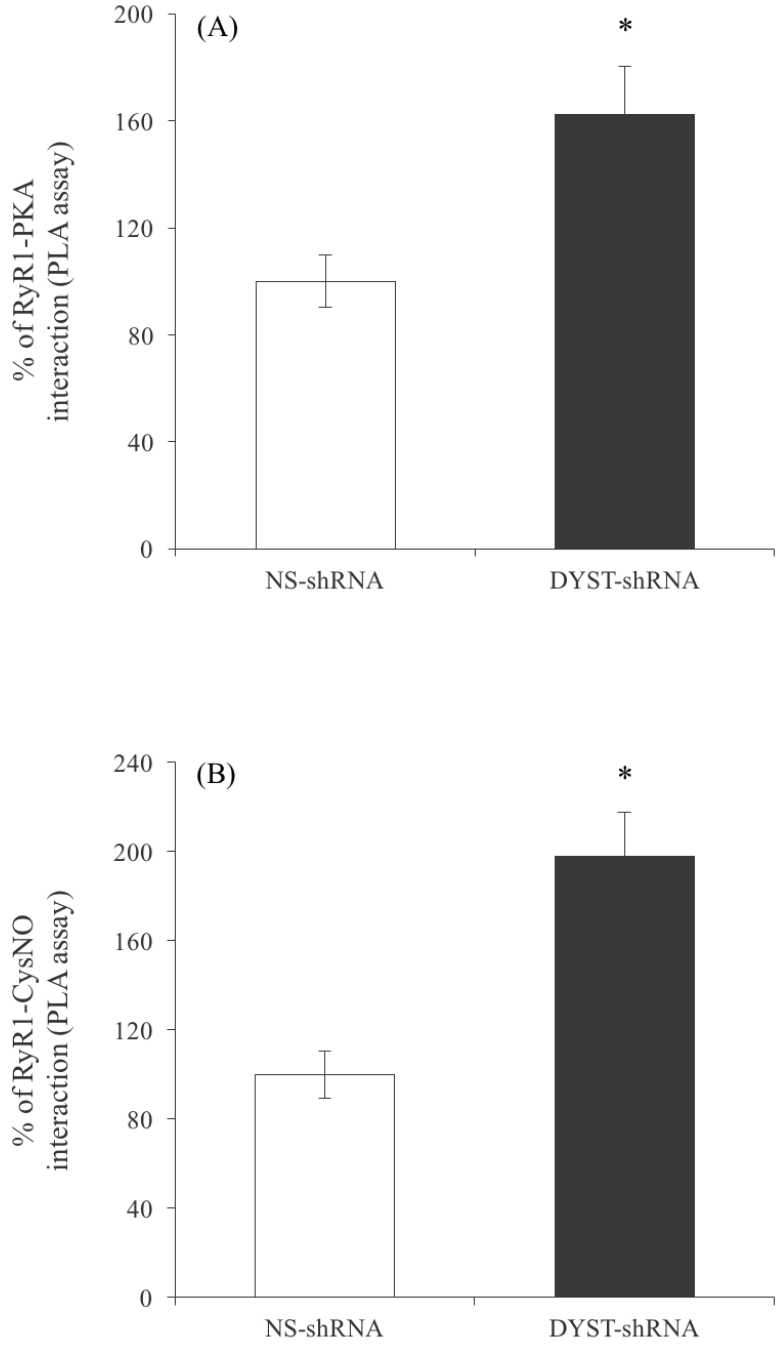

Figure 11. *In situ* proximity ligation assay (PLA) analysis of (A) RyR1 phosphorylation and (B) RyR1 nitrosylation in NS-shRNA infected (NS-shRNA) and DYST-shRNA infected (DYST-shRNA) LHCN-M2 myotubes. Data are represented as percentage of colocalisation. The NS-shRNA infected (NS-shRNA) control was taken as 100%. All data are mean ± SEM, n = 4, * P <0.05 (*t*-test).

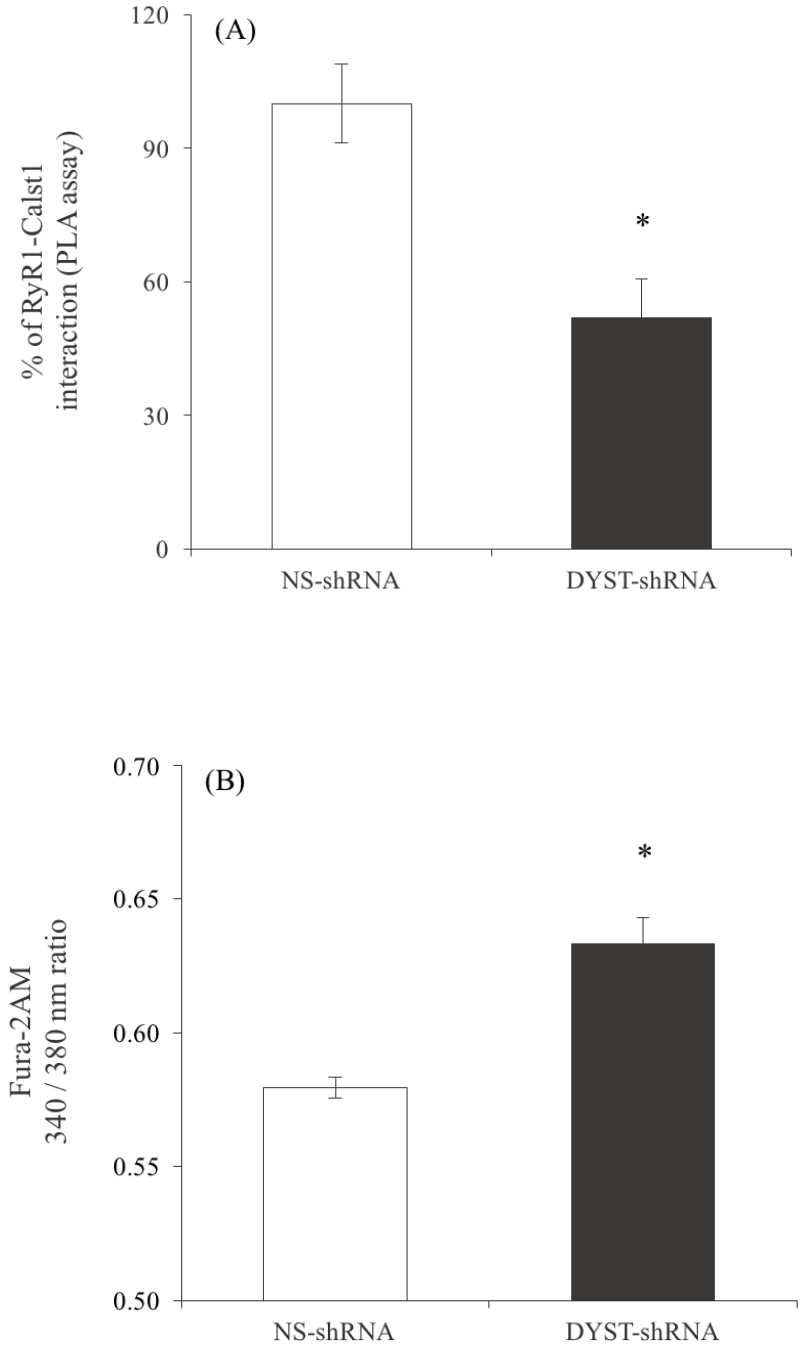

Figure 12. (A) *In situ* proximity ligation assay (PLA) analysis of RyR1-Calst1 in NS-shRNA and DYST-shRNA infected LHCN-M2 myotubes. Data are represented as percentage of colocalisation. The NS-shRNA was taken as 100%. All data are mean ± SEM, n = 11-15 from 3 independent cultures, * P <0.05 (*t*-test). (B) Resting intracellular calcium levels of NS-shRNA and DYST-shRNA myotubes. All data are mean ± SEM, n = 80-100 myotubes from 4 independent cultures, * P <0.05 (*t*-test).

Intracellular calcium levels increased as a consequence of dystrophin deficiency in LHCN-M2 myotubes (Figure 12B). NS-shRNA infected myotubes presented resting intracellular calcium levels of 0.58 ± 0.004, whereas in DYST-shRNA myotubes calcium levels significantly increased to 0.63 ± 0.01 (*t*-test, $P < 0.05$).

Effect of AHK compounds in DYST-shRNA and NS-shRNA myotubes

In vitro treatment of DYST-shRNA myotubes with AHK compounds significantly increased RyR1-Calst1 binding, leading to a reduction of resting intracellular calcium levels (*t*-test, $P < 0.05$). After overnight treatment with 150 nM A6 and A7, RyR1-Calst1 binding significantly increased in a 20 and 27%, respectively in DYST-shRNA myotubes compared to non-treated myotubes (Figure 13A). In contrast, treatments did not change RyR1-Calst1 interaction in NS-shRNA myotubes (*t*-test, $P > 0.05$) (Figure 13B).

The observed increase in RyR1-Calst1 binding drive the subsequent reduction of resting intracellular calcium levels in DYST-shRNA myotubes (Figure 14). Overnight treatment with 50 nM A6 and A7 significantly reduced intracellular calcium levels in DYST-shRNA myotubes to 0.58 ± 0.004 and 0.58 ± 0.003, respectively, compared to non-treated myotubes that showed 0.63 ± 0.01 levels (*t*-test, $P < 0.05$) (Figure 15A). However, these treatments did not change calcium levels in NS-shRNA myotubes (*t*-test, $P > 0.05$) (Figure 15B).

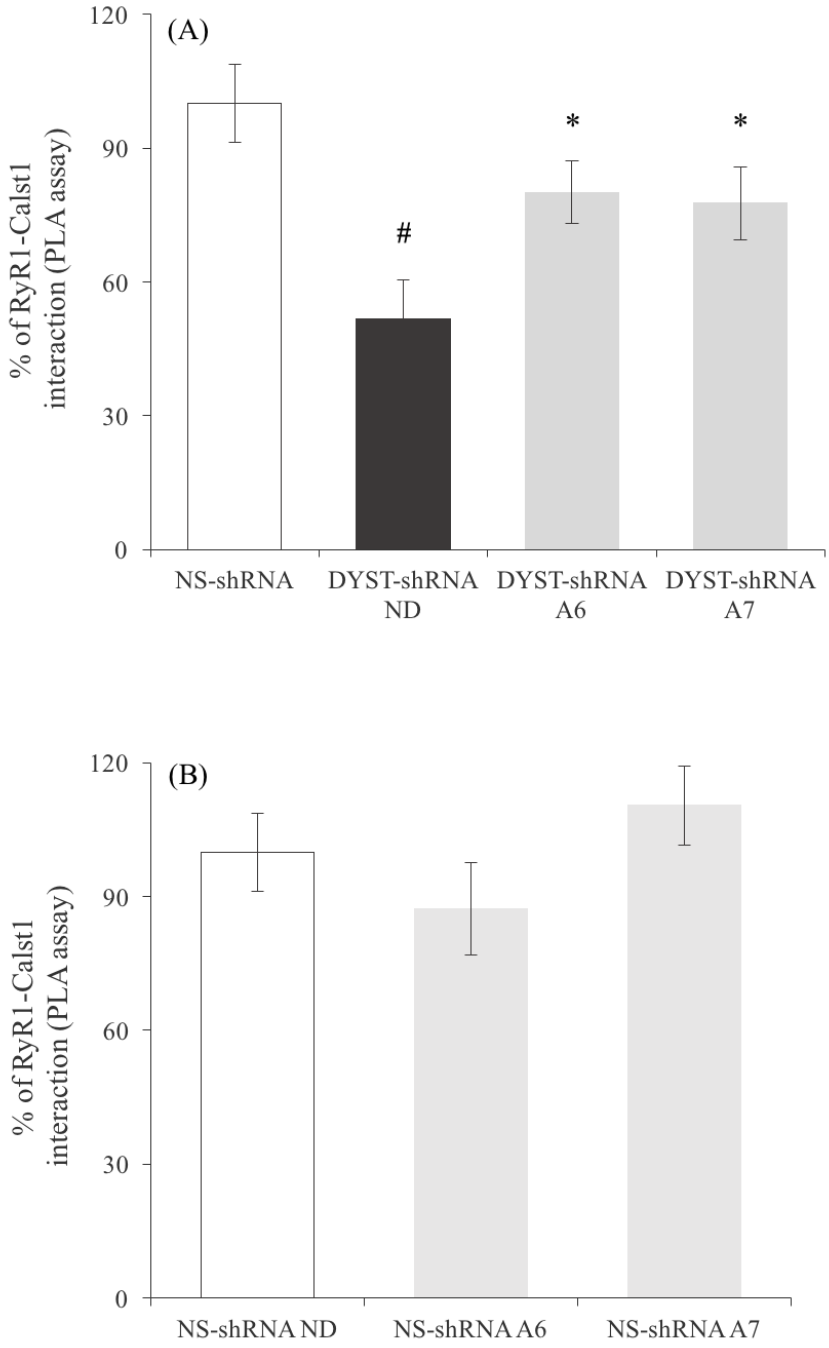

Figure 13. *In situ* proximity ligation assay (PLA) analysis of RyR1-Calst1 in non-treated (ND), A6 treated (A6) and A7 treated (A7) (A) DYST-shRNA infected (DYST-shRNA) and (B) NS-shRNA infected (NS-shRNA) LHCN-M2 myotubes. Data are represented as percentage of colocalisation. The non-treated NS-shRNA infected myotubes (NS-shRNA ND) value was taken as 100%. All data are mean ± SEM, n = 11-15 from 4 independent cultures, # vs NS-shRNA ND and * vs DYST-shRNA ND $P < 0.05$ (*t*-test).

In contrast, treatment of DYST-shRNA myotubes with a higher dose of 150 nM A6 or A7 resulted in a significant reduction of calcium levels only with A6 treatment (0.60 ± 0.01) (Figure 16A). Conversely, both treatments provoked a significant increase of calcium levels in control myotubes to 0.65 ± 0.02 and 0.62 ± 0.01, respectively, compared to non-treated control myotubes that showed 0.58 ± 0.004 levels (*t*-test, $P < 0.05$) (Figure 16B).

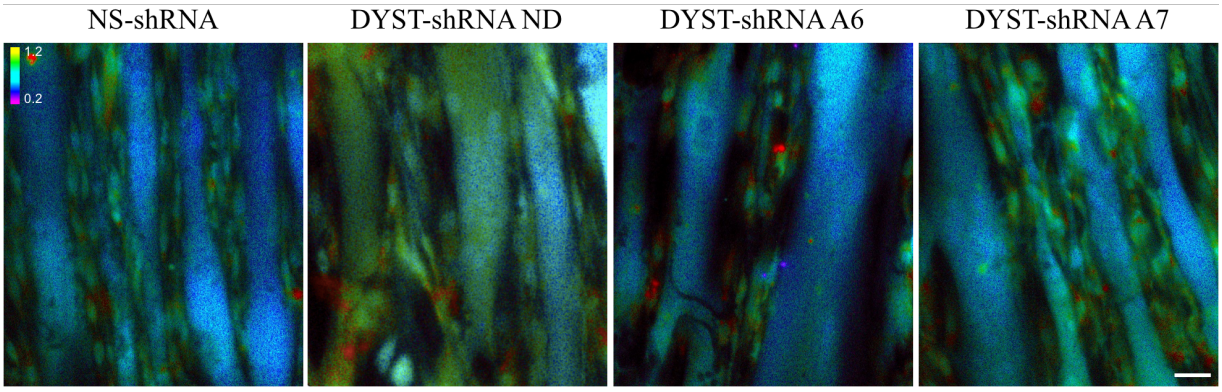

Figure 14. Representative pseudocolor images of Fura-2AM loaded NS-shRNA infected control myotubes (NS-shRNA) and DYST-shRNA infected non-treated dystrophic myotubes (DYST-shRNA ND), A6 treated dystrophic myotubes (DYST-shRNA A6) and A7 treated dystrophic myotubes (DYST-shRNA A7). Scale bar 25 µm.

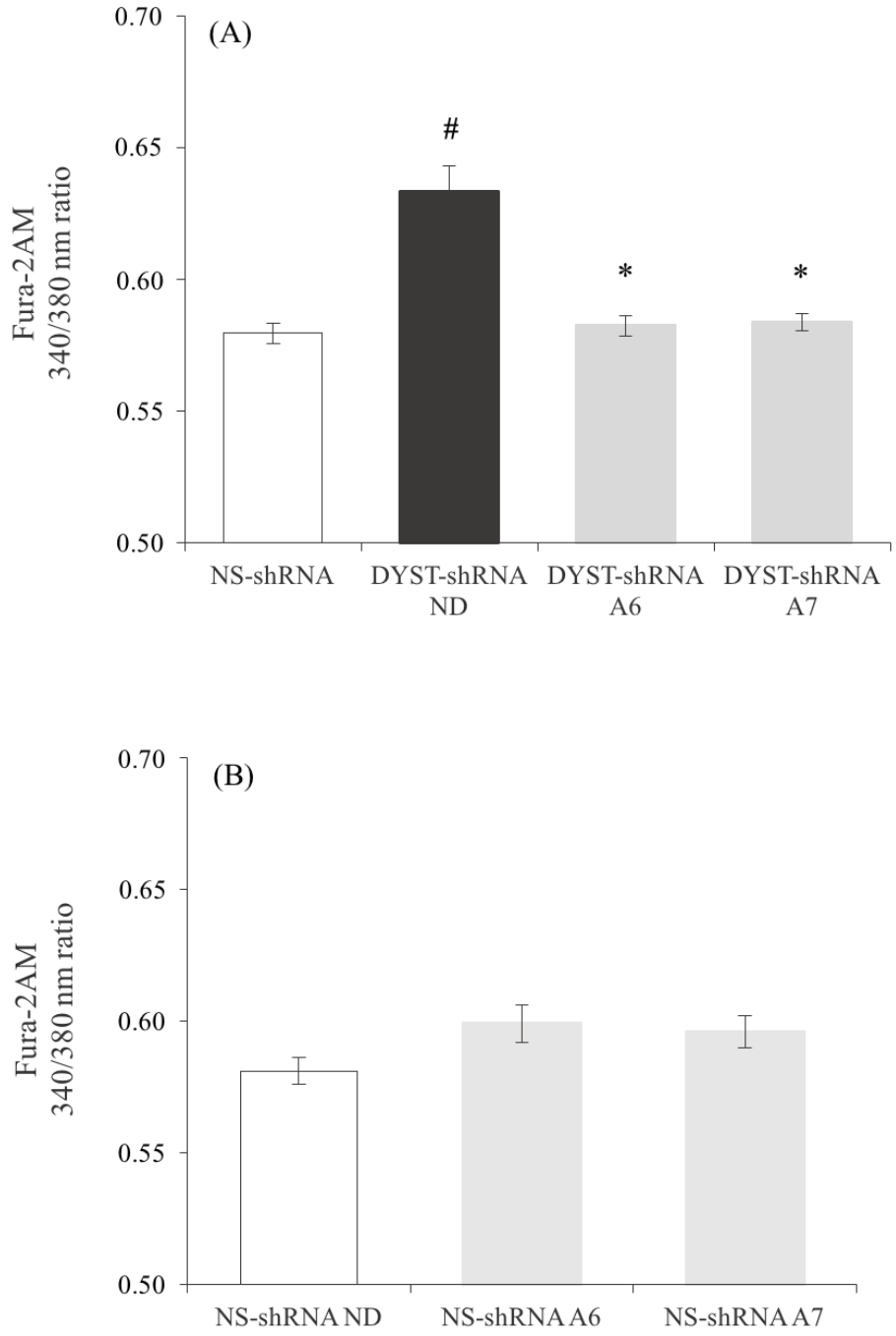

Figure 15. Resting intracellular calcium levels of non-treated (ND), 50 nM A6 treated (A6) and 50 nM A7 treated (A7) (A) DYST-shRNA infected (DYST-shRNA) and (B) NS-shRNA infected (NS-shrRNA) LHCN-M2 myotubes at 8 days in differentiation. All data are mean ± SEM, n = 80-100 myotubes from 2-3 independent cultures, # vs NS-shRNA ND and * vs DYST-shRNA ND P <0.05 (*t*-test).

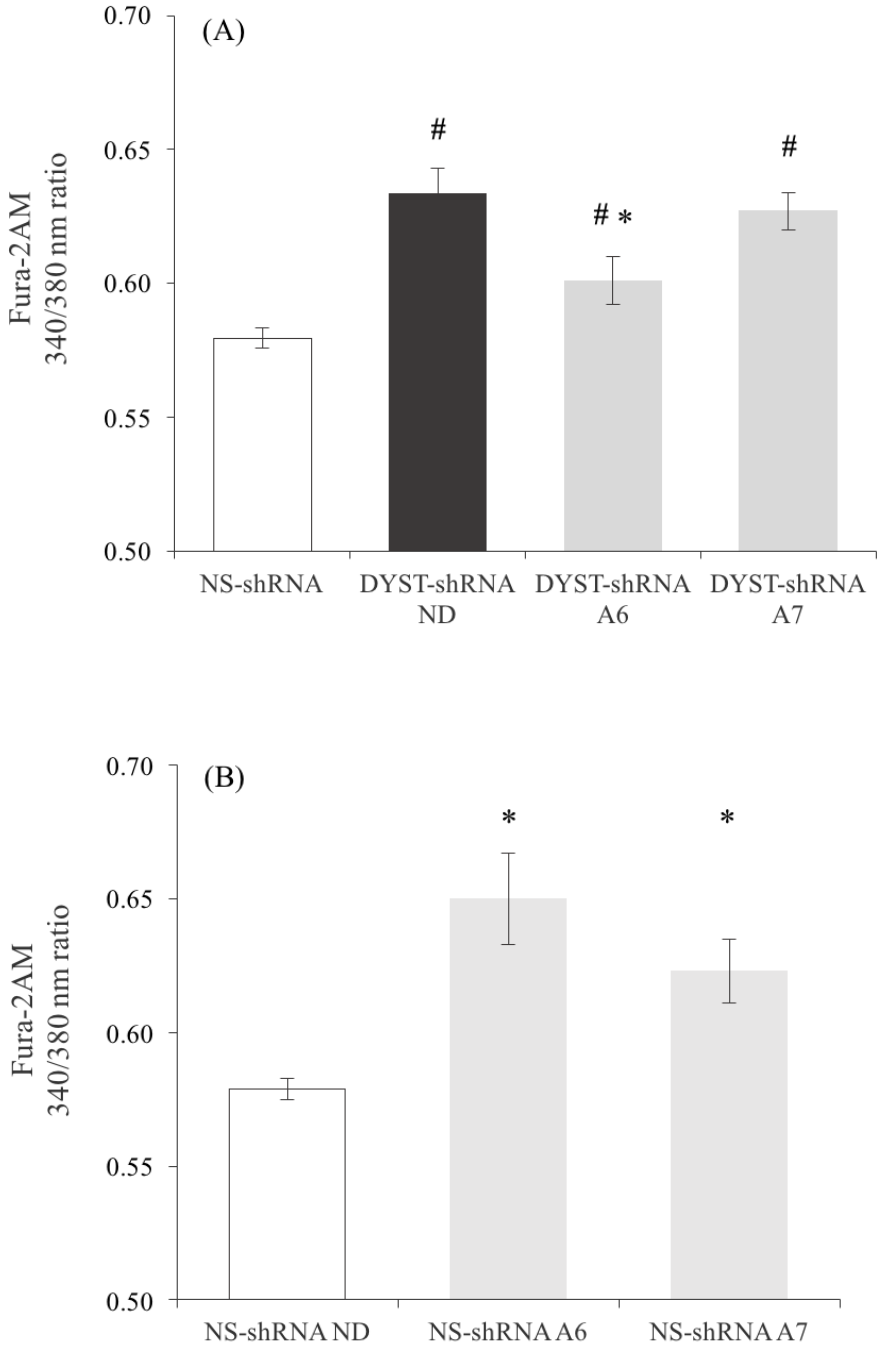

Figure 16. Resting intracellular calcium levels of non-treated (ND), 150 nM A6 treated (A6) and 150 nM A7 treated (A7) (A) DYST-shRNA infected (DYST-shRNA) and (B) NS-shRNA infected (NS-shRNA) LHCN-M2 myotubes at 8 days in differentiation. All data are mean ± SEM, n = 80-100 myotubes from 3 independent cultures, # vs NS-shRNA ND and * vs DYST-shRNA ND P <0.05 (*t*-test).

DISCUSSION

Experimental *in vitro* models of muscular dystrophies are essential tools to understand the mechanisms underlying disease progression and to develop and screen novel therapies. In the past, animal models of DMD were mainly used in these studies but since pathological mechanisms and treatment response could differ between species, special effort is being placed in the development of human models[138]. Within the existing models, patient-derived myoblasts present high physiological relevance but have limited proliferative potential and undergo senescence-induced phenotypic changes that hinder working with a homogeneous cell population over time[137,231]. Immortalisation of human myoblasts may solve this issue since it produces stable cell lines, while preserving the main characteristics of the parental population[151–153]. Additionally, it should be noted that the expression of calcium handling proteins and as a consequence intracellular calcium levels, change during myotube differentiation process[237–239]. Hence, when working with myotubes from healthy and dystrophic patients, it is essential to compare myotubes at same maturation stage, in order to discriminate dystrophic features from differentiation induced changes. For this reason, in this study morphology and differentiation of two different human models, based on immortalised human myoblasts, were evaluated in order to select the optimum model to test the effect of AHK compounds.

First, patient-derived immortalised human myoblasts from two healthy donors and a DMD patient were analysed. In order to select the control that better matched DMD cells, all the lines were compared for morphology and maturation. Myotube width was used to assess morphology, whereas CK activity and the expression (at mRNA and protein level) of several maturation markers was used to analyse maturation. The results showed that differences in myotube width and CK activity were present not only between control and dystrophic myotubes but also between the two control cell lines, suggesting that myotubes did not reach the same maturation stage in culture. This observation was further confirmed by analysing the expression levels of several maturation-related genes and proteins. Thus, taking into account CK activity and

CAPN3 and CK mRNA levels, we found that CTRL2 and DMD myotubes reached a similar maturation stage, while CTRL1 myotubes were more mature (Figure 2 and 3A). However, protein expression levels indicate the opposite result, where dystrophic myotubes maturation was more similar to CTRL1 myotubes than to CTRL2 (Figure 4). All together, these results indicate that none of the control myotubes studied in this work was appropriate for our dystrophic cell line due to differences in the differentiation stages of the myotubes from different donors. This fact makes comparison among different cell lines very challenging, since it is difficult to discriminate between dystrophic features and maturation-induced differences. Overall, the inter-individual variability found among the cell lines used in these experiments has been previously described by several authors as a characteristic of primary myotubes and it has been attributed to the combination of different factors, such as genetic background, physiologic conditions or medical history[137,159].

Next, in order to reduce the inter-individual variability found between cells from different donors, a new model was developed using long-term gene silencing of dystrophin in a healthy myoblast line. Thus, dystrophin was knocked down using lentiviral infections with shRNA specific for dystrophin in LHCN-M2 immortalised myoblasts. In contrast to the previous model, no differences were found in morphology or maturation between NS-shRNA and DYST-shRNA myotubes, indicating that this model resolves the inter-individual variability observed in the previous model, when using myotubes from different donors. After verifying that cells were at the same maturation stage, dystrophin knock-down was confirmed at mRNA and protein levels. Interestingly, in this model, dystrophin deficiency was accompanied by a reduction of α-sarcoglycan protein levels, which is a phenotypic feature of DMD[100,115,120,240]. Overall, these results show that silencing dystrophin in myoblasts enable the study of phenotypic variations that are induced by dystrophin deficiency using the same cell line as a control. For this reason, within the proposed models, DYST-shRNA silencing model was selected to study RyR1 macromolecular complex structure and calcium homeostasis in DMD and to test the effect of AHK compounds.

In the present study, RyR1 was found to be abnormally S-nitrosylated and PKA-phosphorylated in DYST-deficient human myotubes leading to a reduction of Calst1 binding (Figure 11 and 12). This mechanism has been previously found in animal models of DMD and other pathologies such as LGMD, chronic exercise, aging and heart failure[56,58,197,207]. In humans, evidences of RyR1-Calst1 complex disruption have been described after chronic exercise, heart failure and in patients under mechanic ventilation[58,207,241]. However, to our knowledge, this is the first evidence of RyR1-Calst1 disruption in a human model of DMD.

Interestingly, in DYST-deficient myotubes Calst1 depletion from RyR1 was accompanied by a significant increase in intracellular calcium levels. This result is in accordance with previous works were leaky RyR1 has been proposed to contribute to the dysregulation of intracellular calcium levels in dystrophic muscles[56,75]. In addition, several works have described elevated intracellular calcium levels in mouse models, patient-derived human DMD myotubes[75,124,194,242] and biopsies from DMD patients[30,37,243]. However, it has been previously suggested that myotube contraction was essential to induce an increase of intracellular calcium levels *in vitro* in dystrophic myotubes[141]. Interestingly, the results obtained in this work suggest that obtaining highly mature myotubes could be enough to detect dysregulation of calcium homeostasis on human *in vitro* myotubes.

AHK compounds are RyR1 stabilisers that have been designed to increase RyR1-Calst1 binding and regulate intracellular calcium levels in the muscle. The results obtained in this study demonstrated that the AHK compounds A6 and A7 efficiently increased RyR1-Calst1 binding and reduced intracellular calcium levels in a human DMD model (Figure 13 and 15), suggesting that these compounds could also be used as a therapeutic alternative to treat DMD patients. These results are consistent with our previous studies showing that AHK compounds increase RyR1-Calst1 binding in human myotubes under peroxinitrite-induced stress, reduce intracellular calcium levels in mdx dystrophic fibres, and improve dystrophic phenotype of mdx mice (unpublished data; Chapters 1 and 2). Since calcium dysregulation is considered one of the initial triggers

of DMD pathogenesis[30,75], compounds such as AHK molecules that target this early event may result in potential pharmacological treatments for dystrophic patients.

Intriguingly, when analysing the concentration-effect relationship of AHK compounds, treating cells with higher concentration of AHK compounds did not produce more effect in terms of reduction of intracellular calcium levels (Figure 15 and 16). In fact, in A7 treated DYST-shRNA myotubes no effect was shown with 150 nM treatment, whereas a significant reduction of calcium levels was observed after treating cells with a 50 nM concentration. Conversely, in control myotubes 150 nM AHK significantly increased intracellular calcium levels while no effect was observed with 50 nM treatment (Figure 15B and 16B). Although further studies should be done to elucidate the exact mechanisms underlying this event, our results suggest that AHK compounds have a dose-effect that may be due to different conformational changes on RyR1-Calst1 interaction depending on their concentration or to unspecific activation of other calcium-handling proteins. This biphasic effect has been repeatedly related to drugs that produce allosteric modulation of their target proteins and it is especially prevalent in drugs targeting ion channels[244,245]. Furthermore, allosteric regulation of RyR by different regulatory proteins and ligands has been previously decribed[36,62,246,247]. Thus, in future studies, the exact mechanism of action of AHK compounds should be further characterised in order to determine compounds safety dosage and off targets.

In summary, our results indicate that the human DMD model based on silencing dystrophin expression with shRNA in myotubes, recapitulates several features of DMD, validating its relevance for studying this disease. Accordingly, the model was successfully used to validate, for the first time, the RyR1-Calst1 target in a human DMD model and to test novel compounds that modulate this interaction. Furthermore, the AHK compounds A6 and A7 demonstrated their efficacy in human muscle cells, using RyR1-Calst1 binding and intracellular calcium levels as endpoints. Since dysregulation of calcium homeostasis is a mechanism proposed to trigger muscle degeneration in DMD patients, we expect that AHK compounds will constitute a promising therapeutic alternative for dystrophic patients.

CONCLUSIONS

CONCLUSIONS

1. In mouse and human myotube cultures, AHK compounds show very low or undetectable *in vitro* toxicity, in contrast to another RyR modulator, rycal S107, which is cytotoxic at 1 mM concentration.

2. *In situ* proximity ligation assay (PLA) technique has been used to effectively quantify RyR post-translational modifications and Calst1 binding in human myotube cultures.

3. In human myotubes, the peroxynitrite donor SIN-1 induces RyR1 PKA-phosphorylation, RyR1 S-nitrosylation, and Calst1 depletion from RyR1 complexes. This model can be useful for screening drug candidates targeting these events.

4. The AHK compounds A6 and A7, as well as S107 increase RyR1-Calst1 interaction in human myotubes under peroxynitrite-induced stress, while they do not affect RyR1-Calst1 interaction in control myotubes.

5. *In vitro* and *in vivo* treatments with AHK compounds and S107 normalise resting intracellular calcium levels of isolated muscle fibres from dystrophic mdx mice.

6. In mdx mice, 5-week treatments with the AHK compounds A6 and A7, as well as S107, reduce histopathological and biochemical evidence of muscle damage and ameliorate overall muscle weakness. In contrast, these RyR modulators do not have any obvious effect in wild type mice.

7. The *in vitro* human model of DMD, generated by silencing dystrophin expression with shRNAs in the human immortalised LHCN-M2 myoblasts, recapitulates many features of DMD muscles, such as reduced α-sarcoglycan expression, increased RyR1 PKA-dependent phosphorylation and S-nitrosylation, reduced RyR1-Calst1 interaction and increased intracellular calcium levels.

8. In dystrophin-deficient human myotubes, AHK compounds significantly increase RyR1-Calst1 binding and they normalise intracellular calcium levels, which support their potential as alternative therapeutic drugs for DMD patients.

THESIS

The Ahulken compounds, targeting RyR1-Calst1 interaction, tested in this PhD thesis has proven to be useful as a treatment for Duchenne muscular dystrophy. Additionally, using mouse and human models of DMD this work supports the usefulness of RyR1-Calst1 as a therapeutic target for drug development against Duchenne and Becker muscular dystrophies.

REFERENCES

REFERENCES

1. Frontera, W. R. & Ochala, J. Skeletal muscle: a brief review of structure and function. *Calcified tissue international* **96,** 183–195 (2015).

2. Relaix, F. & Zammit, P. S. Satellite cells are essential for skeletal muscle regeneration: the cell on the edge returns centre stage. *Development* **139,** 2845–56 (2012).

3. Rode, C., Siebert, T., Tomalka, A. & Blickhan, R. Myosin filament sliding through the Z-disc relates striated muscle fibre structure to function. *Proc. R. Soc. B Biol. Sci.* **283,** 20153030 (2016).

4. Szentesi, P., Zaremba, R., van Mechelen, W. & Stienen, G. J. ATP utilization for calcium uptake and force production in different types of human skeletal muscle fibres. *J. Physiol.* **531,** 393–403 (2001).

5. Knowles, A. C., Irving, M. & Sun, Y.-B. Conformation of the troponin core complex in the thin filaments of skeletal muscle during relaxation and active contraction. *J. Mol. Biol.* **421,** 125–37 (2012).

6. Rittler, M. R. Sarcoplasmic Reticulum Calcium Handling in Maturing Skeletal Muscle From Two Models of Dystrophic Mice. (2002).

7. Berchtold, M. W., Brinkmeier, H. & Müntener, M. Calcium ion in skeletal muscle: its crucial role for muscle function, plasticity, and disease. *Physiol. Rev.* **80,** 1215–65 (2000).

8. Schiaffino, S. & Reggiani, C. Fiber types in mammalian skeletal muscles. *Physiol.*

Rev. **91,** 1447–531 (2011).

9. Petera, A., Chenga, H., Rossa, R., Knowltona, K. & Chena, J. The costamere bridges sarcomeres to the sarcolemma in striated muscle. *Prog Pediatr Cardiol* **31,** 83–88 (2013).

10. Mishra, P., Varuzhanyan, G., Pham, A. H. & Chan, D. C. Mitochondrial Dynamics Is a Distinguishing Feature of Skeletal Muscle Fiber Types and Regulates Organellar Compartmentalization. *Cell Metab.* **22,** 1033–1044 (2015).

11. Peterson, C. M., Johannsen, D. L. & Ravussin, E. Skeletal muscle mitochondria and aging: A review. *Journal of Aging Research* **2012,** (2012).

12. Caswell, A. H. & Brandt, N. R. Activation of Skeletal Muscle. 1–6 (2012).

13. Scott, W., Stevens, J. & Binder-Macleod, S. A. Human skeletal muscle fiber type classifications. *Phys. Ther.* **81,** 1810–6 (2001).

14. Baylor, S. M. & Hollingworth, S. Intracellular calcium movements during excitation-contraction coupling in mammalian slow-twitch and fast-twitch muscle fibers. *J. Gen. Physiol.* **139,** 261–72 (2012).

15. Westerblad, H., Bruton, J. D. & Katz, A. Skeletal muscle: energy metabolism, fiber types, fatigue and adaptability. *Exp. Cell Res.* **316,** 3093–9 (2010).

16. Schneider, J. S. *et al.* Increased sarcolipin expression and decreased sarco(endo)plasmic reticulum Ca2+ uptake in skeletal muscles of mouse models of Duchenne muscular dystrophy. *J. Muscle Res. Cell Motil.* **34,** 349–56 (2013).

17. Nguyen-Tran, D.-H. *et al.* Molecular mechanism of sphingosine-1-phosphate action in Duchenne muscular dystrophy. *Dis. Model. Mech.* 1–14 (2014).

18. Kramerova, i; Kudryashova, E; Ermolova, N. Impaired calcium calmodulin kinase signaling and muscle adaptation response in the absence of calpain 3. *Hum. Mol. Genet.* **21,** 3193–3204 (2012).

19. Baylor, S. M. & Hollingworth, S. Calcium indicators and calcium signalling in skeletal muscle fibres during excitation-contraction coupling. *Prog. Biophys. Mol. Biol.* **105,** 162–79 (2011).

20. Eltit, J. M. *et al.* Orthograde dihydropyridine receptor signal regulates ryanodine receptor passive leak. *Proc. Natl. Acad. Sci. U. S. A.* **108,** 7046–51 (2011).

21. Witherspoon, J. W. & Meilleur, K. G. Review of RyR1 pathway and associated pathomechanisms. *Acta Neuropathol. Commun.* **4,** 121 (2016).

22. Periasamy, M. & Kalyanasundaram, A. SERCA pump isoforms: Their role in calcium transport and disease. *Muscle and Nerve* **35,** 430–442 (2007).

23. Lamboley, C. R., Murphy, R. M., McKenna, M. J. & Lamb, G. D. Sarcoplasmic reticulum Ca2+ uptake and leak properties, and SERCA isoform expression, in type I and type II fibres of human skeletal muscle. *J. Physiol.* **592,** 1381–95 (2014).

24. Stiber, J. a & Rosenberg, P. B. The role of store-operated calcium influx in skeletal muscle signaling. *Cell Calcium* **49,** 341–9 (2011).

25. Bellinger, A. M., Mongillo, M. & Marks, A. R. Stressed out: the skeletal muscle

ryanodine receptor as a target of stress. *J. Clin. Invest.* **118,** 445–453 (2008).

26. Heizmann, C. W., Berchtold, M. W. & Rowlerson, a M. Correlation of parvalbumin concentration with relaxation speed in mammalian muscles. *Proc. Natl. Acad. Sci. U. S. A.* **79,** 7243–7 (1982).

27. Schwaller, B. *et al.* Prolonged contraction-relaxation cycle of fast-twitch muscles in parvalbumin knockout mice. *Am. J. Physiol.* **276,** C395-403 (1999).

28. Chen, H.-H. *et al.* NRIP is a novel Z-disc protein to activate calmodulin signaling for skeletal muscle contraction and regeneration. *J. Cell Sci.* **44,** 4196–4209 (2015).

29. Sacchetto, R., Bovo, E. & Damiani, E. The Ca 2 + -Calmodulin Dependent Protein Kinase II System of Skeletal Muscle Sarcoplasmic Reticulum. (2005).

30. Vallejo-illarramendi, A., Toral-ojeda, I., Aldanondo, G. & Munain, A. L. De. Dysregulation of calcium homeostasis in muscular dystrophies. *Expert Rev. Mol. Med.* **16,** 1–23 (2014).

31. Lange, S. *et al.* Obscurin determines the architecture of the longitudinal sarcoplasmic reticulum. *J. Cell Sci.* **122,** 2640–50 (2009).

32. Ackermann, M. a *et al.* Integrity of the network sarcoplasmic reticulum in skeletal muscle requires small ankyrin 1. *J. Cell Sci.* **124,** 3619–30 (2011).

33. Inesi, G. & Tadini-Buoninsegni, F. Ca(2+)/H (+) exchange, lumenal Ca(2+) release and Ca (2+)/ATP coupling ratios in the sarcoplasmic reticulum ATPase. *J. Cell Commun. Signal.* **8,** 5–11 (2014).

34. Lamboley, C. R., Murphy, R. M., McKenna, M. J. & Lamb, G. D. Endogenous and maximal sarcoplasmic reticulum calcium content and calsequestrin expression in type I and type II human skeletal muscle fibres. *J. Physiol.* **591,** 6053–68 (2013).

35. Murphy, R. M., Larkins, N. T., Mollica, J. P., Beard, N. A. & Lamb, G. D. Calsequestrin content and SERCA determine normal and maximal Ca 2 + storage levels in sarcoplasmic reticulum of fast- and slow-twitch fibres of rat. *J. Physiol. Physiol.* **2,** 443–460 (2009).

36. Van Petegem, F. Ryanodine receptors: Allosteric ion channel giants. *J. Mol. Biol.* **427,** 31–53 (2015).

37. Farini, A. *et al.* Inositol 1,4,5-trisphosphate (IP3)-dependent Ca2+ signaling mediates delayed myogenesis in Duchenne muscular dystrophy fetal muscle. *Dev.* **143,** 658–669 (2016).

38. Zecchini, E. & Pinton, P. Ca2+ transfer from the ER to mitochondria: when, how and why. *Biochim. Biophys. Acta* **1787,** 1342–1351 (2010).

39. Lanner, J. T., Georgiou, D. K., Joshi, A. D. & Hamilton, S. L. Ryanodine receptors: structure, expression, molecular details, and function in calcium release. *Cold Spring Harb. Perspect. Biol.* **2,** 1–21 (2010).

40. Liu, X. *et al.* Role of Leaky Neuronal Ryanodine Receptors in Stress- Induced Cognitive Dysfunction. *Cell* **150,** 1055–1067 (2012).

41. Guerrero-hernandez, Q. A., Avila, G. & Rueda, A. Ryanodine receptors as leak channels. *Eur. J. Pharmacol.* 1–13 (2013).

42. Dulhunty, A. F., Wei-LaPierre, L., Casarotto, M. G. & Beard, N. A. Core skeletal muscle ryanodine receptor calcium release complex. *Clin. Exp. Pharmacol. Physiol.* **44,** 3–12 (2017).

43. Cherednichenko, G. *et al.* Enhanced Excitation-Coupled Calcium Entry in Myotubes Expressing Malignant Hyperthermia Mutation R163C Is Attenuated by Dantrolene. *Mol Pharmacol.* **73,** 1203–1212 (2009).

44. Avila, G., O'Brien, J. J. & Dirksen, R. T. Excitation--contraction uncoupling by a human central core disease mutation in the ryanodine receptor. *Proc. Natl. Acad. Sci. U. S. A.* **98,** 4215–20 (2001).

45. des Georges, A; Clarke, OB; Zalk, R; Yuan, Q; Condon, KJ; Grassucci, RA; Hendrickson, WA; Marks, AR; Joachim, F. Structural basis for gating and activation of RyR1. *Cell* **150,** 137–143 (2016).

46. Capes, E. M., Loaiza, R. & Valdivia, H. H. Ryanodine receptors. *Skelet. Muscle* **1,** 18 (2011).

47. Wang, S.-Q., Song, L.-S., Lakatta, E. G. & Cheng, H. Ca2+ signalling between single L-type Ca2+ channels and ryanodine receptors in heart cells. *Nature* **410,** 592–596 (2001).

48. O'Brien, F., Venturi, E. & Sitsapesan, R. The ryanodine receptor provides high throughput Ca2+-release but is precisely regulated by networks of associated proteins: a focus on proteins relevant to phosphorylation. *Biochem Soc Trans* **43,** 426–433 (2015).

49. Chaube, R. *et al.* Regulation of the Skeletal Muscle Ryanodine Receptor / Ca 2+

-release Channel RyR1 by S -Palmitoylation *. *J. Biol. Chem.* **289,** 8612–8619 (2014).

50. Breckner, A. *et al.* Effect of Calstabin1 Depletion on Calcium Transients and Energy Utilization in Muscle Fibers and Treatment Opportunities with RyR1 Stabilizers. *PLoS One* **8,** 1–8 (2013).

51. Lam, E. *et al.* A novel FK506 binding protein can mediate the immunosuppressive effects of FK506 and is associated with the cardiac ryanodine receptor. *J. Biol. Chem.* **270,** 26511–26522 (1995).

52. Venturi, E. *et al.* FKBP12.6 activates RyR1: Investigating the amino acid residues critical for channel modulation. *Biophys. J.* **106,** 824–833 (2014).

53. Girgenrath, T. *et al.* N-terminal and central segments of the type 1 ryanodine receptor mediate its interaction with FK506-binding proteins. *J. Biol. Chem.* **288,** 16073–16084 (2013).

54. Mei, Y. *et al.* Stabilization of the Skeletal Muscle Ryanodine Receptor Ion Channel-FKBP12 Complex by the 1 , 4- Benzothiazepine Derivative S107. *PLoS One* **8,** (2013).

55. Bellinger, A. M. *et al.* Hypernitrosylated ryanodine receptor calcium release channels are leaky in dystrophic muscle. *Nat. Med.* **15,** 325–30 (2009).

56. Andersson, D. C. *et al.* Leaky ryanodine receptors in beta-sarcoglycan deficient mice: a potential common defect in muscular dystrophy. *Skelet. Muscle* **2,** 9 (2012).

57. Wehrens, X. H. T. *et al.* Protection from cardiac arrhythmia through ryanodine receptor-stabilizing protein calstabin2. *Science* **304,** 292–296 (2004).

58. Reiken, S. *et al.* PKA phosphorylation activates the calcium release channel (ryanodine receptor) in skeletal muscle: defective regulation in heart failure. *J. Cell Biol.* **160,** 919–28 (2003).

59. Aracena-Parks, P. *et al.* Identification of cysteines involved in S-nitrosylation, S-glutathionylation, and oxidation to disulfides in ryanodine receptor type 1. *J. Biol. Chem.* **281,** 40354–40368 (2006).

60. Aracena, P. & Hamilton, S. L. Effects of S-Glutathionylation and S-Nitrosylation on Calmodulin Binding to Triads and FKBP12 Binding to Type 1 Calcium Release Channels. *Antioxid. Redox Signal.* **7,** 870–881 (2005).

61. Ward, C. W. *et al.* Defects in ryanodine receptor calcium release in skeletal muscle from post-myocardial infarct rats. *FASEB J.* **17,** 1517–9 (2003).

62. Zhao, Y.-T. *et al.* Sensitized signalling between L-type Ca 2+ channels and ryanodine receptors in the absence or inhibition of FKBP12.6 in cardiomyocytes. *Cardiovasc. Res.* 1–11 (2017).

63. O'Reilly, F. M. *et al.* FKBP12 modulation of the binding of the skeletal ryanodine receptor onto the II-III loop of the dihydropyridine receptor. *Biophys. J.* **82,** 145–155 (2002).

64. Gouspillou, G. & Hepple, R. T. Editorial: Mitochondria in Skeletal muscle health, aging and diseases. *Front. Physiol.* **7,** 10–13 (2016).

65. Franzini-armstrong, C. ER-Mitochondria Communication. How Privileged? *Physiology* **22,** 261–268 (2007).

66. Vance, J. E. MAM (mitochondria-associated membranes) in mammalian cells: Lipids and beyond. *Biochim. Biophys. Acta - Mol. Cell Biol. Lipids* **1841,** 595–609 (2014).

67. Dirksen, R. T. Sarcoplasmic reticulum–mitochondrial through-space coupling in skeletal muscleThis paper is one of a selection of papers published in this Special Issue, entitled 14th International Biochemistry of Exercise Conference – Muscles as Molecular and Metabolic . *Appl. Physiol. Nutr. Metab.* **34,** 389–395 (2009).

68. Rizzuto, R. *et al.* Ca(2+) transfer from the ER to mitochondria: when, how and why. *Biochim. Biophys. Acta* **1787,** 1342–51 (2009).

69. Yi, J. *et al.* Mitochondrial calcium uptake regulates rapid calcium transients in skeletal muscle during excitation-contraction (E-C) coupling. *J. Biol. Chem.* **286,** 32436–32443 (2011).

70. Pizzo, P., Drago, I., Filadi, R. & Pozzan, T. Mitochondrial Ca 2+ homeostasis: Mechanism, role, and tissue specificities. *Pflugers Archiv European Journal of Physiology* **464,** 3–17 (2012).

71. Nicholls, D. G. Mitochondria and calcium signaling. *Cell Calcium* **38,** 311–7 (2005).

72. Sohal, S, R., Orr & C, W. The Redox Stress Hypothesis of Aging. *Free radic biol med* **52,** 539–555 (2013).

73. Rossi, A. E., Boncompagni, S., Wei, L., Protasi, F. & Dirksen, R. T. Differential impact of mitochondrial positioning on mitochondrial Ca 2 ∂ uptake and Ca 2 ∂ spark suppression in skeletal muscle. *Am J Physiol Cell Physiol* **301,** 1128–1139 (2011).

74. Mah, J. K. Current and emerging treatment strategies for Duchenne muscular dystrophy. *Neuropsychiatr. Dis. Treat.* **12,** 1795–1807 (2016).

75. Allen, D., Whitehead, N. P., Allen, D. G., Whitehead, N. P. & Froehner, S. C. Absence of Dystrophin Disrupts Skeletal Muscle Signaling: Roles of Ca2+, Reactive Oxygen Species, and Nitric Oxide in the Development of Muscular Dystrophy. *Physiol. Rev.* **96,** 253–305 (2015).

76. Bladen, C. L. *et al.* The TREAT-NMD DMD global database: Analysis of more than 7,000 duchenne muscular dystrophy mutations. *Hum. Mutat.* **36,** 395–402 (2015).

77. Juan-Mateu, J. *et al.* DMD mutations in 576 dystrophinopathy families: A step forward in genotype-phenotype correlations. *PLoS One* **10,** 1–21 (2015).

78. Gentil, C. *et al.* Variable phenotype of del45-55 Becker patients correlated with nNOS m mislocalization and RYR1 hypernitrosylation. *Hum. Mol. Genet.* 1–12 (2012).

79. Bushby, K. *et al.* Diagnosis and management of Duchenne muscular dystrophy, part 1: diagnosis, and pharmacological and psychosocial management. *The Lancet Neurology* **9,** 77–93 (2010).

80. Rae, M. G. & O'Malley, D. Cognitive dysfunction in Duchenne Muscular

Dystrophy: a possible role for neuromodulatory immune molecules. *J. Neurophysiol.* jn.00248.2016 (2016).

81. Anderson, J. L., Head, S. I., Rae, C. & Morley, J. W. Brain function in Duchenne muscular dystrophy. *Brain* **125,** 4–13 (2002).

82. Angelini, C. Muscular dystrophy. *Handb. Clin. Neurol.* **95,** (2010).

83. Archer, J. E., Gardner, A. C., Roper, H. P., Chikermane, A. A. & Tatman, A. J. Duchenne muscular dystrophy: the management of scoliosis. *J. Spine Surg.* **2,** 185–194 (2016).

84. Bushby, K. *et al.* Diagnosis and management of Duchenne muscular dystrophy, part 2: implementation of multidisciplinary care. *Lancet Neurol.* **9,** 177–189 (2010).

85. Klingler, W., Jurkat-Rott, K., Lehmann-Horn, F. & Schleip, R. The role of fibrosis in Duchenne muscular dystrophy. *Acta Myol.* **31,** 184–195 (2012).

86. Polavarapu, K. *et al.* Muscle MRI in Duchenne muscular dystrophy: Evidence of a distinctive pattern. *Neuromuscul. Disord.* **26,** 768–774 (2016).

87. Bonati, U. *et al.* Quantitative muscle MRI: A powerful surrogate outcome measure in Duchenne muscular dystrophy. *Neuromuscul. Disord.* **25,** 679–685 (2015).

88. Willcocks, R. J. *et al.* Multicenter prospective longitudinal study of magnetic resonance biomarkers in a large duchenne muscular dystrophy cohort. *Ann. Neurol.* **79,** 535–547 (2016).

89. Laing, N. G., Davis, M. R., Bayley, K., Fletcher, S. & Wilton, S. D. Molecular diagnosis of duchenne muscular dystrophy: Past, present and future in relation to implementing therapies. *Clin. Biochem. Rev.* **32,** 129–134 (2011).

90. Aartsma-Rus, A., Ginjaar, I. B. & Bushby, K. The importance of genetic diagnosis for Duchenne muscular dystrophy. *J Med Genet* **53,** 145–151 (2016).

91. Flanigan, K. M. *et al.* Mutational Spectrum of DMD Mutations in Dystrophinopathy Patients: Application of Modern Diagnostic Techniques to a Large Cohort. *Hum Mutat.* **30,** 1657–1666 (2012).

92. Suriyonplengsaeng, C. *et al.* Immunohistochemistry of sarcolemmal membrane-associated proteins in formalin-fixed and paraffin-embedded skeletal muscle tissue: a promising tool for the diagnostic evaluation of common muscular dystrophies. *Diagn. Pathol.* **12,** 19 (2017).

93. Lai, Y. *et al.* Dystrophins carrying spectrin-like repeats 16 and 17 anchor nNOS to the sarcolemma and enhance exercise performance in a mouse model of muscular dystrophy. *J. Clin. Invest.* **119,** 624–635 (2009).

94. McGreevy, J. W., Hakim, C. H., McIntosh, M. A. & Duan, D. Animal models of Duchenne muscular dystrophy: from basic mechanisms to gene therapy. *Dis Model Mech* **8,** 195–213 (2015).

95. Nelson, C. E. *et al.* In vivo genome editing improves muscle function in a mouse model of Duchenne muscular dystrophy. *Science (80-.).* **5143,** 1–8 (2015).

96. Nakamura, T. *et al.* Aberrant Protein S-nitrosylation in neurodegenerative diseases. *Neuron* **78,** 596–614 (2013).

97. Sekiguchi, M. *et al.* A deficit of brain dystrophin impairs specific amygdala GABAergic transmission and enhances defensive behaviour in mice. *Brain* **132,** 124–135 (2009).

98. Dumont, N. A. *et al.* Dystrophin expression in muscle stem cells regulates their polarity and asymmetric division. *Nat. Med.* **21,** 1455–1463 (2016).

99. Chang, N. C., Chevalier, F. P. & Rudnicki, M. A. Satellite Cells in Muscular Dystrophy – Lost in Polarity. *Trends Mol. Med.* **22,** 479–496 (2016).

100. Nowak, K. J. & Davies, K. E. Duchenne muscular dystrophy and dystrophin: pathogenesis and opportunities for treatment. *EMBO Rep.* **5,** 872–876 (2004).

101. Burr, A. & Molkentin, J. Genetic evidence in the mouse solidifies the calcium hypothesis of myofiber death in muscular dystrophy. *Cell Death Differ.* **22,** 1402–1412 (2015).

102. Deconinck, N. & Dan, B. Pathophysiology of Duchenne Muscular Dystrophy: Current Hypotheses. *Pediatr. Neurol.* **36,** 1–7 (2007).

103. Millay, D. P. *et al.* Calcium influx is sufficient to induce muscular dystrophy through a TRPC-dependent mechanism. *PNAS* **106,** 19023–19028 (2009).

104. Onopiuk, M. *et al.* Store-operated calcium entry contributes to abnormal Ca2+ signalling in dystrophic mdx mouse myoblasts. *Arch. Biochem. Biophys.* **569,** 1–9 (2015).

105. Kaneko, Y. & Szallasi, A. Transient receptor potential (TRP) channels: A clinical perspective. *Br. J. Pharmacol.* **171,** 2474–2507 (2014).

106. Dorn, G. W. & Maack, C. SR and mitochondria: calcium cross-talk between kissing cousins. *J. Mol. Cell. Cardiol.* **55,** 42–9 (2013).

107. Gehrig, S. M. *et al.* Hsp72 preserves muscle function and shows progression of severe muscular dystrophy. *Nature* **484,** 394–398 (2012).

108. Goonasekera, S. A. *et al.* Mitigation of muscular dystrophy in mice by SERCA overexpression in skeletal muscle. *J. Clin. Invest.* **121,** 1–9 (2011).

109. Morine, K. J., Sleeper, M. M., Barton, E. R. & Sweeney, H. L. Overexpression of SERCA1a in the mdx diaphragm reduces susceptibility to contraction-induced damage. *Hum. Gene Ther.* **21,** 1735–9 (2010).

110. Mazala, D. a. G. *et al.* SERCA1 overexpression minimizes skeletal muscle damage in dystrophic mouse models. *Am. J. Physiol. - Cell Physiol.* **308,** ajpcell.00341.2014 (2015).

111. Lipscomb, L., Piggott, R. W., Emmerson, T. & Winder, S. J. Dasatinib as a treatment for Duchenne muscular dystrophy. *Hum. Mol. Genet.* **25,** 266–274 (2016).

112. Carre-Pierrat, M. *et al.* Pre-clinical study of 21 approved drugs in the mdx mouse. *Neuromuscul. Disord.* **21,** 313–27 (2011).

113. Klymiuk, N. *et al.* Dystrophin-deficient pigs provide new insights into the hierarchy of physiological derangements of dystrophic muscle. *Hum. Mol. Genet.* **22,** 4368–4382 (2013).

114. Kornegay, J. N. *et al.* Canine Models of Duchenne Muscular Dystrophy and Their

Use in Therapeutic Strategies. *Mamm Genome* **23,** 85–108 (2012).

115. Manning, J. & O'Malley, D. What has the mdx mouse model of duchenne muscular dystrophy contributed to our understanding of this disease? *J. Muscle Res. Cell Motil.* **36,** 155–167 (2015).

116. Spurney, C. F. *et al.* Preclinical drug trials in the mdx mouse: assessment of reliable and sensitive outcome measures. *Muscle Nerve* **39,** 591–602 (2009).

117. Briguet, A., Courdier-Fruh, I., Foster, M., Meier, T. & Magyar, J. P. Histological parameters for the quantitative assessment of muscular dystrophy in the mdx-mouse. *Neuromuscul. Disord.* **14,** 675–82 (2004).

118. Whitehead, N. P., Yeung, E. W. & Allen, D. G. Muscle damage in mdx (dystrophic) mice: role of calcium and reactive oxygen species. *Clin. Exp. Pharmacol. Physiol.* **33,** 657–662 (2006).

119. Bates, G. *et al.* Molecular , cellular , and muscle strip mechanics of the mdx mouse diaphragm. *Am J Physiol Cell Physiol* **304,** 873–880 (2013).

120. Hnia, K. *et al.* Pathological pattern of Mdx mice diaphragm correlates with gradual expression of the short utrophin isoform Up71. *Biochim. Biophys. Acta* **1762,** 362–372 (2006).

121. Tkatchenko, A. V, Cam, G. Le, Leger, J. J. & Dechesne, C. A. Large-scale analysis of di ¡ erential gene expression in the hindlimb muscles and diaphragm of mdx mouse. *Biochim. Biophys. Acta* **1500,** (2000).

122. Luca, A. De & Farmacologia, S. Use of grip strength meter to assess the limb

strength of mdx mice. 1–11 (2010).

123. Robin, G., Berthier, C. & Allard, B. Sarcoplasmic reticulum Ca 2 + permeation explored from the lumen side in mdx muscle fibers under voltage control. *J. Gen. Physiol.* **139,** 209–218 (2012).

124. Altamirano, F; Valladares, D; Henríquez-Olguín, C; Casas, M. & López, JR; Allen, PD; Jaimovich, E. Nifedipine Treatment Reduces Resting Calcium Concentration, Oxidative and Apoptotic Gene Expression , and Improves Muscle Function in Dystrophic mdx Mice. *PLoS One* **8,** 4–13 (2013).

125. Fraysse, B. *et al.* The alteration of calcium homeostasis in adult dystrophic mdx muscle fibers is worsened by a chronic exercise in vivo. *Neurobiol. Dis.* **17,** 144–54 (2004).

126. Tinsley, J. *et al.* Expression of full-length utrophin prevents muscular dystrophy in mdx mice. *Nat. Med.* **4,** 1441–1444 (1998).

127. Squire, S. *et al.* Prevention of pathology in mdx mice by expression of utrophin: Analysis using an inducible transgenic expression system. *Human Molecular Genetics* **11,** 3333–3344 (2002).

128. Sacco, A. *et al.* Short Telomeres and Stem Cell Exhaustion Model Duchenne Muscular Dystrophy in mdx/mTR Mice. **143,** 1059–1071 (2011).

129. Chandrasekharan, K. *et al.* Introduction of a human-specific deletion in mouse Cmah increases disease severity in the mdx model of Duchenne muscular dystrophy. *Sci Transl Med* **2,** (2010).

130. Radley-Crabb, H. *et al.* A single 30 min treadmill exercise session is suitable for 'proof-of concept studies' in adult mdx mice: a comparison of the early consequences of two different treadmill protocols. *Neuromuscul. Disord.* **22,** 170–82 (2012).

131. Luca, A. De. Use of treadmill and wheel exercise for impact on mdx mice phenotype. *Neuromuscul. Netw. Protoc.* 1–11 (2011).

132. Isaac, C. *et al.* Dystrophin and Utrophin 'Double Knockout' Dystrophic Mice Exhibit a Spectrum of Degenerative Musculoskeletal Abnormalities. *J orthop res-* **31,** 343–349 (2014).

133. Kobayashi, Y. M., Rader, E. P., Crawford, R. W. & Campbell, K. P. Endpoint measures in the mdx mouse relevant for muscular dystrophy pre-clinical studies. *Neuromuscul. Disord.* **22,** 34–42 (2012).

134. Smith, A. S. T., Davis, J., Lee, G., Mack, D. L. & Kim, D. Muscular dystrophy in a dish- Engineered human skeletal muscle mimetics for disease modeling and drug discovery. **21,** 1387–1398 (2016).

135. Marg, A. *et al.* Human satellite cells have regenerative capacity and are genetically manipulatable. *J Clin Invest* **124,** 4257–4265 (2014).

136. Jarocha, D., Stangel-Wojcikiewicz, K., Basta, A. & Majka, M. Efficient myoblast expansion for regenerative medicine use. *Int. J. Mol. Med.* **34,** 83–91 (2014).

137. Owens, J., Moreira, K. & Bain, G. Characterization of primary human skeletal muscle cells from multiple commercial sources. *In Vitro Cell. Dev. Biol. Anim.* **49,** 695–705 (2013).

138. Boldrin, L., Muntoni, F. & Morgan, J. E. Are Human and Mouse Satellite Cells Really the Same ? The Journal of Histochemistry & Cytochemistry. *Histochemistry* **58,** 941–955 (2010).

139. Juretic, N., Jorquera, G., Caviedes, P., Jaimovich, E. & Riveros, N. Electrical stimulation induces calcium-dependent up-regulation of neuregulin-1beta in dystrophic skeletal muscle cell lines. *Cell Physiol Biochem* **29,** 919–930 (2012).

140. Nikolić, N. *et al.* Electrical pulse stimulation of cultured human skeletal muscle cells as an in vitro model of exercise. *PLoS One* **7,** 1–10 (2012).

141. Deval, E. *et al.* Na+/Ca2+ exchange in human myotubes: Intracellular calcium rises in response to external sodium depletion are enhanced in DMD. *Neuromuscul. Disord.* **12,** 665–673 (2002).

142. Imbert, N. *et al.* Hypoosmotic shocks induce elevation of resting calcium level in duchenne muscular dystrophy myotubes contracting in vitro. *Neuromuscul Disord* **6,** 351–360 (1996).

143. Vandebrouck, C., Duport, G., Raymond, G. & Cognard, C. Hypotonic medium increases calcium permeant channels activity in human normal and dystrophic myotubes. *Neurosci. Lett.* **323,** 239–43 (2002).

144. Vandenburgh, H. *et al.* Automated drug screening with contractile muscle tissue engineered from dystrophic myoblasts. *FASEB J.* **23,** 3325–3334 (2009).

145. Nesmith, A. P. *et al.* A human in vitro model of Duchenne muscular dystrophy muscle formation and contractility. *J. Cell Biol.* **215,** 1–14 (2016).

146. Decary, S. *et al.* Shorter telomeres in dystrophic muscle consistent with extensive regeneration in young children. *Neuromuscul. Disord.* **10,** 113–120 (2000).

147. Charville, G. W. *et al.* Ex Vivo Expansion and In Vivo Self-Renewal of Human Muscle Stem Cells GregoryW. *Stem Cell Reports* **5,** 621–632 (2015).

148. Filareto, A. *et al.* Pax3-induced expansion enables the genetic correction of dystrophic satellite cells. *Skelet. Muscle* **5,** 36 (2015).

149. Ghahramani Seno, M. M. *et al.* Transcriptomic analysis of dystrophin RNAi knockdown reveals a central role for dystrophin in muscle differentiation and contractile apparatus organization. *BMC Genomics* **11,** 345 (2010).

150. Chen, Y. *et al.* Engineering Human Stem Cell Lines with Inducible Gene Knockout using CRISPR/Cas9. *Stem Cell* **17,** 233–244 (2015).

151. Mamchaoui, K. *et al.* Immortalized pathological human myoblasts: towards a universal tool for the study of neuromuscular disorders. *Skelet. Muscle* **1,** 34 (2011).

152. Zhu, C. H. *et al.* Cellular senescence in human myoblasts is overcome by human telomerase reverse transcriptase and cyclin-dependent kinase 4: Consequences in aging muscle and therapeutic strategies for muscular dystrophies. *Aging Cell* **6,** 515–523 (2007).

153. Rokach, O. *et al.* Establishment of a human skeletal muscle-derived cell line: biochemical, cellular and electrophysiological characterization. *Biochem. J.* **455,** 169–77 (2013).

154. Larsen, J. *et al.* Myoblasts generated by lentiviral mediated MyoD transduction of myotonic dystrophy type 1 (DM1) fibroblasts can be used for assays of therapeutic molecules. *BMC Res. Notes* **4,** 490 (2011).

155. Horio, F. *et al.* Functional validation and expression analysis of myotubes converted from skin fibroblasts using a simple direct reprogramming strategy. *eNeurologicalSci* **6,** 9–15 (2017).

156. Abujarour, R. & Valamehr, B. Generation of skeletal muscle cells from pluripotent stem cells: advances and challenges. *Front. Cell Dev. Biol.* **3,** 1–5 (2015).

157. Chal, J. *et al.* Differentiation of pluripotent stem cells to muscle fiber to model Duchenne muscular dystrophy. *Nat. Biotechnol.* **33,** 962–9 (2015).

158. Darabi, R; Arpke, RW; Irion, S; Dimos, JT; Grskovic, M; Kyba, M; Perlingeiro, R. Human ES- and iPS-Derived Myogenic Progenitors Restore Dystrophin and Improve Contractility upon Transplantation in Dystrophic Mice. *Cell Stem Cell* **10,** 610–619 (2013).

159. Shoji, E., Sakurai, H., Nishino, T., Nakahata, T. & Heike, T. Early pathogenesis of Duchenne muscular dystrophy modelled in patient-derived human induced pluripotent stem cells. *Nat. Publ. Gr.* 1–13 (2015).

160. Wilton, SD; Fletcher, S. Novel compounds for the treatment of Duchenne muscular dystrophy : emerging therapeutic agents. *Appl. Clin. Genet.* 29–44 (2011).

161. Huard, J., Mu, X. & Lu, A. Evolving paradigms in clinical pharmacology and

therapeutics for the treatment of Duchenne muscular dystrophy. *Clinical Pharmacology and Therapeutics* **100,** 142–146 (2016).

162. Rodino-Klapac, L. R., Mendell, J. R. & Sahenk, Z. Update on the treatment of Duchenne muscular dystrophy. *Curr. Neurol. Neurosci. Rep.* **13,** 332 (2013).

163. Verhaert, D., Richards, K., Rafael-Fortney, J. A. & Raman, S. V. Cardiac involvement in patients with muscular dystrophies magnetic resonance imaging phenotype and genotypic considerations. *Circ. Cardiovasc. Imaging* **4,** 67–76 (2011).

164. Mcnally, E. M. *et al.* Contemporary Cardiac Issues in Duchenne Muscular Dystrophy Elizabeth. *Circulation* **131,** 1590–1598 (2015).

165. Reinig, A. M., Mirzaei, S. & Berlau, D. J. Advances in the treatment of Duchenne muscular dystrophy: New and emerging pharmacotherapies. *Pharmacotherapy* **38,** 42–49 (2017).

166. Bertoni, C. Emerging gene editing strategies for Duchenne muscular dystrophy targeting stem cells. *Front. Physiol.* **5 APR,** 1–17 (2014).

167. Konieczny, P., Swiderski, K. & Chamberlain, J. S. Gene and cell-mediated therapies for muscular dystrophy. *Muscle Nerve* **47,** 649–663 (2013).

168. Dorota Sienkiewicz, Wojciech Kulak, Bożena Okurowska-Zawada, G. P.-P. & and Katarzyna Kawnik. Duchenne muscular dystrophy: current cell therapies. *Ther. Adv. Neurol. Disord. Ther Adv Neurol Disord* **8,** 166–177 (2015).

169. Niks, E. & Aartsma-Rus, A. Exon skipping: a first in class strategy for Duchenne

muscular dystrophy. *Expert Opin. Biol. Ther.* **17,** 225–236 (2016).

170. Malik, V., Rodino-Klapac, L. R., Viollet, L. & Mendell, J. R. Aminoglycoside-induced mutation suppression (stop codon readthrough) as a therapeutic strategy for Duchenne muscular dystrophy. *Ther. Adv. Neurol. Disord.* **3,** 379–89 (2010).

171. Haas, M. *et al.* European medicines agency review of ataluren for the treatment of ambulant patients aged 5 years and older with Duchenne muscular dystrophy resulting from a nonsense mutation in the dystrophin gene. *Neuromuscul. Disord.* **25,** 5–13 (2015).

172. Welch, E. M. *et al.* PTC124 targets genetic disorders caused by nonsense mutations. *Nature* **447,** 87–91 (2007).

173. Kayali, R. *et al.* Read-through compound 13 restores dystrophin expression and improves muscle function in the MDX mouse model for duchenne muscular dystrophy. *Hum. Mol. Genet.* **21,** 4007–4020 (2012).

174. Li, M., Andersson-Lendahl, M., Sejersen, T. & Arner, A. Muscle dysfunction and structural defects of dystrophin-null sapje mutant zebrafish larvae are rescued by ataluren treatment. *FASEB J.* **28,** 1593–1599 (2014).

175. Bushby, K. *et al.* Ataluren treatment of patients with nonsense mutation dystrophinopathy. *Muscle and Nerve* **50,** 477–487 (2014).

176. Unger, E. F. & Califf, R. M. Regarding 'Eteplirsen for the treatment of Duchenne muscular dystrophy'. *Ann. Neurol.* **81,** 162–164 (2017).

177. Aartsma-Rus, A. & Krieg, A. M. FDA Approves Eteplirsen for Duchenne

Muscular Dystrophy: The Next Chapter in the Eteplirsen Saga. *Nucleic Acid Ther.* **0,** nat.2016.0657 (2016).

178. Lee, T. *et al.* 2′-O-Methyl RNA/Ethylene-Bridged Nucleic Acid Chimera Antisense Oligonucleotides to Induce Dystrophin Exon 45 Skipping. *Genes (Basel).* **8,** 67 (2017).

179. Servais, L. *et al.* Non-Ambulant Duchenne Patients Theoretically Treatable by Exon 53 Skipping have Severe Phenotype. *J. Neuromuscul. Dis.* **2,** 269–279 (2015).

180. Wagner, K. R. Approaching a New Age in Duchenne Muscular Dystrophy Treatment. *Neurotherapeutics* **5,** 583–591 (2008).

181. Fairclough, R. J., Wood, M. J. & Davies, K. E. Therapy for Duchenne muscular dystrophy: renewed optimism from genetic approaches. *Nat. Rev. Genet.* **14,** 373–8 (2013).

182. Zhang, Y. & Duan, D. Novel Mini-Dystrophin Gene Dual Adeno-Associated Virus Vectors Restore Neuronal Nitric Oxide Synthase Expression at the Sarcolemma. *Hum. Gene Ther.* **23,** 98–103 (2012).

183. Li, S. *et al.* A highly functional mini-dystrophin/GFP fusion gene for cell and gene therapy studies of Duchenne muscular dystrophy. *Hum. Mol. Genet.* **15,** 1610–1622 (2006).

184. Mendell, J. R. *et al.* Dystrophin Immunity in Duchenne's Muscular Dystrophy. *N. Engl. J. Med.* **363,** 1429–1437 (2010).

185. Janghra, N. *et al.* Correlation of utrophin levels with the dystrophin protein complex and muscle fibre regeneration in duchenne and becker muscular dystrophy muscle biopsies. *PLoS One* **11,** 1–18 (2016).

186. Heller, K. N. *et al.* AAV-mediated overexpression of human α7 integrin leads to histological and functional improvement in dystrophic mice. *Mol. Ther.* **21,** 520–5 (2013).

187. Tinsley, J. M. *et al.* Daily treatment with SMTC1100, a novel small molecule utrophin upregulator, dramatically reduces the dystrophic symptoms in the mdx mouse. *PLoS One* **6,** e19189 (2011).

188. Murphy, K. T. *et al.* Antibody-directed myostatin inhibition improves diaphragm pathology in young but not adult dystrophic mdx mice. *Am. J. Pathol.* **176,** 2425–2434 (2010).

189. Bish, L. T. *et al.* Long-Term Systemic Myostatin Inhibition via Liver-Targeted Gene Transfer in Golden Retriever Muscular Dystrophy. *Hum. Gene Ther.* **22,** 1499–1509 (2011).

190. Matthias, N., Hunt, S. D., Wu, J. & Darabi, R. Skeletal muscle perfusion and stem cell delivery in muscle disorders using intra-femoral artery canulation in mice. *Exp. Cell Res.* 1–9 (2015).

191. Li, S. *et al.* Stable transduction of myogenic cells with lentiviral vectors expressing a minidystrophin. *Gene Ther.* **12,** 1099–1108 (2005).

192. Benabdallah, B. F. *et al.* Targeted Gene Addition of Microdystrophin in Mice Skeletal Muscle via Human Myoblast Transplantation -. *Mol. Ther. Acids* **2,** 1–9

(2013).

193. Charville, G. W. *et al.* Ex Vivo Expansion and In Vivo Self-Renewal of Human Muscle Stem Cells. *Stem Cell Reports* **5,** 621–632 (2015).

194. Imbert, N. *et al.* Calcium currents and transients in co-cultured contracting normal and Duchenne muscular dystrophy human myotubes. *J. Physiol.* **534,** 343–355 (2001).

195. Fauconnier, J. *et al.* Leaky RyR2 trigger ventricular arrhythmias in Duchenne muscular dystrophy. *Proc Natl Acad Sci U S A* **107,** 1559–1564 (2010).

196. Wehrens, X. H. T. *et al.* Enhancing calstabin binding to ryanodine receptors improves cardiac and skeletal muscle function in heart failure. *Proc. Natl. Acad. Sci. U. S. A.* **102,** 9607–12 (2005).

197. Andersson, D. C. *et al.* Ryanodine Receptor Oxidation Causes Intracellular Calcium Leak and Muscle Weakness in Aging. *Cell Metab.* **14,** 196–207 (2011).

198. Toral-Ojeda, I. *et al.* Calpain 3 deficiency affects SERCA expression and function in the skeletal muscle. *Expert Rev. Mol. Med.* **18,** e7 (2016).

199. Nelson, BR; Makarewich, CA; Anderson, DM; Winders, BR; Troupes, CD; Wu, F; Reese, AL; McAnally, JR; Chen, X; Kavalali, ET; Cannon, SC; Houser, SR; Bassel-Duby, R; Olson, E. A peptide encoded by a transcript annotated as long noncoding RNA enhances SERCA activity in muscle Benjamin. *Science (80-.).* **351,** 271–275 (2016).

200. Kwon, H. W. *et al.* The effect of enalapril and carvedilol on left ventricular

dysfunction in middle childhood and adolescent patients with muscular dystrophy. *Korean Circ. J.* **42,** 184–191 (2012).

201. Kobayashi, Y. M. *et al.* Sarcolemma-localized nNOS is required to maintain activity after mild exercise. *Nat Cell Biol* **456,** 511–515 (2009).

202. Asai, A. *et al.* Primary role of functional ischemia, quantitative evidence for the two-hit mechanism, and phosphodiesterase-5 inhibitor therapy in mouse muscular dystrophy. *PLoS One* **2,** (2007).

203. Hammers, D. W. *et al.* Tadalafil Treatment Delays the Onset of Cardiomyopathy in Dystrophin-Deficient Hearts. *J. Am. Heart Assoc.* **5,** e003911 (2016).

204. Martin, E. A. *et al.* Tadalafil alleviates muscle ischemia in patients with Becker muscular dystrophy. *Sci. Transl. Med.* **4,** 162ra155 (2012).

205. Nelson, M. D. *et al.* PDE5 inhibition alleviates functional muscle ischemia in boys with Duchenne muscular dystrophy. *Neurology* **82,** 2085–2091 (2014).

206. Kakizawa, S. Nitric oxide-induced calcium release: activation of type 1 ryanodine receptor, a calcium release channel, through non-enzymatic post-translational modification by nitric oxide. *Front. Exp. Endocrinol.* **4,** 142 (2013).

207. Bellinger, A. M. *et al.* Remodeling of ryanodine receptor complex causes 'leaky' channels: a molecular mechanism for decreased exercise capacity. *Proc. Natl. Acad. Sci. U. S. A.* **105,** 2198–202 (2008).

208. Niles, A. L., Moravec, R. A. & Riss, T. L. In vitro viability and cytotoxicity testing and same-well multi-parametric combinations for high throughput screening.

Curr. Chem. Genomics **3,** 33–41 (2009).

209. Singh, R. J., Hogg, N., Joseph, J., Konorev, E. & Kalyanaraman, B. The peroxynitrite generator, SIN-1, becomes a nitric oxide donor in the presence of electron acceptors. *Arch. Biochem. Biophys.* **361,** 331–339 (1999).

210. Kohr, MJ; Traynham, CJ; Roof, SR; Davis, JP; Ziolo, M. cAMP-independent Activation of Protein Kinase A by the Peroxynitrite Generator SIN-1 Elicits Positive Inotropic Effects in Cardiomyocytes. *J Mol Cell Cardiol* **44,** 735–745 (2008).

211. Gutiérrez-Martín, Y., Martín-Romero, F. J., Henao, F. & Gutiérrez-Merino, C. Alteration of cytosolic free calcium homeostasis by SIN-1: High sensitivity of L-type Ca2+ channels to extracellular oxidative/nitrosative stress in cerebellar granule cells. *J. Neurochem.* **92,** 973–989 (2005).

212. Söderberg, O. *et al.* Direct observation of individual endogenous protein complexes in situ by proximity ligation. *Nat. Methods* **3,** 995–1000 (2006).

213. Greenwood, C. *et al.* Proximity assays for sensitive quantification of proteins. *Biomol. Detect. Quantif.* **4,** 10–16 (2015).

214. Marks, A. Methods for identifying agents that target leaks in ryanodine receptors. *US Pat.* US 2009/00 (2009).

215. Willmann, R., Possekel, S., Dubach-Powell, J., Meier, T. & Ruegg, M. A. Mammalian animal models for Duchenne muscular dystrophy. *Neuromuscul. Disord.* **19,** 241–249 (2009).

216. Zeiger, U., Mitchell, C. H. & Khurana, T. S. Superior calcium homeostasis of extraocular muscles. *Exp. Eye Res.* **91,** 613–622 (2010).

217. Bertorini, T. E. *et al.* Calcium and magnesium content in fetuses at risk and prenecrotic Duchenne muscular dystrophy. *Neurology* **34,** 1436–40 (1984).

218. Burdi, R. *et al.* Multiple pathological events in exercised dystrophic mdx mice are targeted by pentoxifylline: outcome of a large array of in vivo and ex vivo tests. *J. Appl. Physiol.* **106,** 1311–24 (2009).

219. Hathout, Y. *et al.* Clinical utility of serum biomarkers in Duchenne muscular dystrophy. *Clin. Proteomics* **13,** 9 (2016).

220. Capogrosso, R. F. *et al.* Effects of S48168/Arm210, a new rycal® compound, on pathology related signs of exercised dystrophic mdx mouse. *Neuromuscul. Disord.* **24,** 821–822 (2014).

221. Quinn, J. L. *et al.* Effects of Dantrolene Therapy on Disease Phenotype in Dystrophin Deficient mdx Mice. *Plos Curr. mucular dystrophy* 1–14 (2013).

222. De Luca, A. Pre-clinical drug tests in the mdx mouse as a model of dystrophinopathies: an overview. *Acta Myol.* **31,** 40–7 (2012).

223. Cozzoli, A. *et al.* Evaluation of potential synergistic action of a combined treatment with alpha-methyl-prednisolone and taurine on the mdx mouse model of Duchenne muscular dystrophy. *Neuropathol. Appl. Neurobiol.* **37,** 243–256 (2011).

224. Messina, S. *et al.* Flavocoxid counteracts muscle necrosis and improves functional

properties in mdx mice : A comparison study with methylprednisolone. *Exp. Neurol.* **220,** 349–358 (2009).

225. Cozzoli, A. *et al.* GLPG0492 , a novel selective androgen receptor modulator , improves muscle performance in the exercised-mdx mouse model of muscular dystrophy ☙. *Pharmacol. Res.* **72,** 9–24 (2013).

226. Sinadinos, A. *et al.* P2RX7 Purinoceptor: A Therapeutic Target for Ameliorating the Symptoms of Duchenne Muscular Dystrophy. *PLOS Med.* **12,** e1001888 (2015).

227. Swiderski, K. *et al.* Tranilast administration reduces fibrosis and improves fatigue resistance in muscles of mdx dystrophic mice. 1–8 (2014).

228. Grounds, M. D., Radley, H. G., Lynch, G. S., Nagaraju, K. & De Luca, A. Towards developing standard operating procedures for pre-clinical testing in the mdx mouse model of Duchenne muscular dystrophy. *Neurobiol. Dis.* **31,** 1–19 (2008).

229. Emery, A. E. The muscular dystrophies. *Lancet* **359,** 687–695 (2002).

230. Yablonka-Reuveni, Z. & Anderson, J. E. Satellite cells from dystrophic (mdx) mice display accelerated differentiation in primary cultures and in isolated myofibers. *Dev. Dyn.* **235,** 203–12 (2006).

231. Luin, E., Lorenzon, P., Wernig, A. & Ruzzier, F. Calcium current kinetics in young and aged human cultured myotubes. *Cell Calcium* **44,** 554–566 (2008).

232. Baj, A. *et al.* Culture of skeletal myoblasts from human donors aged over 40 years:

dynamics of cell growth and expression of differentiation markers. *J. Transl. Med.* **3,** 21 (2005).

233. Chaouch, S. *et al.* Immortalized skin fibroblasts expressing conditional MyoD as a renewable and reliable source of converted human muscle cells to assess therapeutic strategies for muscular dystrophies: validation of an exon-skipping approach to restore dystrophin in Duchen. *Hum. Gene Ther.* **20,** 784–790 (2009).

234. Tanaka, A. *et al.* Efficient and Reproducible Myogenic Differentiation from Human iPS Cells: Prospects for Modeling Miyoshi Myopathy In Vitro. *PLoS One* **8,** (2013).

235. Amack, J. D. & Mahadevan, M. S. The myotonic dystrophy expanded CUG repeat tract is necessary but not sufficient to disrupt C2C12 myoblast differentiation. *Hum. Mol. Genet.* **10,** 1879–1887 (2001).

236. Stern-Straeter, J. *et al.* Characterization of human myoblast cultures for tissue engineering. *Int. J. Mol. Med.* **21,** 49–56 (2008).

237. Kiviluoto, S. *et al.* STIM1 as a key regulator for Ca2+ homeostasis in skeletal-muscle development and function. *Skelet. Muscle* **1,** 16 (2011).

238. Coisy-Quivy, M. *et al.* TC10 controls human myofibril organization and is activated by the sarcomeric RhoGEF obscurin. *J. Cell Sci.* **122,** 947–956 (2009).

239. Konig, S., Béguet, A., Bader, C. R. & Bernheim, L. The calcineurin pathway links hyperpolarization (Kir2.1)-induced Ca2+ signals to human myoblast differentiation and fusion. *Development* **133,** 3107–3114 (2006).

240. Kim, M. H. *et al.* Myogenic Akt signaling attenuates muscular degeneration, promotes myofiber regeneration and improves muscle function in dystrophin-deficient mdx mice. *Hum. Mol. Genet.* **20,** 1324–38 (2011).

241. Matecki, S. *et al.* Leaky ryanodine receptors contribute to diaphragmatic muscle weakness during mechanical ventilation. *Am. Thorac. Soc. Int. Conf. Abstr.* **113,** A3885–A3885 (2016).

242. Alderton, J. M. & Steinhardt, R. A. Calcium Influx through Calcium Leak Channels Is Responsible for the Elevated Levels of Calcium-dependent Proteolysis in Dystrophic Myotubes *. *J. Biol. Chem.* **275,** 9452–9460 (2000).

243. Culligan, K. G. & Ohlendieck, K. Abnormal Calcium Handling in Muscular Dystrophy. *Basic Appl Myol 12* **12,** 147–157 (2002).

244. Jun Liu, G. & Madsen, B. W. Biphasic effect of pentobarbitone on chick myotube nicotinic receptor channel kinetics. *Br. J. Pharmacol.* **118,** 1385–1388 (1996).

245. Ledwitch, K. V., Barnes, R. W. & Roberts, A. G. Unravelling the complex drug-drug interactions of the cardiovascular drugs, verapamil and digoxin, with P-glycoprotein. *Biosci. Rep.* **36,** e00309–e00309 (2016).

246. Lau, K. & Petegem, F. Van. Crystal structures of wild type and disease mutant forms of the ryanodine receptor SPRY2 domain. *Nat. Commun.* **5,** 1–11 (2014).

247. Gaburjakova, M. & Gaburjakova, J. Insight towards the identification of cytosolic Ca 2+ -binding sites in ryanodine receptors from skeletal and cardiac muscle. *Acta Physiol* 1–11 (2016).